NUTRIENT SENSING BY THE MONDOA TRANSCRIPTION FACTOR: A ROLE FOR MITOCHONDRIAL ATP

by

Blake Robert Wilde

A dissertation submitted to the faculty of
The University of Utah
in partial fulfillment of the requirements for the degree of

Doctor of Philosophy

Department of Oncological Sciences

The University of Utah

May 2018

The University of Utah Graduate School

STATEMENT OF DISSERTATION APPROVAL

The dissertation of **Blake Robert Wilde**

has been approved by the following supervisory committee members:

Donald Ayer	, Chair	**03/01/2018** Date Approved
Michael Engel	, Member	**03/01/2018** Date Approved
Katharine Ullman	, Member	**03/01/2018** Date Approved
Rodney Stewart	, Member	**03/01/2018** Date Approved
Elizabeth Liebold	, Member	**03/14/2018** Date Approved

and by **Bradley Cairns** , Chair/Dean of

the Department/College/School of **Oncological Sciences**

and by David B. Kieda, Dean of The Graduate School.

ABSTRACT

The MondoA/TXNIP axis controls glucose homeostasis. The transcription factor MondoA senses glucose-6-phosphate (G6P) and responds by driving expression of thioredoxin-interacting protein (TXNIP), a negative regulator of glucose uptake. The transcriptional activity of MondoA requires oxidative phosphorylation, yet the mechanism is unknown. We studied nutrient sensing by MondoA in the context of acidosis treatment and protein synthesis inhibition, both of which drive MondoA transcriptional activity and TXNIP expression. Both acidosis and protein synthesis inhibition converge on increased synthesis of mitochondrial-ATP (mtATP). Intracellular acidification leads to mitochondrial hyperpolarization and mtATP production through the ATP synthase. Protein synthesis inhibitors also drive mtATP production, likely through increased TCA cycle flux. As mtATP is exported from the mitochondria, it is consumed by mitochondria-bound hexokinase in a reaction that produces G6P. The localized production of G6P drives MondoA transcriptional activity. Thus, by simultaneously sensing glucose and mtATP via production of G6P, MondoA acts as a coincidence detector of the cells primary energy sources. We further show that MondoA drives an adaptive transcriptional response to intracellular acidification and protein synthesis inhibition, of which increased TXNIP is a predominant feature. By characterizing the transcriptional consequences of MondoA and TXNIP loss, we show that TXNIP supports MondoA-dependent transcription. Because TXNIP loss causes a shift away from

oxidative metabolism toward aerobic glycolysis, we propose that loss of TXNIP leads to decreased mtATP production, thus restricting MondoA transcriptional activity. Finally, MondoA loss sensitizes cells to Myc-driven cell death. Together these findings further our knowledge of 1) metabolic rewiring during acidosis treatment and protein synthesis inhibition, 2) mtATP and glucose sensing by MondoA, and 3) the biological impacts of MondoA transcriptional activity. Thus, we propose that the MondoA/TXNIP axis is a fundamental attribute of central carbon metabolism and homeostasis.

TABLE OF CONTENTS

LIST OF TABLES

Tables

LIST OF FIGURES

Figures

ACKNOWLEDGMENTS

I would like to first thank my dissertation advisor Donald Ayer. I credit him most for my success in the laboratory. He has the right touch for mentoring students, and I have been lucky to have him as an advisor and friend. Additionally, many faculty members at the Huntsman Cancer Institute and University of Utah have served as mentors and examples for me at this stage of my scientific career.

Next, I would like to thank numerous scientist and nonscientist friends that have helped to encourage and uplift me during graduate school. Among these friends are current and former lab-mates: Mohan Kaadige, John O'Shea, Zhizhou Ye, Kristin Murphy, Tian-Yeh Lim, Erik Eide, Mindy Stone, Thanh Parks, Liangliang Shen, KyongSim Han and many other rotation/visiting students.

I would like to thank my family. From a young age my parents have encouraged my curiosity and ambitions to "figure out how the world works." I appreciate my three brothers who were usually right by my side exploring the world and having fun. I would like to thank my parents-in-law. They are loyal and loving and have been incredibly supportive throughout my time in graduate school. I appreciate my siblings-in-law and their children who are always rooting for my success and constantly making me happy to be related to them.

Finally, I would like to thank my two best friends, my wife Whitney and son Jack. Without them I wouldn't have been able to make it through graduate school. Many days I

would be discouraged by a result in the lab or something else that I felt didn't go the way I wanted it to, but without fail Whitney and Jack found ways to cheer me up. There is nothing better in this life than knowing they are my family. Their constant love and encouragement are essential for me. I love you both more than I can express.

In Salt Lake City, UT

February, 2018

CHAPTER 1

INTRODUCTION

1.1. Metabolic rewiring in cancer

In the early 1900s, Otto Warburg made the seminal observation that cancer cells preferentially metabolize glucose in glycolysis and lactic fermentation, which is different from nontransformed cells that primarily use oxidative phosphorylation (Koppenol et al., 2011; Otto, 2016; Vander Heiden et al., 2009; Warburg, 1956). Dysregulation of glucose metabolism is now a widely recognized hallmark of cancer and is necessary to support the bioenergetic, biosynthetic and redox demands of cancer cells (DeBerardinis and Chandel, 2016; Hanahan and Weinberg, 2011; Pavlova and Thompson, 2016). Defining the metabolic alterations in cancer has had a broad impact on the detection and treatment of cancer; yet there is still much to learn about nutrient acquisition and utilization in cancer.

1.1.1. Glycolysis and pH regulation

Among Warburg's important findings is that cancer cells have elevated glucose uptake relative to surrounding tissues (Hay, 2016; Vander Heiden et al., 2009; Ward and Thompson, 2012). This observation is the key principle behind ^{18}F-deoxyglucose positron emission tomography (FDG-PET), which is routinely used to visualize human tumors in situ. FDG is a glucose analogue and its uptake is controlled by the same mechanisms that control glucose uptake. Accumulation of FDG in tumors is used to assess tumor size and metabolic state. Decreased glucose uptake as measured by FDG-PET is a significant positive prognostic factor (Vander Heiden et al., 2009). Given that increased glucose uptake is a characteristic feature of tumors, substantial work has gone into targeting glucose uptake and metabolism in cancer. There is growing evidence that targeting

glucose uptake directly may lead to selective targeting and eradication of cancer cells (Hay, 2016).

By preferentially converting pyruvate into lactate, cancer cells produce NAD^+, which supports glycolytic flux by serving as a cofactor for glyceraldehyde-3-phosphate dehydrogenase (GAPDH; Figure 1.1; (Pavlova and Thompson, 2016; Vander Heiden et al., 2009). Lactate secretion out of the cell enforces the forward progression of glycolysis and lactic fermentation (Hay, 2016). Lactate secretion is facilitated by monocarboxylate transporters (MCTs), which transport one lactate molecule and one proton to the extracellular space (Figure 1.1). MCTs are upregulated in a number of cancers (Webb et al., 2011). Lactate secretion prevents the accumulation of lactate, which can inhibit the rate limiting glycolytic enzyme phosphofructokinase-1 (PFK1) (Webb et al., 2011). Thus, enhanced lactate production by glycolysis and its export, along with protons, to the extracellular space are key features of metabolic reprogramming towards aerobic glycolysis in cancer. Chapter 2 outlines a mechanism by which intracellular acidification triggers the MondoA/TXNIP axis to control glucose metabolism and pH homeostasis.

MCT-driven export of lactate and protons to the extracellular space leads to intracellular alkalization, a hallmark of cancer metabolism. Increased expression and activity of Na^+-H^+ exchanger 1 (NHE1), carbonic anhydrases and V-ATPases also contribute to intracellular alkalization (Webb et al., 2011). Thus, normal cells have lower intracellular than extracellular pH, and cancer cells have a higher intracellular than extracellular pH. This pH gradient reversal affords cancer cells numerous autonomous and nonautonomous advantages. First, intracellular alkalization increases PFK1 activity about 100-fold, thus increasing glycolysis (Andres et al., 1990; Frieden et al., 1976;

Trivedi and Danforth, 1966). Second, intracellular alkalization drives proliferative signals and restricts cell death signals (Lagadic-Gossmann et al., 2004; Matsuyama et al., 2000; Pouyssegur et al., 1985). Third, acidic extracellular space supports matrix remodeling and cell invasion (Stock and Schwab, 2009). Fourth, the reversal of the pH gradient prevents the cellular retention and efficacy of various chemotherapies (Webb et al., 2011). Fifth, extracellular acidification allows cancer cells to evade death signals from the immune system (Fischer et al., 2007; Webb et al., 2011). Given its predominant role in metabolic rewiring and cancer progression, altered pH might be exploited for cancer-specific therapeutics. In Chapter 2, we show that the MondoA/TXNIP axis is an integral feature of the adaptive response to intracellular acidification.

In addition to acidosis, cancer cells adapt to a milieu of environmental stresses such as hypoxia, acidosis, and attacks by the immune system (Pavlova and Thompson, 2016). Metabolic alterations allow for survival and proliferation in such harsh conditions. Additionally, these stresses are co-opted by cancer as selective pressure for clones that are most resistant to apoptosis (Sloan and Ayer, 2010).

1.1.2. Bioenergetics and biosynthesis

Complementing its role in ATP production, glucose is also an important substrate for the generation of biomass. The first committed step in glucose metabolism is the generation of glucose-6-phosphate (G6P), which is a branching point for numerous biosynthetic pathways. G6P is used in the pentose-phosphate pathway as a major source of NADPH and ribonucleotides (Patra and Hay, 2014). G6P is also used in the hexosamine synthesis pathway, which provides substrates for the glycosylation of

proteins, and in glycogensis, which has a role metabolic reprogramming (Zois and Harris, 2016). Glycerol-3-phosphate is used in fatty-acid synthesis (Hay, 2016). Finally, 3-phosphoglycerate is used to fuel serine and glycine biosynthesis, which generates substrates for one-carbon metabolism and nucleotide production (Yang and Vousden, 2016). Thus glucose-derived glycolytic intermediates serve as precursors for biosynthetic reactions (Figure 1.1).

While cancer cells preferentially convert pyruvate into lactate, a small amount of pyruvate enters the mitochondria where it is metabolized in the TCA cycle (Vander Heiden et al., 2009). Early reports by Warburg and others suggested that mitochondria are nonfunctional in cancer; however, it is now clear that mitochondrial metabolism plays an essential role in cancer progression (King and Attardi, 1989; Koppenol et al., 2011; Sullivan et al., 2015). Pyruvate and glutamine anaplerosis are increased as a source of carbons for the TCA cycle (Altman et al., 2016). Further, Myc and other oncogenes stimulate mitochondrial biogenesis, demonstrating an essential role for the mitochondria in oncogenesis (Dang, 2013; Li et al., 2005). Finally, growing evidence indicates that the electron transport chain (ETC) is essential for redox homeostasis and cancer cell survival (Birsoy et al., 2015; Sullivan et al., 2015).

In a limited number of patients, targeting cancer metabolism has shown great promise. In 1948 Sidney Farber showed that aminopterin, a folate antagonist, and later amethopterin (now methotrexate), induced remission in children with acute lymphocytic leukemia (ALL; (Farber and Diamond, 1948). This was the first successful demonstration of chemotherapy in the clinic (Goodsell, 1999; Rajagopalan et al., 2002; Wright et al., 1951). Mechanistically, methotrexate inhibits dihydrofolate reductase, an important

enzyme in nucleotide biosynthesis. A few years later, Charles Heidelberger demonstrated tumor regression in patients treated with 5-fluorouracil (5-FU; (Heidelberger et al., 1957), which is an inhibitor of thymidylate synthase and nucleotide biosynthesis. 5-FU and methotrexate are the first examples of targeting cancer metabolism. Both therapies are incredibly virulent to cancer and are thus still used in the clinic today; however, widespread toxicity is a major challenge. The new frontier in chemotherapy is to leverage our mechanistic knowledge of cancer to be more specific in the cells and metabolic pathways we target (Luengo et al., 2017). Understanding the full complement of metabolic liabilities in cancer will help to identify other metabolic targets and therapies for cancer patients.

1.2. MondoA and glucose homeostasis

MondoA is the sentinel regulator of glucose-induced transcription, and it controls gene expression circuits that determine cellular fuel choice (Stoltzman et al., 2011; Stoltzman et al., 2008; our unpublished data). Dysregulation of MondoA underlies metabolic reprogramming in diabetes and cancer (O'Shea and Ayer, 2013; Richards et al., 2017a; Richards et al., 2017b). Given its role in metabolic homeostasis, we and others have proposed that the MondoA/TXNIP axis might be a therapeutic target for cancer.

1.2.1 Structure and function

MondoA is a member of the basic helix-loop-helix leucine zipper (bHLH-Zip) family of transcription factors. MondoA requires heterodimerization with Mlx, another bHLH-Zip transcription factor, for DNA-binding and transcriptional activity (Billin et al.,

2000). MondoA:Mlx works within a broader network of bHLH-Zip transcription factors that regulates nutrient utilization and sensing, the Myc-superfamily of transcription factors (Figure 1.2A). ChREBP, or MondoB, is a paralogue of MondoA that also binds Mlx. Both MondoA:Mlx and ChREBP:Mlx sense the metabolic status of the cell and respond by driving expression of genes that control nutrient availability and utilization (O'Shea and Ayer, 2013). Mlx can also dimerize with the transcriptional repressors Mxd1, Mxd4, Mnt or Mga. These heterocomplexes repress genes involved in growth and self-renewal. Mxd1, Mxd4, Mnt, Mga, Mxi1 and Mxd3 can interact with Max to drive the same phenotypes. Finally, Max can interact with c-Myc, N-Myc or L-Myc (collectively Myc). Myc:Max is a master regulator of cell growth, proliferation and motility (Diolaiti et al., 2015; Zhou and Hurlin, 2001). Myc-superfamily heterodimers all bind CANNTG E-boxes. We and others have described transcriptional antagonism between members of the Myc-superfamily (Carroll and Diolaiti, 2016; Carroll et al., 2015; Diolaiti et al., 2015; Wilde and Ayer, 2015; Yang and Hurlin, 2017), yet further work will be required to elucidate how transcription is coordinated by all members of the Myc-superfamily. The simple model that has emerged is that the Myc-superfamily coordinates nutrient utilization and availability.

MondoA and Mlx interact with each other and bind DNA through their bHLH-Zip domains. MondoA:Mlx heterodimers bind carbohydrate-responsive elements (ChoRE), which are two E-boxes separated by five nucleotides. A C-terminal region of both MondoA and Mlx, which we dubbed the dimerization and cytoplasmic localization domain (DCD), is also necessary for MondoA:Mlx interaction and nuclear localization (Figure 1.2B; (Eilers et al., 2002; Peterson et al., 2010). Further, MondoA contains a

strong transactivation domain and five Mondo-conserved domains (MCRs) at the N-terminus (Billin and Ayer, 2006; Billin et al., 2000). The MCRs are highly conserved in MondoA orthologues and control nutrient sensing (McFerrin and Atchley, 2012). An N-terminal region that spans MCRs I-IV has been reported as a low-glucose inhibitory domain (LID) and is involved in repressing transcriptional activation under low glucose conditions (Peterson et al., 2010). A glucose responsive activation element (GRACE), which includes MCRV, is responsible for glucose sensing and glucose-induced transcription (McFerrin and Atchley, 2012). Mechanistically, we showed that MCRII and MCRIII coordinate the glucose-induced nucleocytoplasmic shuttling of MondoA (Eilers et al., 2002). The roles of MCRs I, IV and V have not been well characterized.

Unlike other members of the Myc-superfamily, MondoA is not constitutively nuclear. Rather, it shuttles between the outer-mitochondrial membrane (OMM) and the nucleus (Eilers et al., 2002; Peterson et al., 2010; Sans et al., 2006). We have previously demonstrated that MCRIII interacts with 14-3-3 family members, a class of proteins that bind phosphorylated residues (Figure 1.3A; (Eilers et al., 2002; Morrison, 2009; Peterson et al., 2010). ChREBP also binds 14-3-3, and crystal structures of ChREBP/14-3-3 indicate that the interaction occurs independent of phosphorylated residues in ChREBP: a novel mode of 14-3-3 binding (Ge et al., 2012; Sato et al., 2016). Rather a sulfate ion coordinates the binding. Consistent with this finding, the MondoA/14-3-3 interaction is independent of phosphorylatable residues (Peterson et al., 2010). Functionally, we observed that 14-3-3 binding is necessary for nuclear retention of MondoA (Eilers et al., 2002). Our working model is that 14-3-3 binding to MondoA occludes Crm1 binding at a canonical nuclear-export signal in MCRII (Figure 1.3B). Given the overlapping role for

G6P and 14-3-3 in MondoA activity, we postulated that the MondoA/14-3-3 interaction is coordinated by G6P. Using the published structure of ChREBP and 14-3-3, we conducted molecular modeling to demonstrate that G6P rather than a sulfate ion could coordinate the interaction. G6P fits within steric and electrostatic constraints of the binding interface (Figure 1.3C), leading us to hypothesize that G6P coordinates the interaction between MondoA and 14-3-3, thus leading to a blockage of Crm1 binding to MCRII and the subsequent nuclear retention and transcriptional activity of MondoA.

1.2.2. Nutrient sensing by MondoA

A predominant feature of MondoA is its ability to sense cellular metabolic states. Our work demonstrates that MondoA senses glucose 6-phosphate (G6P) and responds by accumulating in the nucleus, binding the promoters of target genes and recruiting cofactors to initiate transcription (Peterson et al., 2010; Stoltzman et al., 2008). MondoA can sense phosphorylated forms of other nonglucose hexose sugars such as glucosamine, 2-deoxyglucose and 3-O-methylglucose (Stoltzman et al., 2011). Others have suggested that MondoA senses the glycolytic metabolite fructose-2,6-bisphosphate (Petrie et al., 2013). Petrie et al. proposed that fructose-2,6-bisphosphate induces a transcriptional profile that is distinct from G6P-induced transcription. This raises the intriguing possibility that MondoA senses multiple glycolytic metabolites, each potentially driving the distinct gene expression programs. How broadly MondoA senses glycolytic intermediates or potentially other metabolites remains to be explored.

Conceptually, by localizing to the OMM, MondoA is poised to sense metabolic signals from the mitochondria. Consistent with this idea, steady-state and G6P-stimulated

MondoA transcriptional activity requires oxidative phosphorylation (Figure 1.4; (Han and Ayer, 2013; Stoltzman et al.; Yu et al., 2010). The exact molecular mechanism that controls ETC-sensing by MondoA remains unclear. Yu et al. hypothesized that ETC inhibition leads to an increase in glycolytic flux and a decrease in steady-state levels of G6P. They found that restricting glycolytic flux through GAPDH inhibition restored MondoA activity in the face of ETC inhibition. Yet counter to this argument, 2-deoxyglucose (2DG), which is a potent inducer of MondoA transcriptional activity under most circumstances, does not rescue MondoA activity following ETC inhibition (Yu et al., 2010). Thus, glycolytic flux is not the only factor that regulates G6P-driven MondoA activity. Our work on 5-amino-4-imidazolecarboxamide (AICAR)-stimulated MondoA activity showed that MondoA is a direct sensor of adenine nucleotides (Han and Ayer, 2013). In Chapters 2 and 3 we show that mitochondrial-derived ATP is the ETC-derived signal that drives MondoA activity.

MondoA controls the glucose-dependent expression of thioredoxin-interacting protein (TXNIP; (Stoltzman et al. 2008). In nearly all cell types, MondoA is necessary and sufficient to drive TXNIP expression. MondoA binds a ChoRE in the promoter region of TXNIP and recruits cofactors that initiate transcription of TXNIP (Minn et al., 2005). TXNIP is a potent negative-regulator of glucose uptake (see Chapter 1.3 for a detailed discussion of this point). Thus, MondoA and TXNIP form a negative-feedback loop that controls glucose homeostasis. As discussed below, the MondoA/TXNIP axis is downregulated in many cancers. Furthermore, while not the focus of our current work, the MondoA/TXNIP axis is upregulated in insulin-resistance and type-2 diabetes (Richards et al., 2017a; Richards et al., 2017b).

1.3. The MondoA/TXNIP axis in metabolism and cancer

1.3.1. The pleiotropic function of TXNIP

TXNIP has pleiotropic functions in suppressing cell growth and proliferation (Figure 1.5). By restricting thioredoxin (TXN) function, TXNIP drives antiproliferative functions such as oxidative stress, DNA damage and ASK1-mediated apoptosis (Nishiyama et al., 1999; Palde and Carroll, 2015; Saxena et al., 2010). TXNIP interferes with MDM2-mediated p53 ubiquitination and proteolysis, thus driving p53-dependent growth suppression and apoptosis (Jung et al., 2013). During quiescence, MondoA-dependent TXNIP expression is high, enforcing oxidative metabolism; however, downregulation of the MondoA/TXNIP axis is essential for cells to exit quiescence, thus establishing the MondoA/TXNIP axis as a metabolic checkpoint in the cell cycle (Elgort et al., 2010). Further, TXNIP directly inhibits progression through G1 by physically interacting with and stabilizing p27(kip1) (Jeon et al., 2005; Yamaguchi et al., 2008). Finally, our preliminary data suggests that TXNIP is a negative regulator of PI3K activity (our unpublished data).

Based on known functions of TXNIP, it has been generally thought that TXNIP localizes to the cytoplasm, yet recent work has shown TXNIP is enriched in the nucleus and interacts with transcriptional machinery (Huttlin et al., 2017; Huttlin et al., 2015; Saxena et al., 2010; Xu et al., 2013). TXNIP stimulates its own expression through a feed-forward loop (Chen et al., 2014). Though the mechanism has yet to be fully explored, we speculate that TXNIP regulates MondoA function. We address this hypothesis in Chapter 4.

TXNIP expression is elevated in several rodent models of diabetes and in human

diabetes patients (Chen et al., 2010a; Chen et al., 2008a; Chen et al., 2008b). TXNIP stimulates activity of the NRLP3 inflammasome, a process that is linked to pancreatic β-cell death, insulin resistance, and diabetes (Zhou et al., 2010). Further, AMP-activated protein kinase (AMPK), a master regulator of β-cell function, is negatively regulated by TXNIP expression. Conversely, AMPK phosphorylates TXNIP on residue S308, which accelerates its degradation, thus stimulating glucose uptake in an insulin-independent manner (Waldhart et al., 2017; Wu et al., 2013). Further work will be important in defining the functional connections between AMPK and the MondoA/TXNIP axis.

TXNIP has pleiotropic effects on cell metabolism, the most predominant being its ability to suppress glucose uptake. Mechanistically, TXNIP localizes to the plasma membrane where it binds GLUT1 or GLUT4 and initiates clathrin-mediated internalization (Waldhart et al., 2017; Wu et al., 2013). A di-leucine motif in one of the arrestin domains of TXNIP is essential for GLUT internalization and probably serves as a clathrin binding site. Mutating these residues to alanine leads to constitutive glucose uptake (Wu et al., 2013). This is consistent with a report showing that glucose uptake is intrinsic to the arrestin-domains (Patwari et al., 2009). Further, TXNIP negatively regulates GLUT1 mRNA and protein levels, although the mechanism is not known (Wu et al., 2013). A potential explanation is that TXNIP prevents Hypoxia inducible factor 1α (Hif1α) transcriptional activity, which drives the GLUT1 expression. Mechanistically, TXNIP interacts with and stabilizes an isoform of pVHL that controls the nuclear export of Hif1α (Shin et al., 2008). Additionally, TXNIP stabilizes the pVHL/HIF1α interaction, facilitating Hif1α ubiquitination and degradation (Yoshioka and Lee, 2014).

In addition to its effects on carbohydrate metabolism, TXNIP is an important

regulator of lipid homeostasis. TXNIP-knockout mice are hyperlipidemic (Bodnar et al., 2002). Further, loss of TXNIP in skeletal muscles prevents β-oxidation (DeBalsi et al., 2014) of a number of substrates. Our recent work has demonstrated that TXNIP decreases expression of G0S2, an important negative regulator of lipolysis (our unpublished data). Together these results show that TXNIP is important for fatty acid catabolism. Paradoxically, one group found that in cardiomyocytes TXNIP negatively regulates fatty acid oxidation via the increased expression of miR-33a (Chen et al., 2016). Further work will be needed to determine the role of TXNIP in lipid homeostasis.

TXNIP is highly upregulated in response to glucose (Shalev et al., 2002; Stoltzman et al., 2008). A wide variety of metabolic stresses trigger the MondoA/TXNIP axis. In Chapter 2 and 3, we show metabolic rewiring and activation of the MondoA/TXNIP axis in response to acidosis and protein synthesis inhibition, respectively. Further, endoplasmic-reticulum stress drives TXNIP expression by enhancing TXNIP mRNA stability (Lerner et al., 2012).

1.3.2. TXNIP in cancer

TXNIP expression is diminished in many cancers including renal, breast, lung, gastric, colon and hepatocellular carcinoma (Figure 1.6; (Cadenas et al., 2010; Dutta et al., 2005; Kopantzev et al., 2008; Kwon et al., 2010; Lee et al., 2010; Shen et al., 2015; Takahashi et al., 2002). TXNIP expression is decreased in triple-negative breast cancer (TNBC), and overexpression of TXNIP in patient derived TNBC xenografts restricted tumor growth (our unpublished data). However, MondoA and TXNIP have growth promoting effects in B-cell acute lymphocytic leukemia (Wernicke et al., 2012). Further

work will be needed to determine the contexts in which TXNIP is tumor suppressive versus tumor promoting.

We demonstrated that TXNIP is suppressed by many progrowth pathways. First, serum stimulation of cells in quiescence decreases TXNIP expression through the Ras/MAPK and PI3K/AKT pathways (Elgort et al., 2010). Second, mTOR physically interacts with MondoA and sequesters it from Mlx, thus preventing MondoA-dependent TXNIP expression (Kaadige et al., 2015). Third, Myc binds to the TXNIP promoter and drives its transcriptionally repression by competing with MondoA at a shared ChoRE binding site (Shen et al., 2015). Fourth, constitutively active BRAF represses MondoA-dependent TXNIP expression (Parmenter et al., 2014). Fifth, Ras decreases translation of TXNIP mRNA (our unpublished work). Others have shown that IGF1, PI3K, AKT and AMPK all downregulate TXNIP expression (Hong et al., 2016; Nagaraj et al., 2018; Waldhart et al., 2017; Wu et al., 2013). By suppressing TXNIP expression, progrowth signals drive enhanced glucose uptake and glycolytic metabolism.

Our work has focused on TXNIP in triple-negative breast cancer (TNBC). We recently demonstrated that MondoA/TXNIP functions as a tumor suppressor axis in TNBC. We showed that Myc directly competes with MondoA for a binding site on the TXNIP promoter. Restoring TXNIP expression in TNBC restricts glucose uptake and aerobic glycolysis (Shen et al., 2015). These findings are consistent with our work showing that: 1) high TXNIP expression correlates with better overall prognosis in breast cancer patients (Chen et al., 2010b; Shen et al., 2015); 2) overexpression of TXNIP in TNBC patient-derived xenografts restricts tumor growth (our unpublished data); and 3) loss of MondoA or TXNIP in TNBC leads to increased glucose uptake and proliferation

of TNBC cells in culture (data not shown). Collectively, these data suggest that the MondoA/TXNIP axis suppresses tumor growth by limiting nutrient availability. Thus increasing MondoA/TXNIP activity may be efficacious against TNBC. Consistent with these findings, in $BRAF^{V600E}$ melanomas Myc and MondoA also work in opposition. In these tumors, activation of the MondoA/TXNIP axis and downregulation of Myc are required for the therapeutic efficacy of vemurafenib (Parmenter et al., 2014; Wilde and Ayer, 2015). In contrast, in neuroblastoma and Myc-amplified B-cell leukemia, Myc and MondoA cooperate to reprogram metabolism and drive tumorigenesis (Carroll and Diolaiti, 2016; Carroll et al., 2015). A model that addresses this apparent disparity is that as the level of Myc expression determines a requirement for MondoA. When Myc is very high, cells need to activate pathways that counter Myc-driven cell death, of which MondoA is an integral player. Loss of MondoA thus leads to synthetic lethality. In contrast, when Myc is low it needs to rewire transcription to support nutrient uptake to allow for cell growth and proliferation. Thus, by repressing MondoA target genes such as TXNIP, Myc drives an increase in nutrient uptake and utilization. Chapter 4 specifically addresses this model.

1.4. Summary of dissertation

As reviewed above, MondoA is a sensor of the metabolic status of the cell and through its regulation of TXNIP expression, maintains glucose homeostasis. Downregulation of the MondoA/TXNIP axis is a hallmark of cancer, and affords cancer cells bioenergetic and biosynthetic advantages. Triggering MondoA transcriptional activity may be an effective way to target glucose metabolism and treat cancer; however,

this will require characterization of the molecular mechanisms that control MondoA transcriptional activity. Further, deep knowledge of the MondoA-dependent transcriptome will be important for understanding the downstream consequences of restricting MondoA transcriptional activity.

Chapter 2 addresses how acidosis controls TXNIP expression. We show that acidosis drives the synthesis of mitochondrial ATP (mtATP) that is required for MondoA transcriptional activity. We further show that the dependence on mtATP is due to its consumption by mitochondria-bound hexokinase to generate G6P. This finding implicates the mitochondria in transcriptional control of cellular fuel choice. Collectively, our findings show that MondoA acts as a coincidence detector, integrating signals from glycolysis and the ETC to maintain energy balance in the cell.

In Chapter 3, we examined the effects of protein synthesis inhibition on the MondoA/TXNIP axis. Using the translation inhibitors cycloheximide and Rocaglamide A, we observed robust induction of MondoA transcriptional activity. Protein synthesis inhibition drives mtATP synthesis and leads to increased G6P levels. Our working model is that protein synthesis inhibition drives TCA cycle activity and mtATP synthesis. This leads to G6P production by mitochondrial-linked hexokinase and activation of the MondoA/TXNIP axis. This model is consistent with the findings in Chapter 2 showing that MondoA senses mtATP. Further, we showed that activation of the MondoA/TXNIP axis is a key feature of the growth suppressive effects of Rocaglamide A.

Chapter 4 focused on decoding the MondoA-dependent transcriptome. We used CRISPR/Cas9 genome editing to knockout MondoA and TXNIP in two different cell lines. mRNA-sequencing and ChIP-sequencing were employed to characterize

differentially regulated genes and DNA occupancy, respectively. First, we observed that TXNIP supports MondoA transcriptional activity. Second, we showed that MondoA and Myc differentially regulate the same genes. Finally, we showed that MondoA is part of an adaptive response to high Myc levels.

1.5. References

Altman, B.J., Stine, Z.E., and Dang, C.V. (2016). From Krebs to clinic: glutamine metabolism to cancer therapy. Nat Rev Cancer *16*, 749.

Andres, V., Carreras, J., and Cusso, R. (1990). Regulation of muscle phosphofructokinase by physiological concentrations of bisphosphorylated hexoses: effect of alkalinization. Biochem Biophys Res Commun *172*, 328-334.

Billin, A.N., and Ayer, D.E. (2006). The Mlx network: evidence for a parallel Max-like transcriptional network that regulates energy metabolism. Curr Top Microbiol Immunol *302*, 255-278.

Billin, A.N., Eilers, A.L., Coulter, K.L., Logan, J.S., and Ayer, D.E. (2000). MondoA, a novel basic helix-loop-helix-leucine zipper transcriptional activator that constitutes a positive branch of a max-like network. Mol Cell Biol *20*, 8845-8854.

Birsoy, K., Wang, T., Chen, W.W., Freinkman, E., Abu-Remaileh, M., and Sabatini, D.M. (2015). An Essential Role of the Mitochondrial Electron Transport Chain in Cell Proliferation Is to Enable Aspartate Synthesis. Cell *162*, 540-551.

Bodnar, J.S., Chatterjee, A., Castellani, L.W., Ross, D.A., Ohmen, J., Cavalcoli, J., Wu, C., Dains, K.M., Catanese, J., Chu, M.*, et al.* (2002). Positional cloning of the combined hyperlipidemia gene Hyplip1. Nat Genet *30*, 110-116.

Cadenas, C., Franckenstein, D., Schmidt, M., Gehrmann, M., Hermes, M., Geppert, B., Schormann, W., Maccoux, L.J., Schug, M., Schumann, A.*, et al.* (2010). Role of thioredoxin reductase 1 and thioredoxin interacting protein in prognosis of breast cancer. Breast Cancer Res *12*, R44.

Carroll, P.A., and Diolaiti, D. (2016). A novel role for the extended MYC network in cancer cell survival. Mol Cell Oncol *3*, e1026528.

Carroll, P.A., Diolaiti, D., McFerrin, L., Gu, H., Djukovic, D., Du, J., Cheng, P.F., Anderson, S., Ulrich, M., Hurley, J.B.*, et al.* (2015). Deregulated Myc requires MondoA/Mlx for metabolic reprogramming and tumorigenesis. Cancer Cell *27*, 271-285.

Chen, J., Fontes, G., Saxena, G., Poitout, V., and Shalev, A. (2010a). Lack of TXNIP protects against mitochondria-mediated apoptosis but not against fatty acid-induced ER stress-mediated beta-cell death. Diabetes *59*, 440-447.

Chen, J., Hui, S.T., Couto, F.M., Mungrue, I.N., Davis, D.B., Attie, A.D., Lusis, A.J., Davis, R.A., and Shalev, A. (2008a). Thioredoxin-interacting protein deficiency induces Akt/Bcl-xL signaling and pancreatic beta-cell mass and protects against diabetes. FASEB J *22*, 3581-3594.

Chen, J., Jing, G., Xu, G., and Shalev, A. (2014). Thioredoxin-interacting protein stimulates its own expression via a positive feedback loop. Mol Endocrinol *28*, 674-680.

Chen, J., Saxena, G., Mungrue, I.N., Lusis, A.J., and Shalev, A. (2008b). Thioredoxin-interacting protein: a critical link between glucose toxicity and beta-cell apoptosis. Diabetes *57*, 938-944.

Chen, J., Young, M.E., Chatham, J.C., Crossman, D.K., Dell'Italia, L.J., and Shalev, A. (2016). TXNIP regulates myocardial fatty acid oxidation via miR-33a signaling. Am J Physiol Heart Circ Physiol *311*, H64-75.

Chen, J.L., Merl, D., Peterson, C.W., Wu, J., Liu, P.Y., Yin, H., Muoio, D.M., Ayer, D.E., West, M., and Chi, J.T. (2010b). Lactic acidosis triggers starvation response with paradoxical induction of TXNIP through MondoA. PLoS Genet *6*, e1001093.

Dang, C.V. (2013). MYC, metabolism, cell growth, and tumorigenesis. Cold Spring Harb Perspect Med *3*, 1-13.

DeBalsi, K.L., Wong, K.E., Koves, T.R., Slentz, D.H., Seiler, S.E., Wittmann, A.H., Ilkayeva, O.R., Stevens, R.D., Perry, C.G., Lark, D.S.*, et al.* (2014). Targeted metabolomics connects thioredoxin-interacting protein (TXNIP) to mitochondrial fuel selection and regulation of specific oxidoreductase enzymes in skeletal muscle. J Biol Chem *289*, 8106-8120.

DeBerardinis, R.J., and Chandel, N.S. (2016). Fundamentals of cancer metabolism. Sci Adv *2*, e1600200.

Diolaiti, D., McFerrin, L., Carroll, P.A., and Eisenman, R.N. (2015). Functional interactions among members of the MAX and MLX transcriptional network during oncogenesis. Biochim Biophys Acta *1849*, 484-500.

Dutta, K.K., Nishinaka, Y., Masutani, H., Akatsuka, S., Aung, T.T., Shirase, T., Lee, W.H., Yamada, Y., Hiai, H., Yodoi, J.*, et al.* (2005). Two distinct mechanisms for loss of thioredoxin-binding protein-2 in oxidative stress-induced renal carcinogenesis. Lab Invest *85*, 798-807.

Eilers, A.L., Sundwall, E., Lin, M., Sullivan, A.A., and Ayer, D.E. (2002). A novel heterodimerization domain, CRM1, and 14-3-3 control subcellular localization of the MondoA-Mlx heterocomplex. Mol Cell Biol *22*, 8514-8526.

Elgort, M.G., O'Shea, J.M., Jiang, Y., and Ayer, D.E. (2010). Transcriptional and translational downregulation of thioredoxin interacting protein is required for metabolic reprogramming during G(1). Genes Cancer *1*, 893-907.

Farber, S., and Diamond, L.K. (1948). Temporary remissions in acute leukemia in children produced by folic acid antagonist, 4-aminopteroyl-glutamic acid. N Engl J Med *238*, 787-793.

Fischer, K., Hoffmann, P., Voelkl, S., Meidenbauer, N., Ammer, J., Edinger, M., Gottfried, E., Schwarz, S., Rothe, G., Hoves, S.*, et al.* (2007). Inhibitory effect of tumor cell-derived lactic acid on human T cells. Blood *109*, 3812-3819.

Frieden, C., Gilbert, H.R., and Bock, P.E. (1976). Phosphofructokinase. III. Correlation of the regulatory kinetic and molecular properties of the rabbit muscle enzyme. J Biol Chem *251*, 5644-5647.

Ge, Q., Huang, N., Wynn, R.M., Li, Y., Du, X., Miller, B., Zhang, H., and Uyeda, K. (2012). Structural characterization of a unique interface between carbohydrate response element-binding protein (ChREBP) and 14-3-3beta protein. J Biol Chem *287*, 41914-41921.

Goodsell, D.S. (1999). The molecular perspective: methotrexate. Stem Cells *17*, 314-315.

Han, K.S., and Ayer, D.E. (2013). MondoA senses adenine nucleotides: transcriptional induction of thioredoxin-interacting protein. Biochem J *453*, 209-218.

Hanahan, D., and Weinberg, R.A. (2011). Hallmarks of cancer: the next generation. Cell *144*, 646-674.

Hay, N. (2016). Reprogramming glucose metabolism in cancer: can it be exploited for cancer therapy? Nat Rev Cancer *16*, 635-649.

Heidelberger, C., Chaudhuri, N.K., Danneberg, P., Mooren, D., Griesbach, L., Duschinsky, R., Schnitzer, R.J., Pleven, E., and Scheiner, J. (1957). Fluorinated pyrimidines, a new class of tumour-inhibitory compounds. Nature *179*, 663-666.

Hong, S.Y., Yu, F.X., Luo, Y., and Hagen, T. (2016). Oncogenic activation of the PI3K/Akt pathway promotes cellular glucose uptake by downregulating the expression of thioredoxin-interacting protein. Cell Signal *28*, 377-383.

Huttlin, E.L., Bruckner, R.J., Paulo, J.A., Cannon, J.R., Ting, L., Baltier, K., Colby, G., Gebreab, F., Gygi, M.P., Parzen, H.*, et al.* (2017). Architecture of the human interactome defines protein communities and disease networks. Nature *545*, 505-509.

Huttlin, E.L., Ting, L., Bruckner, R.J., Gebreab, F., Gygi, M.P., Szpyt, J., Tam, S., Zarraga, G., Colby, G., Baltier, K.*, et al.* (2015). The BioPlex Network: a systematic exploration of the human interactome. Cell *162*, 425-440.

Jeon, J.H., Lee, K.N., Hwang, C.Y., Kwon, K.S., You, K.H., and Choi, I. (2005). Tumor suppressor VDUP1 increases p27(kip1) stability by inhibiting JAB1. Cancer Res *65*, 4485-4489.

Jung, H., Kim, M.J., Kim, D.O., Kim, W.S., Yoon, S.J., Park, Y.J., Yoon, S.R., Kim, T.D., Suh, H.W., Yun, S.*, et al.* (2013). TXNIP maintains the hematopoietic cell pool by switching the function of p53 under oxidative stress. Cell Metab *18*, 75-85.

Kaadige, M.R., Yang, J., Wilde, B.R., and Ayer, D.E. (2015). MondoA-Mlx transcriptional activity is limited by mTOR-MondoA interaction. Mol Cell Biol *35*, 101-110.

King, M.P., and Attardi, G. (1989). Human cells lacking mtDNA: repopulation with exogenous mitochondria by complementation. Science *246*, 500-503.

Kopantzev, E.P., Monastyrskaya, G.S., Vinogradova, T.V., Zinovyeva, M.V., Kostina, M.B., Filyukova, O.B., Tonevitsky, A.G., Sukhikh, G.T., and Sverdlov, E.D. (2008). Differences in gene expression levels between early and later stages of human lung development are opposite to those between normal lung tissue and non-small lung cell carcinoma. Lung Cancer *62*, 23-34.

Koppenol, W.H., Bounds, P.L., and Dang, C.V. (2011). Otto Warburg's contributions to current concepts of cancer metabolism. Nat Rev Cancer *11*, 325-337.

Kwon, H.J., Won, Y.S., Suh, H.W., Jeon, J.H., Shao, Y., Yoon, S.R., Chung, J.W., Kim, T.D., Kim, H.M., Nam, K.H.*, et al.* (2010). Vitamin D3 upregulated protein 1 suppresses TNF-alpha-induced NF-kappaB activation in hepatocarcinogenesis. J Immunol *185*, 3980-3989.

Lagadic-Gossmann, D., Huc, L., and Lecureur, V. (2004). Alterations of intracellular pH homeostasis in apoptosis: origins and roles. Cell Death Differ *11*, 953-961.

Lee, J.H., Jeong, E.G., Choi, M.C., Kim, S.H., Park, J.H., Song, S.H., Park, J., Bang, Y.J., and Kim, T.Y. (2010). Inhibition of histone deacetylase 10 induces thioredoxin-interacting protein and causes accumulation of reactive oxygen species in SNU-620 human gastric cancer cells. Mol Cells *30*, 107-112.

Lerner, A.G., Upton, J.P., Praveen, P.V., Ghosh, R., Nakagawa, Y., Igbaria, A., Shen, S., Nguyen, V., Backes, B.J., Heiman, M.*, et al.* (2012). IRE1alpha induces thioredoxin-interacting protein to activate the NLRP3 inflammasome and promote programmed cell death under irremediable ER stress. Cell Metab *16*, 250-264.

Li, F., Wang, Y., Zeller, K.I., Potter, J.J., Wonsey, D.R., O'Donnell, K.A., Kim, J.W., Yustein, J.T., Lee, L.A., and Dang, C.V. (2005). Myc stimulates nuclearly encoded mitochondrial genes and mitochondrial biogenesis. Mol Cell Biol *25*, 6225-6234.

Luengo, A., Gui, D.Y., and Vander Heiden, M.G. (2017). Targeting metabolism for cancer therapy. Cell Chem Biol *24*, 1161-1180.

Matsuyama, S., Llopis, J., Deveraux, Q.L., Tsien, R.Y., and Reed, J.C. (2000). Changes in intramitochondrial and cytosolic pH: early events that modulate caspase activation during apoptosis. Nat Cell Biol *2*, 318-325.

McFerrin, L.G., and Atchley, W.R. (2012). A novel N-terminal domain may dictate the glucose response of Mondo proteins. PLoS One *7*, e34803.

Minn, A.H., Hafele, C., and Shalev, A. (2005). Thioredoxin-interacting protein is stimulated by glucose through a carbohydrate response element and induces beta-cell apoptosis. Endocrinology *146*, 2397-2405.

Morrison, D.K. (2009). The 14-3-3 proteins: integrators of diverse signaling cues that impact cell fate and cancer development. Trends Cell Biol *19*, 16-23.

Nagaraj, K., Lapkina-Gendler, L., Sarfstein, R., Gurwitz, D., Pasmanik-Chor, M., Laron, Z., Yakar, S., and Werner, H. (2018). Identification of thioredoxin-interacting protein (TXNIP) as a downstream target for IGF1 action. Proc Natl Acad Sci U S A *115*, 1045-1050.

Nishiyama, A., Matsui, M., Iwata, S., Hirota, K., Masutani, H., Nakamura, H., Takagi, Y., Sono, H., Gon, Y., and Yodoi, J. (1999). Identification of thioredoxin-binding protein-2/vitamin D(3) up-regulated protein 1 as a negative regulator of thioredoxin function and expression. J Biol Chem *274*, 21645-21650.

O'Shea, J.M., and Ayer, D.E. (2013). Coordination of nutrient availability and utilization by MAX- and MLX-centered transcription networks. Cold Spring Harb Perspect Med *3*, a014258.

Otto, A.M. (2016). Warburg effect(s)-a biographical sketch of Otto Warburg and his impacts on tumor metabolism. Cancer Metab *4*, 5.

Palde, P.B., and Carroll, K.S. (2015). A universal entropy-driven mechanism for thioredoxin-target recognition. Proc Natl Acad Sci U S A *112*, 7960-7965.

Parmenter, T.J., Kleinschmidt, M., Kinross, K.M., Bond, S.T., Li, J., Kaadige, M.R., Rao, A., Sheppard, K.E., Hugo, W., Pupo, G.M., *et al.* (2014). Response of BRAF-mutant melanoma to BRAF inhibition is mediated by a network of transcriptional regulators of glycolysis. Cancer Discov *4*, 423-433.

Patra, K.C., and Hay, N. (2014). The pentose phosphate pathway and cancer. Trends Biochem Sci *39*, 347-354.

Patwari, P., Chutkow, W.A., Cummings, K., Verstraeten, V.L., Lammerding, J., Schreiter, E.R., and Lee, R.T. (2009). Thioredoxin-independent regulation of metabolism by the alpha-arrestin proteins. J Biol Chem *284*, 24996-25003.

Pavlova, N.N., and Thompson, C.B. (2016). The emerging hallmarks of cancer metabolism. Cell Metab *23*, 27-47.

Peterson, C.W., Stoltzman, C.A., Sighinolfi, M.P., Han, K.S., and Ayer, D.E. (2010). Glucose controls nuclear accumulation, promoter binding, and transcriptional activity of the MondoA-Mlx heterodimer. Mol Cell Biol *30*, 2887-2895.

Petrie, J.L., Al-Oanzi, Z.H., Arden, C., Tudhope, S.J., Mann, J., Kieswich, J., Yaqoob, M.M., Towle, H.C., and Agius, L. (2013). Glucose induces protein targeting to glycogen in hepatocytes by fructose 2,6-bisphosphate-mediated recruitment of MondoA to the promoter. Mol Cell Biol *33*, 725-738.

Pouyssegur, J., Franchi, A., L'Allemain, G., and Paris, S. (1985). Cytoplasmic pH, a key determinant of growth factor-induced DNA synthesis in quiescent fibroblasts. FEBS Lett *190*, 115-119.

Rajagopalan, P.T., Zhang, Z., McCourt, L., Dwyer, M., Benkovic, S.J., and Hammes, G.G. (2002). Interaction of dihydrofolate reductase with methotrexate: ensemble and single-molecule kinetics. Proc Natl Acad Sci U S A *99*, 13481-13486.

Richards, P., Ourabah, S., Montagne, J., Burnol, A.F., Postic, C., and Guilmeau, S. (2017a). MondoA/ChREBP: The usual suspects of transcriptional glucose sensing: Implication in pathophysiology. Metabolism *70*, 133-151.

Richards, P., Rachdi, L., Oshima, M., Marchetti, P., Bugliani, M., Armanet, M., Postic, C., Guilmeau, S., and Scharfmann, R. (2017b). MondoA is an essential glucose responsive transcription factor in human pancreatic beta cells. Diabetes *67*, 461-472.

Sans, C.L., Satterwhite, D.J., Stoltzman, C.A., Breen, K.T., and Ayer, D.E. (2006). MondoA-Mlx heterodimers are candidate sensors of cellular energy status: mitochondrial localization and direct regulation of glycolysis. Mol Cell Biol *26*, 4863-4871.

Sato, S., Jung, H., Nakagawa, T., Pawlosky, R., Takeshima, T., Lee, W.R., Sakiyama, H., Laxman, S., Wynn, R.M., Tu, B.P.*, et al.* (2016). Metabolite regulation of nuclear localization of Carbohydrate-response Element-binding Protein (ChREBP): role of amp as an allosteric inhibitor. J Biol Chem *291*, 10515-10527.

Saxena, G., Chen, J., and Shalev, A. (2010). Intracellular shuttling and mitochondrial function of thioredoxin-interacting protein. J Biol Chem *285*, 3997-4005.

Shalev, A., Pise-Masison, C.A., Radonovich, M., Hoffmann, S.C., Hirshberg, B., Brady, J.N., and Harlan, D.M. (2002). Oligonucleotide microarray analysis of intact human pancreatic islets: identification of glucose-responsive genes and a highly regulated TGFbeta signaling pathway. Endocrinology *143*, 3695-3698.

Shen, L., O'Shea, J.M., Kaadige, M.R., Cunha, S., Wilde, B.R., Cohen, A.L., Welm, A.L., and Ayer, D.E. (2015). Metabolic reprogramming in triple-negative breast cancer through Myc suppression of TXNIP. Proc Natl Acad Sci U S A *112*, 5425-5430.

Shin, D., Jeon, J.H., Jeong, M., Suh, H.W., Kim, S., Kim, H.C., Moon, O.S., Kim, Y.S., Chung, J.W., Yoon, S.R., *et al.* (2008). VDUP1 mediates nuclear export of HIF1alpha via CRM1-dependent pathway. Biochim Biophys Acta *1783*, 838-848.

Sloan, E.J., and Ayer, D.E. (2010). Myc, mondo, and metabolism. Genes Cancer *1*, 587-596.

Stock, C., and Schwab, A. (2009). Protons make tumor cells move like clockwork. Pflugers Arch *458*, 981-992.

Stoltzman, C.A., Kaadige, M.R., Peterson, C.W., and Ayer, D.E. (2011). MondoA senses non-glucose sugars: regulation of thioredoxin-interacting protein (TXNIP) and the hexose transport curb. J Biol Chem *286*, 38027-38034.

Stoltzman, C.A., Peterson, C.W., Breen, K.T., Muoio, D.M., Billin, A.N., and Ayer, D.E. (2008). Glucose sensing by MondoA:Mlx complexes: a role for hexokinases and direct regulation of thioredoxin-interacting protein expression. Proc Natl Acad Sci U S A *105*, 6912-6917.

Sullivan, L.B., Gui, D.Y., Hosios, A.M., Bush, L.N., Freinkman, E., and Vander Heiden, M.G. (2015). Supporting aspartate biosynthesis is an essential function of respiration in proliferating cells. Cell *162*, 552-563.

Takahashi, Y., Nagata, T., Ishii, Y., Ikarashi, M., Ishikawa, K., and Asai, S. (2002). Up-regulation of vitamin D3 up-regulated protein 1 gene in response to 5-fluorouracil in colon carcinoma SW620. Oncol Rep *9*, 75-79.

Trivedi, B., and Danforth, W.H. (1966). Effect of pH on the kinetics of frog muscle phosphofructokinase. J Biol Chem *241*, 4110-4112.

Vander Heiden, M.G., Cantley, L.C., and Thompson, C.B. (2009). Understanding the Warburg effect: the metabolic requirements of cell proliferation. Science *324*, 1029-1033.

Waldhart, A.N., Dykstra, H., Peck, A.S., Boguslawski, E.A., Madaj, Z.B., Wen, J., Veldkamp, K., Hollowell, M., Zheng, B., Cantley, L.C., *et al.* (2017). Phosphorylation of TXNIP by AKT mediates acute influx of glucose in response to insulin. Cell Rep *19*, 2005-2013.

Warburg, O. (1956). On respiratory impairment in cancer cells. Science *124*, 269-270.

Ward, P.S., and Thompson, C.B. (2012). Metabolic reprogramming: a cancer hallmark even warburg did not anticipate. Cancer Cell *21*, 297-308.

Webb, B.A., Chimenti, M., Jacobson, M.P., and Barber, D.L. (2011). Dysregulated pH: a perfect storm for cancer progression. Nat Rev Cancer *11*, 671-677.

Wernicke, C.M., Richter, G.H., Beinvogl, B.C., Plehm, S., Schlitter, A.M., Bandapalli, O.R., Prazeres da Costa, O., Hattenhorst, U.E., Volkmer, I., Staege, M.S., *et al.* (2012).

MondoA is highly overexpressed in acute lymphoblastic leukemia cells and modulates their metabolism, differentiation and survival. Leuk Res *36*, 1185-1192.

Wilde, B.R., and Ayer, D.E. (2015). Interactions between Myc and MondoA transcription factors in metabolism and tumourigenesis. Br J Cancer *113*, 1529-1533.

Wright, J.C., Prigot, A., Wright, B., Weintraub, S., and Wright, L.T. (1951). An evaluation of folic acid antagonists in adults with neoplastic diseases: a study of 93 patients with incurable neoplasms. J Natl Med Assoc *43*, 211-240.

Wu, N., Zheng, B., Shaywitz, A., Dagon, Y., Tower, C., Bellinger, G., Shen, C.H., Wen, J., Asara, J., McGraw, T.E*., et al.* (2013). AMPK-dependent degradation of TXNIP upon energy stress leads to enhanced glucose uptake via GLUT1. Mol Cell *49*, 1167-1175.

Xu, G., Chen, J., Jing, G., and Shalev, A. (2013). Thioredoxin-interacting protein regulates insulin transcription through microRNA-204. Nat Med *19*, 1141-1146.

Yamaguchi, F., Takata, M., Kamitori, K., Nonaka, M., Dong, Y., Sui, L., and Tokuda, M. (2008). Rare sugar D-allose induces specific up-regulation of TXNIP and subsequent G1 cell cycle arrest in hepatocellular carcinoma cells by stabilization of p27kip1. Int J Oncol *32*, 377-385.

Yang, G., and Hurlin, P.J. (2017). MNT and emerging concepts of MNT-MYC antagonism. Genes (Basel) *8*, 1-12.

Yang, M., and Vousden, K.H. (2016). Serine and one-carbon metabolism in cancer. Nat Rev Cancer *16*, 650-662.

Yoshioka, J., and Lee, R.T. (2014). Thioredoxin-interacting protein and myocardial mitochondrial function in ischemia-reperfusion injury. Trends Cardiovasc Med *24*, 75-80.

Yu, F.X., Chai, T.F., He, H., Hagen, T., and Luo, Y. (2010). Thioredoxin-interacting protein (Txnip) gene expression: sensing oxidative phosphorylation status and glycolytic rate. J Biol Chem *285*, 25822-25830.

Zhou, R., Tardivel, A., Thorens, B., Choi, I., and Tschopp, J. (2010). Thioredoxin-interacting protein links oxidative stress to inflammasome activation. Nat Immunol *11*, 136-140.

Zhou, Z.Q., and Hurlin, P.J. (2001). The interplay between Mad and Myc in proliferation and differentiation. Trends Cell Biol *11*, S10-14.

Zois, C.E., and Harris, A.L. (2016). Glycogen metabolism has a key role in the cancer microenvironment and provides new targets for cancer therapy. J Mol Med (Berl) *94*, 137-154.

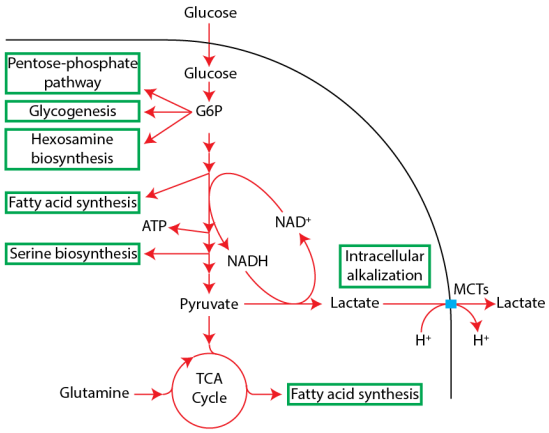

Figure 1.1. Metabolic rewiring in cancer
Glucose uptake is increased in cancer. Glycolytic intermediates are used to fuel biosynthetic pathways including the pentose-phosphate pathway, glycogenesis, fatty acid synthesis and serine biosynthesis. Lactic fermentation enhances glycolytic rate by generating NAD+. TCA cycle intermediates support biosynthetic pathways, in particular fatty acid synthesis. While pyruvate entry into the TCA cycle is decreased, glutamine conversion to α-ketoglutarate supports TCA cycling.

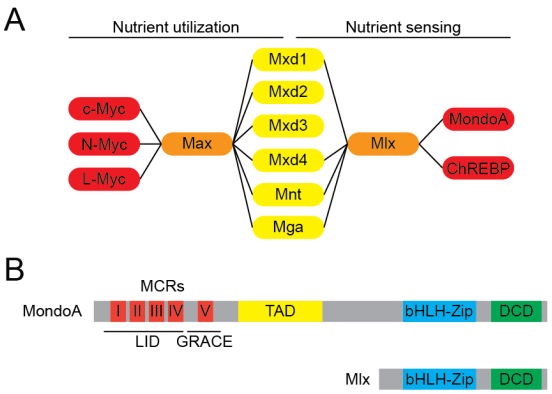

Figure 1.2. The Myc-superfamily of transcription factors
(**A**) The Myc-superfamily of transcription factors are centered on Max and Mlx and regulate nutrient utilization. The transcription factors are physically connected by sharing binding partners. cMyc, N-Myc and L-Myc all interact with Max. Max also interacts with the Mad family of transcriptional repressors, Mnt and Mga. MondoA and MondoB (ChREBP) interact with Mlx. Mlx also interacts with Mxd1, Mxd4, Mnt and Mga. (**B**) Diagrams of MondoA and Mlx. MondoA and Mlx interact through the bHLH-Zip and dimerization and cytoplasmic localization domains (DCD). MondoA has a strong transactivation domain (Cadenas et al., 1957) as well as Mondo-conserved regions (MCR), which control nucleocytoplasmic shuttling. MCRs I-IV make up a low-glucose inhibitory domain (LID) and MCRV is a glucose-responsive activation element (GRACE).

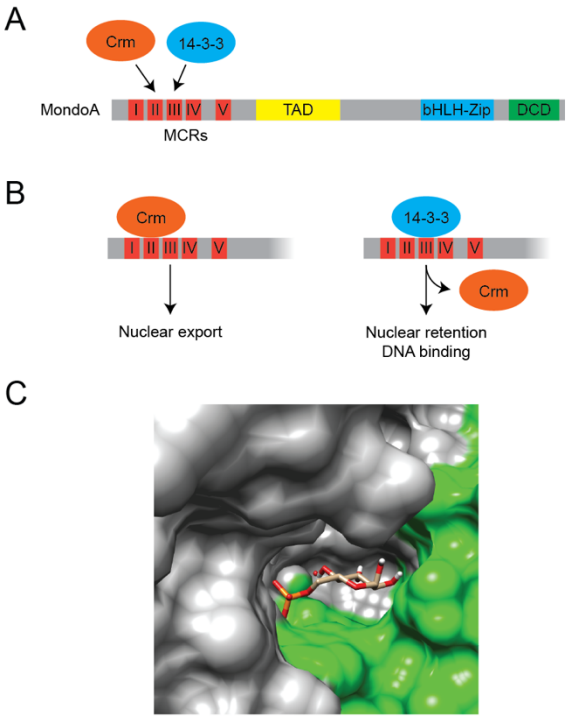

Figure 1.3. MCRs II and III control glucose-responsive nucleocytoplasmic shuttling Schematics showing (**A**) overall MondoA structure and the regions where Crm1 and 14-3-3 bind MondoA, and (**B**) the consequences of Crm1 and 14-3-3 binding. (**C**) Molecular modeling shows that G6P could coordinate the interaction between ChREBP (green) and 14-3-3 (gray).

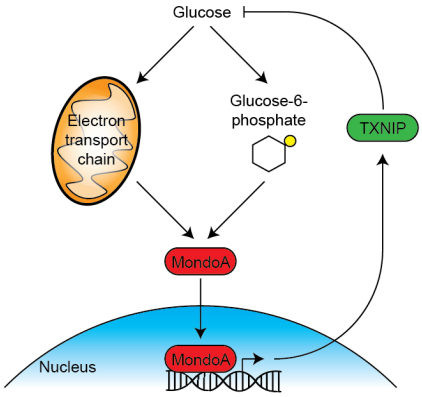

Figure 1.4. The MondoA/TXNIP axis
The first committed step of glycolysis is the conversion of glucose into glucose-6-phosphate, which stimulates MondoA translocation to the nucleus, DNA binding in the promoter of target-genes, and recruitment of cofactors to initiate transcription. The most well-characterized target gene, TXNIP, negatively regulates glucose uptake. Thus MondoA/TXNIP make up a negative-feedback loop that maintains glucose homeostasis in the cell. Notably, the transcriptional activity of MondoA is dependent on the electron transport chain.

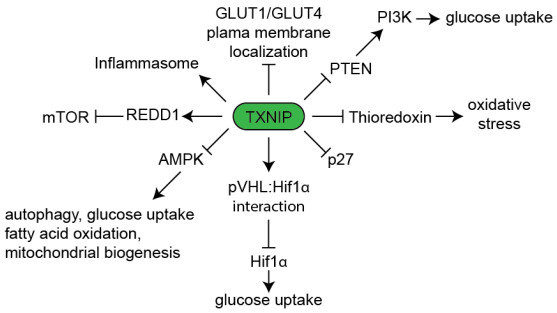

Figure 1.5. TXNIP is a master regulator of catabolic and anabolic metabolism
TXNIP controls bioenergetics, biosynthetic and redox metabolism. It directly opposes GLUT expression on the plasma membrane. As a negative regulator of AMPK, TXNIP prevents lipolysis, glucose uptake, autophagy and mitochondrial biogenesis. It stabilizes the interaction of pVHL and Hif1α, thus driving ubiquitination and degradation of Hif1α. Finally, by inhibiting thioredoxin, TXNIP drives oxidative stress.

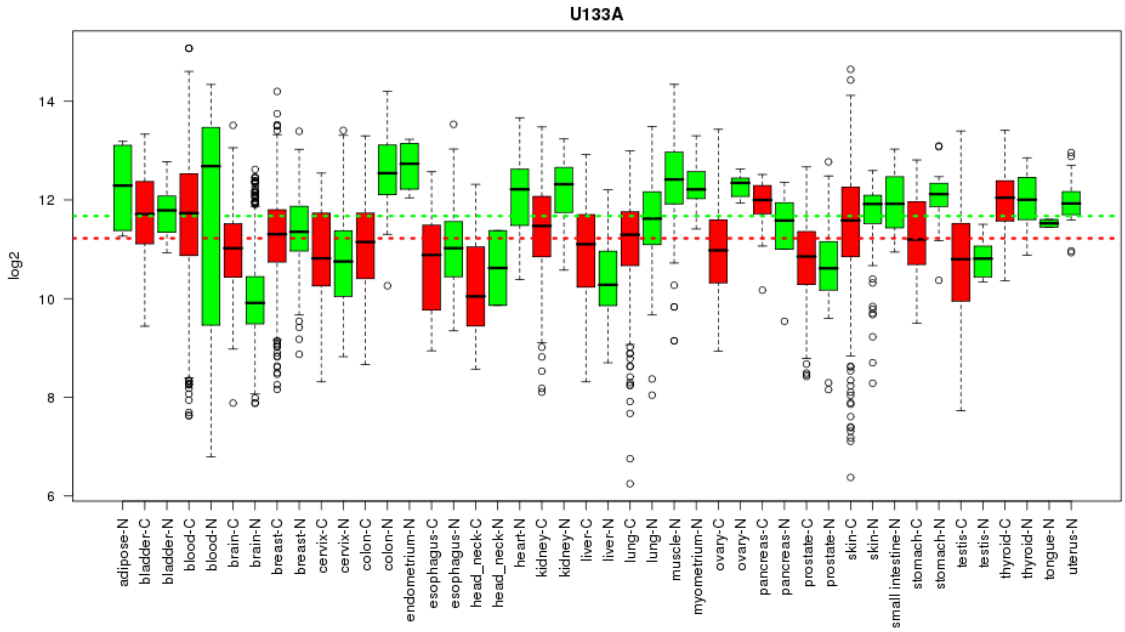

Figure 1.6. Expression of TXNIP in cancer
Relative expression of TXNIP as reported in The Cancer Genome Atlas (TCGA). Affymetrix U133A microarray was used to quantify expression in cancerous (red) and noncancerous tissues (green). Dotted lines indicate average expression level. TXNIP is generally decreased in cancer relative to normal tissues. Of note, the most dramatic difference occurs in colon cancer.

CHAPTER 2

MONDOA SIMULTANEOUSLY SENSES MITOCHONDRIAL ATP AND GLUCOSE

2.1. Abstract

The MondoA transcription factor and its target-gene thioredoxin-interacting protein (TXNIP) constitute a metabolic axis that senses and controls nutrient availability. A predominant feature of the MondoA/TXNIP axis is an adaptive response to metabolic challenges. The molecular mechanisms that dictate how MondoA senses diverse nutrients and stresses are poorly understood. To elucidate these mechanisms, we focused our studies on one particular metabolic stress, acidosis, which triggers the MondoA/TXNIP axis. We found that acidosis drives mitochondrial ATP (mtATP) synthesis. The subsequent export of mtATP from the mitochondrial matrix via adenine-nucleotide transporter and voltage-dependent anion channel, and the enzymatic activity of mitochondria-bound hexokinase results in the production of glucose-6-phosphate (G6P), a potent activator of MondoA transcriptional activity. MondoA localizes to the outer-mitochondrial membrane (OMM), and in response to G6P, shuttles to the nucleus and drives transcription. Thus, the OMM serves as a scaffold for a glucose/mtATP signaling center of which MondoA is a central feature. Our findings establish MondoA as a coincidence detector, monitoring signals from glycolysis and oxidative phosphorylation. Further, we show that MondoA plays a predominant role in the transcriptional response to acidosis, and that loss of MondoA prevents the viability of cells exposed to acidosis.

2.2. Introduction

Glucose is a major source of carbons for the production of ATP and biosynthetic intermediates. Dysregulation of glucose uptake and metabolism underlies many diseases including cancer and diabetes (Hay, 2016; Petersen et al., 2017). The precise molecular

mechanisms that regulate glucose homeostasis in normal and pathological settings are yet to be fully explored.

MondoA is the sentinel regulator of glucose-induced transcription and its activity is highly, if not entirely, dependent on glucose (Billin and Ayer; Richards et al. 2017; Stoltzman et al. 2008). In response to glucose-6-phosphate (G6P), MondoA shuttles from the outer mitochondrial membrane (OMM) to the nucleus where it drives transcriptional circuits that control cellular fuel choice (Billin et al., 2000; Sans et al., 2006; Stoltzman et al., 2008). A functional electron transport chain (ETC) is also absolutely required for MondoA activity, yet the ETC-derived signal remains unknown (Han and Ayer, 2013; Yu et al., 2010). Nevertheless, because MondoA responds to both glycolysis and mitochondrial respiration, MondoA is poised to be a master regulator of central carbon metabolism.

MondoA controls the glucose-dependent expression of thioredoxin-interacting protein (TXNIP), which has a number of critical cellular functions. Among these, the best characterized is as a suppressor of glucose uptake. Thus, MondoA and TXNIP make up a negative feedback loop that maintains cellular glucose homeostasis. High TXNIP is anti-correlated with glucose uptake in human tumors and is a predictor of better overall survival in cancer patients, establishing the MondoA/TXNIP axis as an important prognostic factor in cancer (our unpublished data; Chen et al., 2010; Shen et al., 2015).

Intracellular acidification is a metabolic stress innate to proliferative cells. Cancer cells initiate an adaptive response to intracellular acidification that includes 1) secreting protons to the extracellular space, 2) slowing glycolytic flux and 3) restricting glucose uptake (Gunnink et al., 2014; Webb et al., 2011). While pH-regulation of glycolytic flux

and proton transport have been well studied, it is unknown how intracellular pH regulates glucose uptake. We previously showed that lactic acidosis triggers MondoA-dependent TXNIP expression and decreased glucose uptake. Further, the suppression of glucose uptake following lactic acidosis treatment required both MondoA and TXNIP (Chen et al., 2010). Therefore, the MondoA/TXNIP axis is critical for the cellular response to lactic acidosis.

Here we show here that intracellular acidosis drives MondoA-dependent TXNIP expression, and requires a functional ETC. Mechanistically, acidosis treatment leads to intracellular acidification, hyperpolarizes the mitochondria and leads to increased mitochondrial ATP (mtATP) synthesis. As mtATP is exported from the mitochondria, it is consumed by mitochondria-bound hexokinase to generate G6P, which subsequently activates the MondoA/TXNIP axis. Finally, we observed that MondoA is an essential component of the transcriptional response to acidosis, and that loss of MondoA restricts adaptive metabolism and cell viability.

2.3. Results

2.3.1. Intracellular acidosis drives MondoA-dependent TXNIP expression

Intracellular pH is primarily regulated by the monocarboxylate transporters (MCTs) and sodium-hydrogen antiporter 1 (NHE1; (Webb et al., 2011). MCTs are a family of plasma membrane transporters that facilitate the cotransport of protons and monocarboxylates to the extracellular space. NHE1 controls pH by the electroneutral exchange of protons and sodium ions to the extracellular and intracellular space, respectively. We used publicly available gene expression data to compare the expression

levels of TXNIP and genes that control intracellular pH. TXNIP expression inversely correlates with MCT4 in breast cancer, MCT1 in lung cancer and NHE1 in brain cancer (Figure 2.1A). TXNIP expression is also anticorrelated with MCTs and NHE1 in nontransformed tissues (Figures 2.2A and 2.2B). Further, we identified a correlation between TXNIP expression and an acidosis-driven gene-signature in breast cancer (Figure 2.1B).

To better understand how intracellular acidification effects TXNIP expression, we treated cells with Hank's balanced salt solution (HBSS), which mimics the nutrient-poor extracellular environment cancer cells are exposed to *in vivo*. HBSS has minimal pH-buffering capacity and in 5% CO_2 has a pH of ~ 6.4. Consistent with our previous findings, HBSS treatment leads to increased TXNIP mRNA and protein expression, and also decreases glucose uptake (Figures 2.3A-B and 2.4A; (Chen et al., 2010). HBSS is weakly buffered due to its low levels of sodium bicarbonate. We therefore supplemented HBSS with sodium bicarbonate to the same level as in DMEM, which raised the pH to 7.5: this prevented TXNIP induction (Figures 2.3C and 2.4B). To determine whether TXNIP induction is mediated by sodium bicarbonate or pH, we clamped the pH to 7.4 by adding 25mM HEPES and adjusting the pH with NaOH. This prevented TXNIP induction in response to low levels of sodium bicarbonate (Figure 2.3D), confirming that low pH is primarily responsible for HBSS-driven MondoA activity. We extended this finding to other cell types and media. We observed that low pH DMEM (pH 6.5, hereafter referred to as acidosis) induced TXNIP expression in HEK293T, HepG2 and HeLa cells (Figure 2.4C).

Given our findings that MondoA is both necessary and sufficient for TXNIP

expression, we sought to determine the requirement for MondoA in HBSS-driven TXNIP. We treated MondoA$^{-/-}$ mouse embryonic fibroblasts (MEFs) with HBSS. TXNIP was not induced in response to HBSS in MondoA$^{-/-}$ MEFs, yet their reconstitution with wild type MondoA rescued TXNIP induction (Figure 2.3E). MondoA requires binding with Mlx for its nuclear translocation and DNA binding, and a single point mutation, I766P in MondoA, prevents their interaction (Peterson et al., 2010; Stoltzman et al., 2011). In MondoA$^{-/-}$ MEFs expressing MondoA(I766P), TXNIP was not induced in response to HBSS (Figure 2.3E), indicating that HBSS-driven TXNIP is dependent on the MondoA:Mlx heterocomplex.

Since the induction of TXNIP is entirely dependent on MondoA, we hypothesized that HBSS drives MondoA transcriptional activity. MondoA binds to the TXNIP promoter at a carbohydrate response element (ChoRE), about 80 bp upstream of the transcription start site (Minn et al., 2005; Stoltzman et al., 2008). We performed a luciferase-reporter assay in which luciferase expression was driven from the TXNIP promoter or the TXNIP promoter with a mutation in the ChoRE (ChoRE $_{mut}$). HBSS drove luciferase expression from the wild type promoter, yet we observed no induction of luciferase from the ChoRE$_{mut}$ promoter (Figure 2.5A). Consistent with this finding, we also observed that HBSS treatment led to increased MondoA occupancy of the TXNIP promoter (Figure 2.5B). Together these data show that HBSS drives MondoA transcriptional activity.

Previous reports show that treating cells with low pH media for short periods of time drives intracellular acidification (Adams et al., 2006; Wahl et al., 2000). pH has significant impacts on chemical reactions and macromolecular functions; thus, it is not

surprising that organelles greatly vary in their steady-state pH and compartmentalization of protons is essential for organelle function (Casey et al., 2010). Therefore, we used compartment-selective ionophores to alter proton concentrations in various cellular compartments. The monovalent ionophore monensin, which mediates the electroneutral exchange of an extracellular Na^+ ion for an intracellular proton leading to cytosolic alkalization, abrogated HBSS-induced TXNIP expression (Figure 2.6A). By contrast, the dibasic ionophore chloroquine that disrupts acidification of endosomes/lysosomes had no effect on TXNIP induction (Figure 2.6A). Finally, the mitochondrial ionophore FCCP, which uncouples electron transport and ATP generation by the F_0F_1-ATPase (ATP synthase), prevented HBSS-driven TXNIP expression (Figure 2.6B). Together these results suggest that mitochondrial proton usage, but not pH-dependent changes in the endosome/lysosome, is critical for the activation of the MondoA/TXNIP axis.

2.3.2. MondoA is dependent upon mitochondrial ATP

We next sought to evaluate the impact of the ETC on the MondoA/TXNIP axis using a genetic approach. To accomplish this, we used ρ^0 cells that lack mtDNA and are respiration deficient. TXNIP was induced in 143B osteosarcoma cells treated with acidosis (Figure 2.7A); however, acidosis driven TXNIP expression was blunted in 143Bρ^0 cells (Figure 2.7B). Repopulating 143Bρ^0 cells with wild type mitochondria rescued TXNIP induction (Figure 2.7C). These results illustrate MondoA's dependence on a functional ETC.

ETC complexes I-IV cooperatively build a proton gradient by pumping protons from the mitochondrial matrix to the inner membrane space. ATP synthase harnesses the

resultant proton motive force to phosphorylate ADP. We therefore hypothesized that acidosis leads to intracellular acidification, hyperpolarization of the inner-mitochondrial membrane and ATP production. We measured intracellular pH using the pH-sensitive dye BCECF-AM. We observed that acidosis treatment shifted intracellular pH from 7.2 to 6.5 (Figure 2.7D). This was accompanied by an increase in mitochondrial membrane potential as measured by JC1 (Figure 2.7E). Further, acidosis drove an increase in total cellular ATP levels (Figure 2.7F). Collectively these data suggest that acidosis drives ATP synthesis, which may support MondoA transcriptional activity.

A number of recent publications have demonstrated that measuring metabolic changes from whole cells may be vastly different from what is observed at specific organelles (Abu-Remaileh et al., 2017; Chen et al., 2016). We therefore sought to determine how acidosis affects mitochondrial ATP (mtATP). To accomplish this, we used a mitochondrial-targeted fluorescence resonance energy transfer (FRET) ATP biosensor (Mit-ATEAM). This biosensor consists of cp173-Venus fused to mseCFP via an ATP-binding linker region (Imamura et al., 2009). As a control, we used constructs with mutations in the ATP binding domain that prevent ATP binding and FRET signaling (Figure 2.10A-2.10F). HeLa cells treated with acidosis showed increased FRET signal over time, indicating that acidosis drives an increase in mtATP (Figures 2.9A and 2.10C).

We next determined whether mtATP synthesis is required to trigger the MondoA/TXNIP axis. The ATP synthase inhibitor oligomycin completely blocked TXNIP induction in response to acidosis or HBSS (Figures 2.6A and 2.6B). We next used 143Bρ^0:ΔATP6/ΔATP8 cybrid cells, which have a single point mutation in mtDNA that causes ATP8 truncation and disruption of the ATP6 start codon (Boominathan et al.,

2016; Jonckheere et al., 2008). These cells lack expression of both ATP6 and ATP8 and thus lack a functional ATP synthase. Acidosis-driven TXNIP expression was blunted in these cells (Figure 2.9C), but ATP synthase and TXNIP induction is partially rescued by nuclear-encoded versions of ATP6 and ATP8 that are targeted to the mitochondria (Boominathan et al., 2016) (Figure 2.9C). Similarly, knock down of nuclear-encoded ATP5I, an essential component of the ATP synthase (Figure 2.9B), prevented TXNIP induction in response to acidosis (Figure 2.9D). Importantly, ATP5I knock down decreased the steady state level and the acidosis-driven increase in mtATP (Figures 2.9E and 2.11A). These data show that acidosis drives mtATP production through the ATP synthase and that mATP synthesis correlates with TXNIP induction.

2.3.3. MondoA senses G6P produced by mitochondrial-hexokinase

Mitochondria-bound hexokinase has preferential access to mtATP that is exported from the mitochondria (Wilson, 2003). Thus, enhanced mtATP synthesis and export from the mitochondria leads to increased production of G6P, which is a potent activator of MondoA transcriptional activity. We speculated that an increase in mtATP synthesis would drive G6P production and trigger the MondoA/TXNIP axis. We used GC/MS to determine how acidosis treatment affects central carbon metabolism. While there was a general decrease in glycolytic intermediates, we observed a significant increase in steady state G6P levels (Figure 2.12A).

MondoA, Mlx and HK2 are all residents of the outer mitochondrial membrane (Figure 2.12C; Sans et al., 2006). We speculated that increase in mtATP production and export would lead to increased utilization by mitochondrial-bound HK2 to generate G6P,

which could then activate mitochondria-localized MondoA (Figure 2.12B). To test this model, we blocked export of mtATP. In HeLa cells, the most highly expressed mitochondrial transporter of ATP is ANT2 (SLC25A5). Using siRNA, we blunted expression of ANT2. This prevented TXNIP induction (Figure 2.12D), suggesting that export of mtATP from the mitochondria is critical for acidosis-driven MondoA activity. siRNA pools against HK2 also blocked TXNIP induction (Figure 2.12E). Overexpression of HK2(D657A), which lacks kinase activity, also blocked TXNIP induction (Figure 2.12F).

Hexokinase localizes to the outer-mitochondrial membrane via interactions the voltage-dependent anion channel (VDAC; (Wilson, 2003). The N-terminal 25 amino acids of hexokinase and Glu72 of VDAC1 are necessary for hexokinase/VDAC interaction. Mutating VDAC-E72 prevents the VDAC/hexokinase interaction and disrupts the mitochondrial localization of hexokinase (Abu-Hamad et al., 2008; Zaid et al., 2005). To address the requirement of mitochondrial-localization of hexokinase for induction of the MondoA/TXNIP axis, we overexpressed a mutant version of the mouse orthologue of VDAC1, mVDAC1(E72Q), which has a dominant negative effect on hexokinase localization to the mitochondria. As expected, we observed a decrease in mitochondrial-localization of HK2, and complete loss of acidosis-driven TXNIP (Figure 2.12G).

We next sought to rescue the effect of mVDAC1(E72Q). To accomplish this goal, we artificially tethered HK2 to the mitochondria in a manner completely independent of the N-terminal 25 amino acids of HK2, which is its known mitochondrial tether, and Glu72 of VDAC. We tagged mVDAC1 with the first 10 β-strands of GFP (mVDAC1-

GFP(1-10)) and tagged HK2 with the last β-strand of GFP (HK2-GFP(11)). When coexpressed, the β-strands of GFP self-assemble, linking mVDAC1 and HK2 (Figure 2.12H). Notably, neither mVDAC1-GFP(1-10) nor HK2-GFP(11) alone fluoresce, but when assembled, fluorescence is observed in a mitochondrial pattern (Figure 2.13A). Mirroring the results with mVDAC1(E72Q) from above, overexpression of mVDAC1(E72Q)-GFP(1-10) alone decreases the amount of HK2 on the mitochondria and prevents TXNIP induction (Figures 2.12H and 2.12I). However, coexpression of mVDAC1(E72Q)-GFP(1-10) and HK2-GFP(11) rescues HK2 mitochondrial localization and TXNIP induction (Figures 2.12H and 2.12I). Together these data show that mitochondrial-localized HK2 is both necessary and sufficient for acidosis-driven MondoA activity.

2.3.4. MondoA is a predominant feature of an adaptive response to acidosis

We next determined the impact of acidosis on MondoA-dependent transcription. Using CRISPR/Cas9 genome editing, we knocked out MondoA in HeLa cells (HeLa:MondoA-KO cells). This was done by expressing CRISPR/Cas9, three sgRNAs and a homology-directed repair (HDR) construct containing a puromycin-resistance cassette. HDR incorporation into the MondoA locus conferred puromycin resistance. We confirmed the loss of MondoA expression by immunoblot analysis (Figure 2.14A). We next conducted mRNA-sequencing on parental and HeLa:MondoA-KO cells treated with normal media or acidosis. We determined the genes that are differentially regulated by acidosis each cell type. Using a $\log_2$(fold change) greater than one, parental cells had 169 differentially regulated genes, about 50% of which were not differentially regulated in

HeLa:MondoA-KO cells (Figure 2.14B), indicating that MondoA is an essential feature of the adaptive response to acidosis. Using overrepresentation analysis, we determined that acidosis drives an adaptive immune response and cholesterol biosynthesis, of which cholesterol biosynthesis is specific to MondoA (Figure 2.14C). Finally, loss of MondoA decreased the viability of HeLa cells treated with acidosis (Figure 2.14D). Together these data indicate that MondoA is a necessary component of an adaptive response to acidosis.

2.4. Discussion

In describing key features of metabolic rewiring in cancer, Otto Warburg noted that increased sodium bicarbonate and increased pH favor glycolysis (Koppenol et al., 2011; Warburg, 1925). Intracellular alkalization is now a widely accepted hallmark of cancer metabolism (Webb et al., 2011), and has pleiotropic effects on tumorigenesis, the most predominant being a transition from oxidative metabolism to aerobic glycolysis (Reshkin et al., 2000). A central feature of this conversion to aerobic glycolysis is an increase in glucose uptake (Xie et al., 2014). Consistent with this observation, the MondoA/TXNIP axis is suppressed under alkaline conditions. By contrast, the MondoA/TXNIP axis is activated by acidosis. Thus, we propose that the MondoA/TXNIP axis plays a critical role in how cells sense and respond to dysregulated glycolytic metabolism and pH.

Changes in cytosolic pH influence multiple aspects of mitochondrial function (Matsuyama and Reed, 2000; Wu et al., 2017). During intracellular acidification protons can contribute to the proton gradient at the mitochondria (Wu et al., 2017). Additionally, chronic acidosis increases mitochondrial-membrane potential and enhances oxidative

phosphorylation (Khacho et al. 2014). These findings are consistent with our data showing that acidosis treatment causes intracellular acidification, hyperpolarization of the inner-mitochondrial membrane and ATP production.

We previously showed that MondoA senses G6P and the ETC; however, the specific ETC derived signal was unknown. Multiple hypotheses have been put forward to explain the dependence of MondoA on ETC, the predominant being that ETC inhibitors cause increased glycolytic flux and decreased steady state G6P levels, thus restricting G6P-stimulated MondoA. Inhibiting the glycolytic enzyme GAPDH rescued TXNIP from blockade in ETC activity. Yet coadministration of ETC inhibitors and 2-deoxyglucose, a glycolytic inhibitor, does not rescue MondoA activity, suggesting that the mechanism involves more than only glycolytic flux (Yu et al., 2010). By dissecting acidosis-induction of MondoA transcriptional activity, we discovered that MondoA senses mitochondrial ATP (mtATP). Further, we show that as mtATP is exported from the mitochondria, it becomes a substrate in the production of G6P by mitochondria-bound hexokinase. Our findings establish MondoA as a coincidence detector, which simultaneously senses mtATP and glucose through the generation of G6P. Conceptually, by detecting mitochondrial ATP and cytosolic glucose metabolism, MondoA is poised to be a master regulator of central carbon metabolism. The mechanistic details of how MondoA senses G6P and the impact on cell metabolism remains to be clarified.

MondoA, Mlx and hexokinase all localize to the outer-mitochondrial membrane where they make up a nutrient sensing center. Mitochondria-bound hexokinase preferentially uses mtATP, thereby coupling G6P production to mtATP availability. By binding to the mitochondria, hexokinase has increased specific activity and decreased

feedback inhibition by G6P (Robey and Hay, 2006). By localizing to the mitochondria and sensing G6P derived from mitochondria-bound hexokinase, we propose that MondoA couples its activity to mitochondrial metabolism and oxidative phosphorylation. Our results show that mtATP pools instead of cytosolic pools of ATP control MondoA transcriptional activity, illustrating that not all pools of ATP are equal. It further illustrates that site-specific ATP synthesis is an important determinant in controlling nutrient homeostasis.

TXNIP expression is downregulated by progrowth signals such as mTOR, PI3K, Ras and Myc (Elgort et al., 2010; Kaadige et al., 2015; Shen et al., 2015). We previously showed that TXNIP repression is essential for enhanced glucose uptake and a shift away from mitochondrial metabolism toward aerobic glycolysis. The resultant decrease in mtATP synthesis further restricts MondoA transcriptional activity and TXNIP expression. This feed-forward restriction of TXNIP enforces high glucose availability to support the metabolic demands of growing cells. We propose that reactivating the MondoA/TXNIP axis would restrict aerobic glycolysis and cell proliferation. One potential approach would be to drive intracellular acidification by inhibiting NHE1 with amiloride, which has antiglycolytic and anticancer properties (Reshkin et al., 2000; Xue et al., 2010).

We show that the MondoA/TXNIP axis is a predominant feature of an adaptive response to intracellular acidification. In particular MondoA is essential for acidosis-driven expression of cholesterol biosynthesis genes. This finding is consistent with other data showing that MondoA drives expression of genes involved in cholesterol biosynthesis (Carroll et al., 2015). The full impact of MondoA/TXNIP axis on cholesterol

biosynthesis remains to be explored. During tumor development, there are multiple times in which cells experience pH-related metabolic stress. Additional studies will be important in determining the impact of the MondoA/TXNIP axis on an adaptive response to intracellular acidification *in vivo* and the impact on tumorigenesis.

2.5. Experimental methods

2.5.1. Experimental model and subject details

A list of cell lines used is provided in the Key Resources Table. All cells were maintained in DMEM +10% FBS (Gibco), 100 units/mL penicillin (Gibco) and 100 units/mL streptomycin (Gibco). MDA-MB-231 were additionally cultured with non-essential amino acids. 143Bρ^0 and cybrids were cultured with 1 mM sodium pyruvate and 50 μg/mL uridine. Cells were passaged and treated in an incubator set at 37 °C and 5% CO_2.

2.5.2. Treatments

HBSS was supplemented with glucose to 20 mM prior to treatment. Acidosis treatment media was prepared from DMEM powder without glutamine, glucose, pyruvate, sodium bicarbonate and phenol red. The following were added: glutamine to 2 mM, glucose to 20 mM, pyruvate 1 mM, sodium bicarbonate to 0.35 g/L and phenol red to 16 mg/L. For live cell imaging, phenol red was omitted.

2.5.3. Plasmid construction

Plasmids were created using either standard restriction digest and ligation or Gibson assembly (NEB). A list of plasmids used, the vector backbone and their source is provided in the Key Resources Table.

2.5.4. Quantitative PCR

Total RNA was extracted from cells using a Quick RNA Miniprep Kit (Zymo Research) according to manufacturer's recommendations. cDNA was synthesized from 200 ng mRNA using the GoScript Reverse Transcription System (Promega) with oligo-dT primers. A 100-fold dilution was used in a PCR reaction containing SYBR Green and analyzed on a CFX Connect Real Time System. Values were determined by a standard curve. For each sample, three technical replicates were performed and averages determined.

2.5.5. Immunoblotting

Equal concentrations of denatured protein lysates were resolved on 10% SDS-PAGE gel with a stacking gel. Proteins were electrotransferred to PDVF membrane (Genesee Scientific). Membranes were incubated in 5% (weight/volume) blotting-grade nonfat dry milk (Bio-Rad) in TBST (Tris-buffered saline, pH 7.4 and 0.1% Tween-20) for 30 minutes at room temperature with gentle rocking. Membranes were then transferred to antibody-dilution buffer (20 mM Tris, pH 8.0; 200 mM NaCl; 0.25% Tween-20; 2% bovine serum albumin; 0.1% sodium azide) and incubated for one hour at room temperature or overnight at 4 °C with gentle rocking. Membranes were washed

with TBST and vigorous rocking at room temperature. Membranes were then incubated in secondary antibody diluted in 5% (weight/volume) blotting-grade nonfat dry milk (Bio-Rad) in TBST for one hour at room temperature with gentle rocking. Membranes were then washed again and proteins were detected with chemiluminescence using standard or high sensitivity ECL (Genesee Scientific or Thermo Fisher, respectively). Antibodies were used at the following dilutions: Anti-GFP 1:1000; Anti-HK2 1:1,000; Anti-Mlx 1:1,000; Anti-MondoA 1:2,000; Anti-SDHA 1:15,000; Anti-Tubulin 1:50,000; Anti-TXNIP 1:2,000; Anti-goat HRP 1:20,000; Anti-mouse HRP 1:5,000 and Anti-rabbit HRP 1:15,000.

2.5.6. ATP quantification

After treatment, cells were washed once with cold PBS. Cells were scraped into boiling TE buffer (1 mL per 3.5 cm dish), which was collected into 1.5 mL centrifuge tube. Cells were then boiled at 100°C for five minutes. Tubes were then spun at 20,000xg for five minutes. 10 μL of supernatant was used for analysis. ATP determination kit (Thermo Fisher) was used to detect ATP. A standard curve was generated using purified ATP.

2.5.7. Glucose uptake

Cells were incubated with deoxy-D-glucose-2[1,2-3H(N)] (American Radiolabeled Chemicals, Inc.) in KRH buffer (NaCl,116 mM; KCl, 4 mM; $MgCl_2$, 1 mM; $CaCl_2$, 1.8 mM; 2-deoxy-D-glucose, 20 mM; HEPES pH 7.4, 10 mM) for 10 minutes. Cells were then washed, harvested and analyzed for radioactivity using a

scintillation counter. A standard was used to determine the exact molar content in each sample. deoxy-D-glucose-2[1,2-3H(N)] was normalized to protein content as determined by a Bradford Protein Assay (Bio-Rad).

2.5.8. Cell viability/proliferation

Cells were seeded in 6-well dishes (1000 cells/well). When cells were harvested, media was aspirated and 1 mL of crystal violet staining solution was added to wells (0.05% crystal violet, 1% formaldehyde and 1% methanol in PBS). Plates were rocked gently at room temperature for one hour. Staining solution was then aspirated and water was used to wash wells several times until washes came out clear. Plates were then dried overnight.

To quantify crystal violet retention, 1 mL of 1% SDS in H_2O was added to each well. Plates were rocked gently at room temperature for one hour. Supernatant from each well was analyzed by absorbance spectroscopy at 590 nm. Values were only considered if absorbance was ≤ 0.90. If absorbance was higher, samples were diluted in 1% SDS in H_2O.

2.5.9. Mitochondrial membrane potential

Cells were plated on 8-well Nunc™ Lab-Tek™ II Chambered Coverglass (Thermo Fisher). Forty-five minutes prior to experiment, cells were preloaded with JC1 (1 μg/mL). Cells were treated acidosis media lacking phenol red or DMEM lacking phenol red. A Nikon A1 confocal and NIS Elements AR were used to capture images over the course of four hours. For each time point images were captured by exciting with

488 nm and reading emission at 530 nm (green) and 595 nm (red). The ratio of red to green is used to quantify changes in membrane potential. JC1 signal was dramatically reduced one hour after treatment; therefore, the one-hour time point was used to report mitochondrial membrane potential.

2.5.10. Intracellular pH

Cells were plated on 3.5 mm glass bottom culture dishes (MatTek Corporation). The next day cells were treated with normal or low pH DMEM for four hours. Cells were treated with BCECF-AM (1 μM) 30 minutes prior to the end of the experiment. A standard curve was generated by treating cells with Nigericin (5 μM) and media of varying pHs for 30 minutes prior to BCECF-AM treatment. A Nikon A1 confocal and NIS Elements AR were used to capture images by exciting with 488 nm and reading emission at 530 nm and 595 nm. The 595/530 nm fluorescence emission ratio was used to generate a calibration curve and determine intracellular pH for acidosis-treated cells.

2.5.11. Mitochondria purification

Mitochondria were purified from ~20×10^6 cells using a Mitochondria Isolation Kit for Cultured Cells (Thermo Fisher). Cells were processed using the dounce homogenation method. Following purification, mitochondria were resuspended in 100 μl radioimmunoprecipitation buffer. 100 μl of both mitochondria and cytosolic fractions were sonicated at using a Bioruptor sonication device. Sonication was performed 4°C using 30 second on/off pulses at the high setting. Following sonication, lysates were centrifuged and supernatants were collected and analyzed for protein content using a

Bradford Protein Assay (Bio-Rad). 1-5 μg of sample were used for immunoblot analysis.

2.5.12. Luciferase assay

Cells were seeded and the next day transfected with constructs containing TXNIP promoter (or a mutant)-driven luciferase and CMV-driven beta-galactosidase. Cells were harvested in 1X Buffer RLB (Promega). Luciferase was detected using the Luciferase Detection System (Promega), and beta-galactosidase was detected using Galacto-Light™ Reaction Buffer Diluent with Galacto-Plus™ Substrate (Thermo Fisher). Luminescence was determined using a GloMax 96 Microplate Luminometer (Promega). Luciferase values were normalized to beta-galactosidase.

2.5.13. GC-MS

Following treatment, cells were collected into a 1.5 mL microcentrifuge tube then snap frozen using liquid nitrogen. Cells were kept at -80°C until metabolite extraction was performed. 450 μL of cold 90% methanol and internal standards were added to cells and incubated at -20°C for one hour. Tubes were then centrifuged at -20,000×g for five minutes at 4°C. Supernatants were dried using a speed-vac.

Samples were converted into volatile derivatives amenable to GC-MS. Briefly, dried samples were resuspended in O-methoxylamine hydrochloride (40 mg/mL) then mixed with 40 μL N-methyl-N-trimethylsilyltrifluoracetamide and mixed at 37°C. After incubation, 3 μL fatty acid methyl ester standard solution was added. One μL of this final solution was injected into gas chromatograph with an inlet temperature of 250°C. A 10:1 split ratio was used. Three temperatures were ramped with a final temperature of

350°C and a final three-minute incubation. A 30 m Phenomex ZB5-5 MSi column was used. Helium was used as carrier gas at 1 mL/minute. Samples were analyzed again with a 10-fold dilution.

Data was collected using MassLynx 4.1 software (Evan et al., 1992). Metabolites were identified and peak area was determined using QuanLynx. Data was normalized using Metaboanalyst 3.6 (http://www.metaboanalyst.ca/). Quantile normalization, log transformation and Pareto scaling were used. Normal distribution of values was used to determine fold changes.

2.5.14. RNA-sequencing library construction and analysis

Total RNA was extracted from cells using a Quick RNA Miniprep Kit (Zymo Research) according to manufacturer's recommendations. mRNA was isolated and library production performed using a Stranded mRNA-Seq Kit with mRNA Capture Beads (Kapa). Library quality was analyzed using an Agilent High Sensitivity D1000 ScreenTape. Single-end sequencing for 50 cycles was performed using an Illumina HiSeq. The resulting FASTQ files were aligned to the human genome (hg19) using Novoalign. DESeq2 was used to quantify transcript abundance and differential expression.

Overrepresentation analysis was performed using ConsensusPathDB. Pathway-based sets were analyzed from Wikipathways. A p-value cutoff of 0.01 and a minimum overlap of 2 genes was used. Enriched pathways were verified by comparing fold-changes obtained from DESeq2.

2.5.15. Live cell imaging: Widefield microscopy

Widefield microscopy was used for Figures 2.9 and 2.11. Cells were plated on 3.5 mm glass bottom culture dishes (MatTek Corporation). The following day 100 ng DNA was transfected using Lipofectamine 3000 (Thermo Fisher) according to manufacturer's recommendations. The next day cells were treated acidosis media lacking phenol red. A Nikon [scope info] with a 40X lens and [camera] was used to capture images over the course of eight hours. For each time point we took images using / (YFP), / (CFP), and / (FRET) excitement/emission.

Images were analyzed using ImageJ. We used the YFP channel to identify and isolate mitochondrial regions for each image. We isolated these same regions from the CFP and FRET channel. Total intensity was determined for each image. FRET/CFP ratios were determined and normalized to the two-hour time point. RatioPlus was used to make pseudo-colored images.

2.5.16. Live cell imaging: Confocal microscopy

Confocal microscopy was used for Figure 2.10. Cells were plated on 8-well Nunc™ Lab-Tek™ II Chambered Coverglass (Thermo Fisher). The following day 200 ng DNA was transfected using Lipofectamine 3000 (Thermo Fisher) according to manufacturer's recommendations. The next day cells were treated acidosis media lacking phenol red or DMEM lacking phenol red with CCCP. A Nikon [scope info] with a 20X lens and [camera] was used to capture images over the course of eight hours. For each time point we took images using / (YFP), / (CFP), and / (FRET) excitement/emission. Images were analyzed using ImageJ. RatioPlus was used to make pseudo-colored images.

Total intensity was determined.

2.5.17. Gene signature

mRNA expression z-scores were obtained for 2509 breast cancer tumors (Pereira et al., 2016). Acidosis regulated genes were determined from the gene set GO_RESPONSE_TO_ACIDIC_PH in the Molecular Signature Database. Principal component analysis was conducted for all tumors using the expression levels of acidosis regulated genes. Gene signature scores were determined as the first principle component. This was compared to TXNIP expression for the same tumors.

2.5.18. Quantification and statistical analysis

Data is presented as mean ± standard deviation. One-way ANOVA was used to account for variation and significance was determined using a two-tailed Student's t-test.

2.6. References

Abu-Hamad, S., Zaid, H., Israelson, A., Nahon, E., and Shoshan-Barmatz, V. (2008). Hexokinase-I protection against apoptotic cell death is mediated via interaction with the voltage-dependent anion channel-1: mapping the site of binding. J Biol Chem *283*, 13482-13490.

Abu-Remaileh, M., Wyant, G.A., Kim, C., Laqtom, N.N., Abbasi, M., Chan, S.H., Freinkman, E., and Sabatini, D.M. (2017). Lysosomal metabolomics reveals V-ATPase- and mTOR-dependent regulation of amino acid efflux from lysosomes. Science *358*, 807-813.

Adams, D.J., Wahl, M.L., Flowers, J.L., Sen, B., Colvin, M., Dewhirst, M.W., Manikumar, G., and Wani, M.C. (2006). Camptothecin analogs with enhanced activity against human breast cancer cells. II. Impact of the tumor pH gradient. Cancer Chemother Pharmacol *57*, 145-154.

Billin, A.N., and Ayer, D.E. (2006). The Mlx network: evidence for a parallel Max-like transcriptional network that regulates energy metabolism. Curr Top Microbiol Immunol *302*, 255-278.

Billin, A.N., Eilers, A.L., Coulter, K.L., Logan, J.S., and Ayer, D.E. (2000). MondoA, a novel basic helix-loop-helix-leucine zipper transcriptional activator that constitutes a positive branch of a max-like network. Mol Cell Biol *20*, 8845-8854.

Boominathan, A., Vanhoozer, S., Basisty, N., Powers, K., Crampton, A.L., Wang, X., Friedricks, N., Schilling, B., Brand, M.D., and O'Connor, M.S. (2016). Stable nuclear expression of ATP8 and ATP6 genes rescues a mtDNA Complex V null mutant. Nucleic Acids Res *44*, 9342-9357.

Cadenas, C., Franckenstein, D., Schmidt, M., Gehrmann, M., Hermes, M., Geppert, B., Schormann, W., Maccoux, L.J., Schug, M., Schumann, A.*, et al.* (2010). Role of thioredoxin reductase 1 and thioredoxin interacting protein in prognosis of breast cancer. Breast Cancer Res *12*, R44.

Carroll, P.A., Diolaiti, D., McFerrin, L., Gu, H., Djukovic, D., Du, J., Cheng, P.F., Anderson, S., Ulrich, M., Hurley, J.B.*, et al.* (2015). Deregulated Myc requires MondoA/Mlx for metabolic reprogramming and tumorigenesis. Cancer Cell *27*, 271-285.

Casey, J.R., Grinstein, S., and Orlowski, J. (2010). Sensors and regulators of intracellular pH. Nat Rev Mol Cell Biol *11*, 50-61.

Chen, J.L., Merl, D., Peterson, C.W., Wu, J., Liu, P.Y., Yin, H., Muoio, D.M., Ayer, D.E., West, M., and Chi, J.T. (2010). Lactic acidosis triggers starvation response with paradoxical induction of TXNIP through MondoA. PLoS Genet *6*, e1001093.

Chen, W.W., Freinkman, E., Wang, T., Birsoy, K., and Sabatini, D.M. (2016). Absolute quantification of matrix metabolites reveals the dynamics of mitochondrial metabolism. Cell *166*, 1324-1337 e1311.

Elgort, M.G., O'Shea, J.M., Jiang, Y., and Ayer, D.E. (2010). Transcriptional and translational downregulation of thioredoxin interacting protein is required for metabolic reprogramming during G(1). Genes Cancer *1*, 893-907.

Evan, G.I., Wyllie, A.H., Gilbert, C.S., Littlewood, T.D., Land, H., Brooks, M., Waters, C.M., Penn, L.Z., and Hancock, D.C. (1992). Induction of apoptosis in fibroblasts by c-myc protein. Cell *69*, 119-128.

Gunnink, S.M., Kerk, S.A., Kuiper, B.D., Alabi, O.D., Kuipers, D.P., Praamsma, R.C., Wrobel, K.E., and Louters, L.L. (2014). Alkaline pH activates the transport activity of GLUT1 in L929 fibroblast cells. Biochimie *99*, 189-194.

Han, K.S., and Ayer, D.E. (2013). MondoA senses adenine nucleotides: transcriptional induction of thioredoxin-interacting protein. Biochem J *453*, 209-218.

Hay, N. (2016). Reprogramming glucose metabolism in cancer: can it be exploited for cancer therapy? Nat Rev Cancer *16*, 635-649.

Heidelberger, C., Chaudhuri, N.K., Danneberg, P., Mooren, D., Griesbach, L., Duschinsky, R., Schnitzer, R.J., Pleven, E., and Scheiner, J. (1957). Fluorinated pyrimidines, a new class of tumour-inhibitory compounds. Nature *179*, 663-666.

Imamura, H., Nhat, K.P., Togawa, H., Saito, K., Iino, R., Kato-Yamada, Y., Nagai, T., and Noji, H. (2009). Visualization of ATP levels inside single living cells with fluorescence resonance energy transfer-based genetically encoded indicators. Proc Natl Acad Sci U S A *106*, 15651-15656.

Jonckheere, A.I., Hogeveen, M., Nijtmans, L.G., van den Brand, M.A., Janssen, A.J., Diepstra, J.H., van den Brandt, F.C., van den Heuvel, L.P., Hol, F.A., Hofste, T.G.*, et al.* (2008). A novel mitochondrial ATP8 gene mutation in a patient with apical hypertrophic cardiomyopathy and neuropathy. J Med Genet *45*, 129-133.

Kaadige, M.R., Yang, J., Wilde, B.R., and Ayer, D.E. (2015). MondoA-Mlx transcriptional activity is limited by mTOR-MondoA interaction. Mol Cell Biol *35*, 101-110.

Khacho, M., Tarabay, M., Patten, D., Khacho, P., MacLaurin, J.G., Guadagno, J., Bergeron, R., Cregan, S.P., Harper, M.E., Park, D.S.*, et al.* (2014). Acidosis overrides oxygen deprivation to maintain mitochondrial function and cell survival. Nat Commun *5*, 3550.

Koppenol, W.H., Bounds, P.L., and Dang, C.V. (2011). Otto Warburg's contributions to current concepts of cancer metabolism. Nat Rev Cancer *11*, 325-337.

Matsuyama, S., and Reed, J.C. (2000). Mitochondria-dependent apoptosis and cellular pH regulation. Cell Death Differ *7*, 1155-1165.

Minn, A.H., Hafele, C., and Shalev, A. (2005). Thioredoxin-interacting protein is stimulated by glucose through a carbohydrate response element and induces beta-cell apoptosis. Endocrinology *146*, 2397-2405.

Pereira, B., Chin, S.F., Rueda, O.M., Vollan, H.K., Provenzano, E., Bardwell, H.A., Pugh, M., Jones, L., Russell, R., Sammut, S.J.*, et al.* (2016). The somatic mutation profiles of 2,433 breast cancers refines their genomic and transcriptomic landscapes. Nat Commun *7*, 11479.

Petersen, M.C., Vatner, D.F., and Shulman, G.I. (2017). Regulation of hepatic glucose metabolism in health and disease. Nat Rev Endocrinol *13*, 572-587.

Peterson, C.W., Stoltzman, C.A., Sighinolfi, M.P., Han, K.S., and Ayer, D.E. (2010). Glucose controls nuclear accumulation, promoter binding, and transcriptional activity of the MondoA-Mlx heterodimer. Mol Cell Biol *30*, 2887-2895.

Reshkin, S.J., Bellizzi, A., Caldeira, S., Albarani, V., Malanchi, I., Poignee, M., Alunni-Fabbroni, M., Casavola, V., and Tommasino, M. (2000). Na+/H+ exchanger-dependent intracellular alkalinization is an early event in malignant transformation and plays an essential role in the development of subsequent transformation-associated phenotypes. FASEB J *14*, 2185-2197.

Richards, P., Ourabah, S., Montagne, J., Burnol, A.F., Postic, C., and Guilmeau, S. (2017). MondoA/ChREBP: the usual suspects of transcriptional glucose sensing: implication in pathophysiology. Metabolism *70*, 133-151.

Robey, R.B., and Hay, N. (2006). Mitochondrial hexokinases, novel mediators of the antiapoptotic effects of growth factors and Akt. Oncogene *25*, 4683-4696.

Sans, C.L., Satterwhite, D.J., Stoltzman, C.A., Breen, K.T., and Ayer, D.E. (2006). MondoA-Mlx heterodimers are candidate sensors of cellular energy status: mitochondrial localization and direct regulation of glycolysis. Mol Cell Biol *26*, 4863-4871.

Shen, L., O'Shea, J.M., Kaadige, M.R., Cunha, S., Wilde, B.R., Cohen, A.L., Welm, A.L., and Ayer, D.E. (2015). Metabolic reprogramming in triple-negative breast cancer through Myc suppression of TXNIP. Proc Natl Acad Sci U S A *112*, 5425-5430.

Stoltzman, C.A., Kaadige, M.R., Peterson, C.W., and Ayer, D.E. (2011). MondoA senses non-glucose sugars: regulation of thioredoxin-interacting protein (TXNIP) and the hexose transport curb. J Biol Chem *286*, 38027-38034.

Stoltzman, C.A., Peterson, C.W., Breen, K.T., Muoio, D.M., Billin, A.N., and Ayer, D.E. (2008). Glucose sensing by MondoA:Mlx complexes: a role for hexokinases and direct regulation of thioredoxin-interacting protein expression. Proc Natl Acad Sci U S A *105*, 6912-6917.

Wahl, M.L., Pooler, P.M., Briand, P., Leeper, D.B., and Owen, C.S. (2000). Intracellular pH regulation in a nonmalignant and a derived malignant human breast cell line. J Cell Physiol *183*, 373-380.

Warburg, O. (1925). The metabolism of carcinoma cells. Cancer Res *9*, 148-163.

Webb, B.A., Chimenti, M., Jacobson, M.P., and Barber, D.L. (2011). Dysregulated pH: a perfect storm for cancer progression. Nat Rev Cancer *11*, 671-677.

Wilson, J.E. (2003). Isozymes of mammalian hexokinase: structure, subcellular localization and metabolic function. J Exp Biol *206*, 2049-2057.

Wu, K.C., Cheng, K.S., Wang, Y.W., Chen, Y.F., Wong, K.L., Su, T.H., Chan, P., and Leung, Y.M. (2017). Perturbation of Akt signaling, mitochondrial potential, and ADP/ATP ratio in acidosis-challenged rat cortical astrocytes. J Cell Biochem *118*, 1108-1117.

Xie, J., Wu, H., Dai, C., Pan, Q., Ding, Z., Hu, D., Ji, B., Luo, Y., and Hu, X. (2014). Beyond Warburg effect--dual metabolic nature of cancer cells. Sci Rep *4*, 4927.

Xue, J., Mraiche, F., Zhou, D., Karmazyn, M., Oka, T., Fliegel, L., and Haddad, G.G. (2010). Elevated myocardial Na+/H+ exchanger isoform 1 activity elicits gene expression that leads to cardiac hypertrophy. Physiol Genomics *42*, 374-383.

Yu, F.X., Chai, T.F., He, H., Hagen, T., and Luo, Y. (2010). Thioredoxin-interacting protein (Txnip) gene expression: sensing oxidative phosphorylation status and glycolytic rate. J Biol Chem *285*, 25822-25830.

Zaid, H., Abu-Hamad, S., Israelson, A., Nathan, I., and Shoshan-Barmatz, V. (2005). The voltage-dependent anion channel-1 modulates apoptotic cell death. Cell Death Differ *12*, 751-760.

Table 2.1. Key Resources

REAGENT or RESOURCE	SOURCE	IDENTIFIE
Antibodies		
Anti-GFP (B-2)	Santa Cruz	sc-9996
Anti-HK2 (anti-HXKII)	Santa Cruz	sc6521
Anti-MLX (D8G6W)	Cell Signaling	85570S
Anti-MondoA (Anti-MLXIP)	Proteintech	13614-1-AP
Anti-SDHA [2E3GC12FB2AE2]	Abcam	AB147
Anti-Tubulin	Molecular Probes	236-10501
Anti-TXNIP	Abcam	ab188865
Donkey anti-goat IgG-HRP	Santa Cruz	sc-2056
Mouse IgG, HRP-linked whole Ab (from sheep)	GE Life Science	NA-931
Rabbit IgG, HRP-linked whole Ab (from donkey)	GE Life Science	NA-934
Chemicals, Peptides, and Recombinant Proteins		
BCECF-AM	Thermo Fisher	B1170
Blotting Grade Blocker Non-fat Dry Milk	Bio-Rad	1706404XTU
CCCP	Sigma Aldrich	C2759
Chloroquine	Sigma Aldrich	415480
Deoxy-D-Glucose, 2-[1,2-3H(N)]	American Radiolabeled Chemicals, Inc.	0103-250
DMEM	Gibco	11995-065
DMEM Powder without sodium bicarbonate, glucose, L-glutamine, sodium pyruvate and phenol red	Cellgro	90-113-PB
DMEM, no glucose	Gibco	11966025
DMSO	Fisher	BP231
FCCP	Sigma Aldrich	C2920
Fetal bovine serum (FBS)	Gibco	26140-079
Galacto-Light™ Reaction Buffer Diluent with Galacton-Plus™	Thermo Fisher	T1055
Glucose	Fisher	D16-1
Glutamine	Cellgro	25-005-Cl
HBSS	Gibco	24020-117
HCl	Fisher	A144SI-212
HEPES	Sigma Aldrich	H3375
JC1	Thermo Fisher	T3168
Luciferase Assay System	Promega	E4550
Metformin	Sigma Aldrich	D150959
Monensin	Sigma Aldrich	M5273

more

Table 2.1. continued.

NaOH	Fisher	S-320-1
Non-essential amino acids	Gibco	11140-050
Oligomycin A	Sigma Aldrich	75351
Pennicillin/Streptomycin	Gibco	15140-112
Phenol Red	Sigma Aldrich	P-0290
ProSignal Pico ECL	Genesee Scientific	20-300B
Reporter 5X Lysis Buffer	Promega	E4030
Sodium bicarbonate	Fisher	L-23200
Sodium pyruvate	Gibco	11360-070
SuperSignal West Femto	Thermo Fisher	34094
Trypsin-EDTA (0.25%)	Gibco	25200-056
Tween-20	Fisher	BP-337
Critical Commercial Assays		
Quick RNA miniprep kit	Genesee Scientific	R1055
ATP determination kit	Thermo Fisher	A22066
Mitochondria isolation kit for cultured cells	Thermo Fisher	89874
Stranded mRNA-Seq kit with mRNA capture beads	Kapa Biosystems	KK8421
Experimental Models: Cell Lines		
MondoA $^{-/-}$ mouse embryonic fibroblasts	Peterson et al. 2008	N/A
MondoA Δ/Δ mouse embryonic fibroblasts	Peterson et al. 2008	N/A
143B	Weinberg et al. 2010	N/A
143Bρ^0	Weinberg et al. 2010	N/A
143Bρ^0:Wild type cybrid	Weinberg et al. 2010	N/A
143Bρ^0:ΔCYTB cybrid	Weinberg et al. 2010	N/A
143Bρ^0:ΔATP6/ΔATP8 cybrid	Boominathan et al. 2016	N/A
143Bρ^0:ΔATP6/ΔATP8 cybrid + ATP6$_{nuc}$ +ATP8$_{nuc}$	Boominathan et al. 2016	N/A
HeLa	ATCC	CCL-2
MDA-MB-231	ATCC	HTB-26
BJ-Tert	ATCC	CRL-4001
MDA-MB-231:MondoA-KO1	This paper	N/A
MDA-MB-231:MondoA-KO2	This paper	N/A
MDA-MB-231:MondoA-KO3	This paper	N/A
Oligonucleotides		
TXNIP_forward (human): TGACTTTGGCCTACAGTGGG	Peterson et al. 2010	N/A
TXNIP_reverse (human): TTGCGCTTCTCCAGATACTGC	Peterson et al. 2010	N/A
TXNIP_forward (mouse): CCTGACCTAATGGCACC	Peterson et al. 2010	N/A

more

Table 2.1. continued.

TXNIP_reverse (mouse): GAGATGTCATCACCTTCAC	Peterson et al. 2010	N/A
ATP5I_forward: CAGGTCTCTCCGCTCATCAAG	This paper	N/A
ATP5I_reverse: GCCCGAGGTTTTAGGTAATTGT	This paper	N/A
Actin_forward: TCCATCATGAAGTGTGACGT	Peterson et al. 2010	N/A
Actin_reverse: TACTCCTGCTTGCTGATCCAC	Peterson et al. 2010	N/A
Recombinant DNA		
LXSH	Stoltzman et al. 2008	N/A
LXSH-MondoA	Stoltzman et al. 2008	N/A
LXSH-MondoA(I766P)	Stoltzman et al. 2008	N/A
pcDNA3-AT1.03 (ATEAM)	Imamura et al. 2009	N/A
pcDNA3-mitAT1.03 (Mit-ATEAM)	Imamura et al. 2009	N/A
pcDNA3-AT1.03 R122K/R126K	Imamura et al. 2009	N/A
pcDNA3-mitAT1.03 R122K/R126K	Imamura et al. 2009	N/A
pEGFP-N1-mVDAC1	Zaid et a. 2005	N/A
pEGFP-N1-mVDAC1(E72Q)	Zaid et a. 2005	N/A
pCDV-SPORT6-HK2	Stoltzman et al. 2008	N/A
pCDV-SPORT6-HK2(D657A)	Stoltzman et al. 2008	N/A
pcDNA3.1-mVDAC1-GFP(1-10)	This paper	N/A
pcDNA3.1-mVDAC1(E72Q)-GFP(1-10)	This paper	N/A
pcDNA3.1-HK2-GFP(11)	This paper	N/A
pGL3Basic-TXNIP_Promoter	Peterson et al. 2010	N/A
pGL3Basic-TXNIP_Promoter($ChoRE_{mut}$)	Peterson et al. 2010	N/A
Software and Algorithms		
Prism	Graphpad Software	N/A
ImageJ	N/A	N/A
CFX Manager 3.1	Bio-Rad	N/A
R	N/A	N/A
NIS Elements	Nikon	N/A
Other		
siRNA: Dharmacon ON-TARGETplus control siRNA	GE Life Sciences	D00-1810-10-20

more

Table 2.1. continued.

siRNA: siATP5I SmartPool	GE Life Sciences	M-019688-01
siRNA: siSLC25A5 SmartPool (siANT2)	GE Life Sciences	M-007486
siRNA: siHK2 SmartPool	GE Life Sciences	L-006735-00-0005
Nunc™ Lab-Tek™ II Chambered Coverglass, 8-well	Thermo Fisher	155409PK
3.5 mm glass bottom culture dishes	MatTek Corporation	P35G-.15-14-C
Hybond P PVDF Membrane; 0.45 μm	Genesee Scientific	83-646R

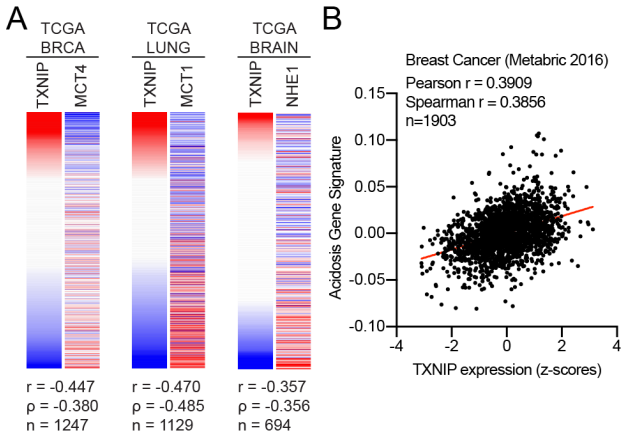

Figure 2.1. TXNIP expression anticorrelates with genes that control intracellular pH (**A**) Heatmaps depicting the expression of TXNIP mRNA compared to MCT4 (breast cancer), MCT1 (lung cancer) and NHE1 (brain cancer). All expression data was collected from TCGA. Spearman and Pearson correlation statistics are reported as r and ρ, respectively. (**B**) An acidosis gene signature was determined for the 2016 METABRIC breast cancer dataset. These scores were compared to TXNIP expression from the dataset and correlation statistics were performed.

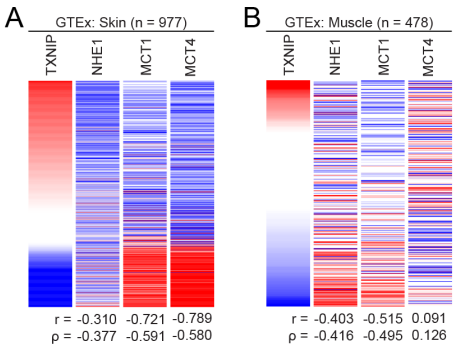

Figure 2.2. Supplement: TXNIP expression anticorrelates with genes that control intracellular pH

Heatmaps depicting the expression of TXNIP mRNA compared to MCT4, MCT1 and NHE1 for normal (**A**) skin and (**B**) muscle tissues. All expression data was collected from GTEx. Spearman and Pearson correlation statistics are reported as r and ρ, respectively.

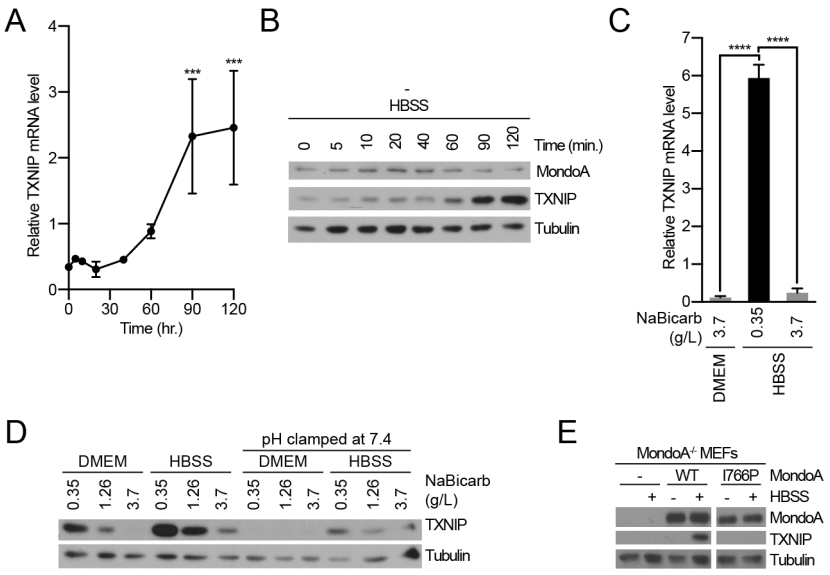

Figure 2.3. Acidosis drives MondoA-dependent TXNIP expression
Mouse embryonic fibroblasts (MEFs) treated with HBSS for the indicated amounts of time and (**A**) TXNIP mRNA levels were determined by reverse transcriptase-quantitative PCR (RT-qPCR) and (**B**) TXNIP and MondoA protein levels were determined immunoblotting. (**C**) TXNIP mRNA from MEFs treated with DMEM, HBSS and HBSS supplemented with sodium bicarbonate to the same level as in DMEM (3.7 g/L). HBSS with high sodium bicarbonate brought the pH to 7.5. (**D**) TXNIP protein levels in MEFs treated with DMEM and HBSS containing the indicated amounts of sodium bicarbonate. Additionally, the same treatments were clamped to pH 7.4 by adding 25mM HEPES and adjusting pH with NaOH. (**E**) Immunoblot examining TXNIP induction in response to HBSS in MondoA-knockout MEFs complemented with empty vector, wild type MondoA or MondoA(I766P). ***p<0.001; ****p<0.0001; ns – not significant

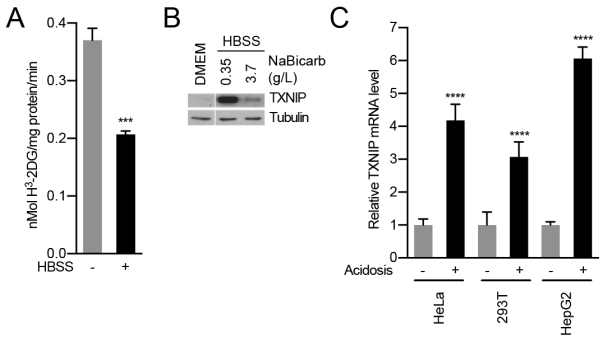

Figure 2.4. Supplement: HBSS drives MondoA-dependent TXNIP expression
(**A**) Glucose uptake was determined by quantifying the rate of H^3-2-deoxyglucose uptake in cells treated with HBSS. (**B**) TXNIP immunoblot of MEFs treated with DMEM, HBSS and HBSS supplemented with sodium bicarbonate to the same degree as DMEM (3.7 g/L). (**C**) TXNIP mRNA levels in HEK-293T, HeLa and HepG2 cells treated with acidosis.

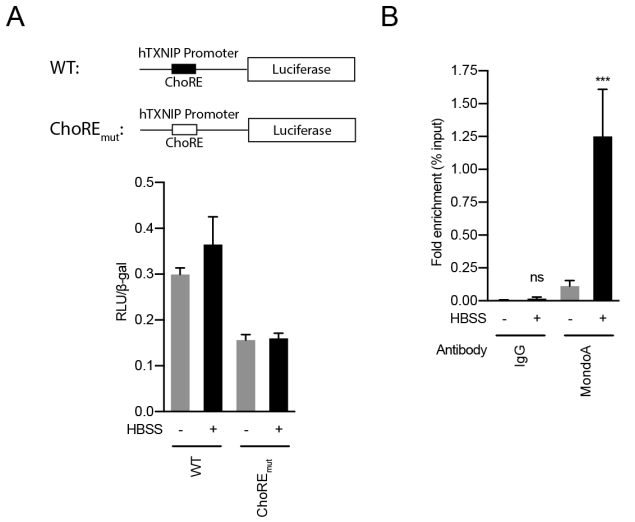

Figure 2.5. Supplement: The MondoA/TXNIP axis is triggered by acidosis
(**A**) Schematic depicting luciferase reporter assay. A construct was made that contained a mutation in the carbohydrate-responsive element (ChoRE$_{mut}$). Luciferase constructs were transfected into MEFs and HBSS treatment results in a slight induction of luciferase. Using the ChoRE$_{mut}$ TXNIP promoter, initial luciferase expression was lower and HBSS treatment had no effect on luciferase. (**B**) Chromatin-immunoprecipitation performed on MEFs treated with HBSS. Antibodies against MondoA and IgG were used.

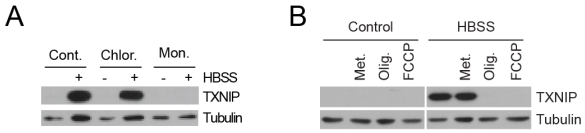

Figure 2.6. Supplement: TXNIP induction by HBSS occurs through regulation of mitochondrial protons

(**A**) TXNIP protein levels in MEFs treated with ionophores chloroquine (Chlor., 25 μM) and monensin (Mon., 5 μM), which cause lysosomal and cytosolic alkalization, respectively. (**B**) TXNIP protein levels in MEFs treated with HBSS and the mitochondrial ionophore FCCP or the ETC complex inhibitors metformin (Met., 1 mM) and oligomycin (Olig., 1 μM).

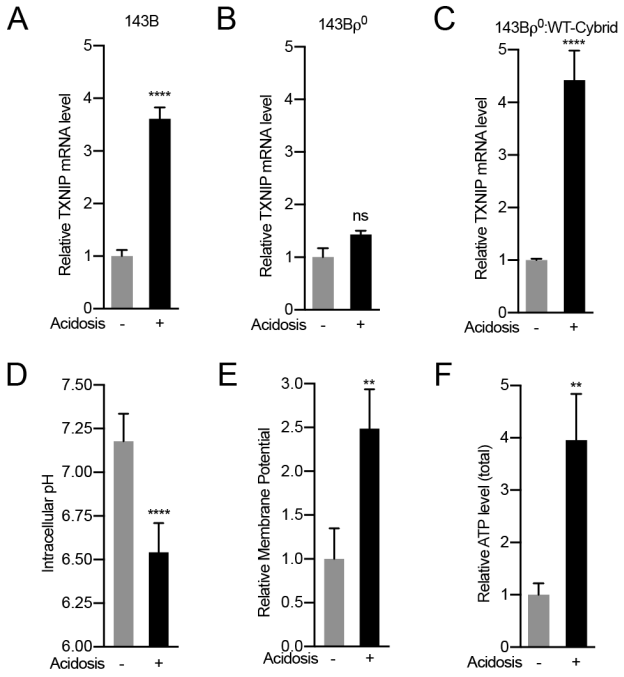

Figure 2.7. Acidosis drives ETC-dependent MondoA transcriptional activity
TXNIP mRNA level following treatment with acidosis in (**A**) 143B osteosarcoma cells, (**B**) 143Bρ^0 cells, which lack mtDNA, and (**C**) WT-Cybrid cells, which have restored wild type mitochondria. (**D**) Intracellular pH was determined by BCECF-AM staining. (**E**) Mitochondrial membrane potential was determined by JC1 staining. (**F**) Relative ATP levels were determined using an ATP-luciferase assay. * $p<0.05$; ** $p<0.01$; ****$p<0.0001$; ns – not significant

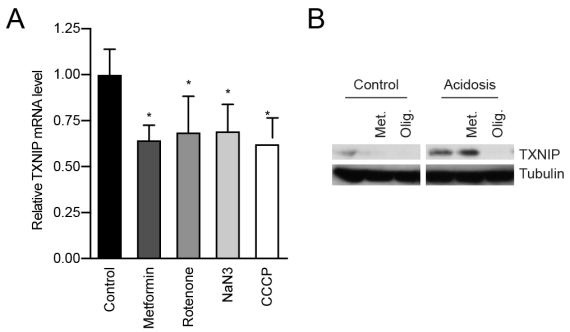

Figure 2.8. Supplement: Acidosis-driven MondoA activity requires the ATP synthase

(**A**) TXNIP mRNA levels in HeLa cells after treatment with the ETC poisons metformin (complex I, 5 mM), rotenone (complex I, 1 μM), NaN_3 (complex IV, 1 mM) and CCCP (disrupts the proton gradient, 1 μM). (**B**) TXNIP protein levels in MEFs treated with the mitochondrial ionophore FCCP and the ETC complex inhibitors metformin (Met., 1 mM) and oligomycin (Olig., 1 μM).

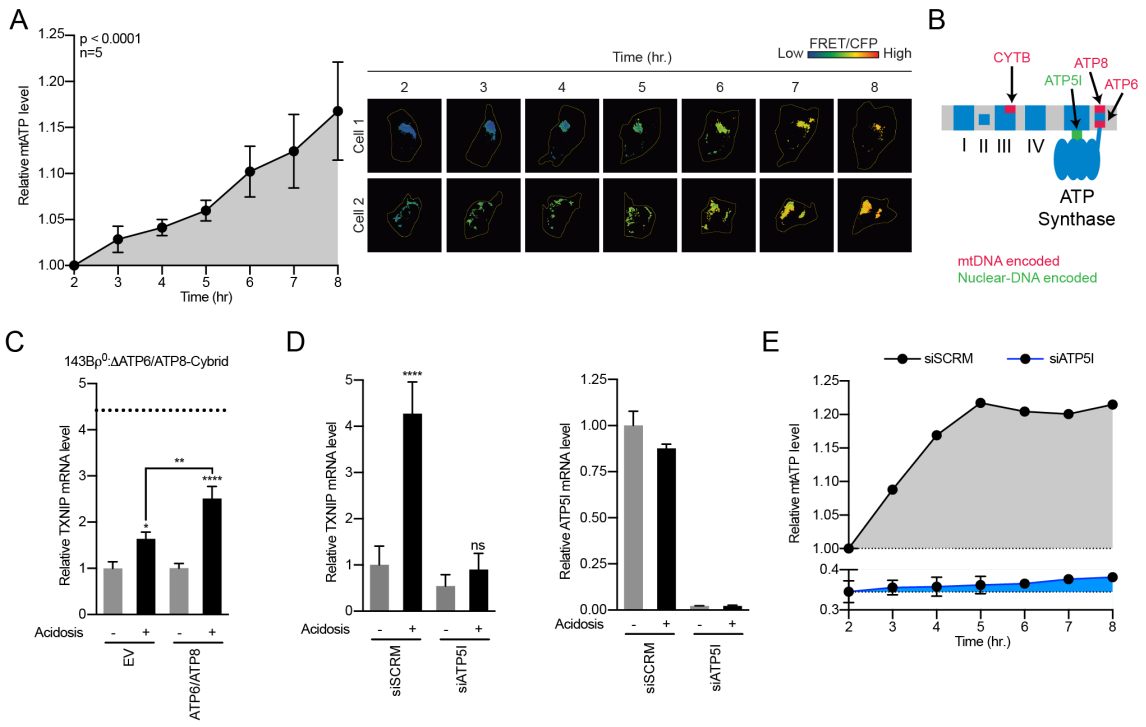

Figure 2.9. MondoA senses mitochondrial ATP
(**A**) Mit-ATEAM, a mitochondrial-targeted ATP-biosensor, was used to determine how acidosis affects mitochondrial ATP. Widefield microscopy was used to capture images in the FRET and CFP channels. After images were obtained, mitochondria were analyzed for FRET and CFP signal. FRET signal was normalized using CFP. (**B**) A schematic depicting nuclear- and mitochondrial-DNA encoded components of the ETC. (**C**) TXNIP mRNA level following treatment with acidosis of 143Bρ^0:ΔATP6/ATP8-Cybrid cells, which do not express ATP6 or ATP8, critical components of the ATP synthase. Empty vector or mitochondrial-targeted versions of the ATP6 and ATP8 were expressed. The dotted line indicates the level to which TXNIP was induced in 143Bρ^0:WT-cybrid cells. (**D**) TXNIP mRNA level following acidosis treatment of HeLa cells expressing scrambled or ATP5I-specific siRNA (siSCRM or siATP5I). ATP5I knock down was confirmed by measuring ATP5I mRNA levels. (**F**) Mit-ATEAM was used to determine how acidosis affects mitochondrial ATP production in the context of siSCRM or siATP5I. * p<0.05; ** p<0.01; ****p<0.0001; ns – not significant

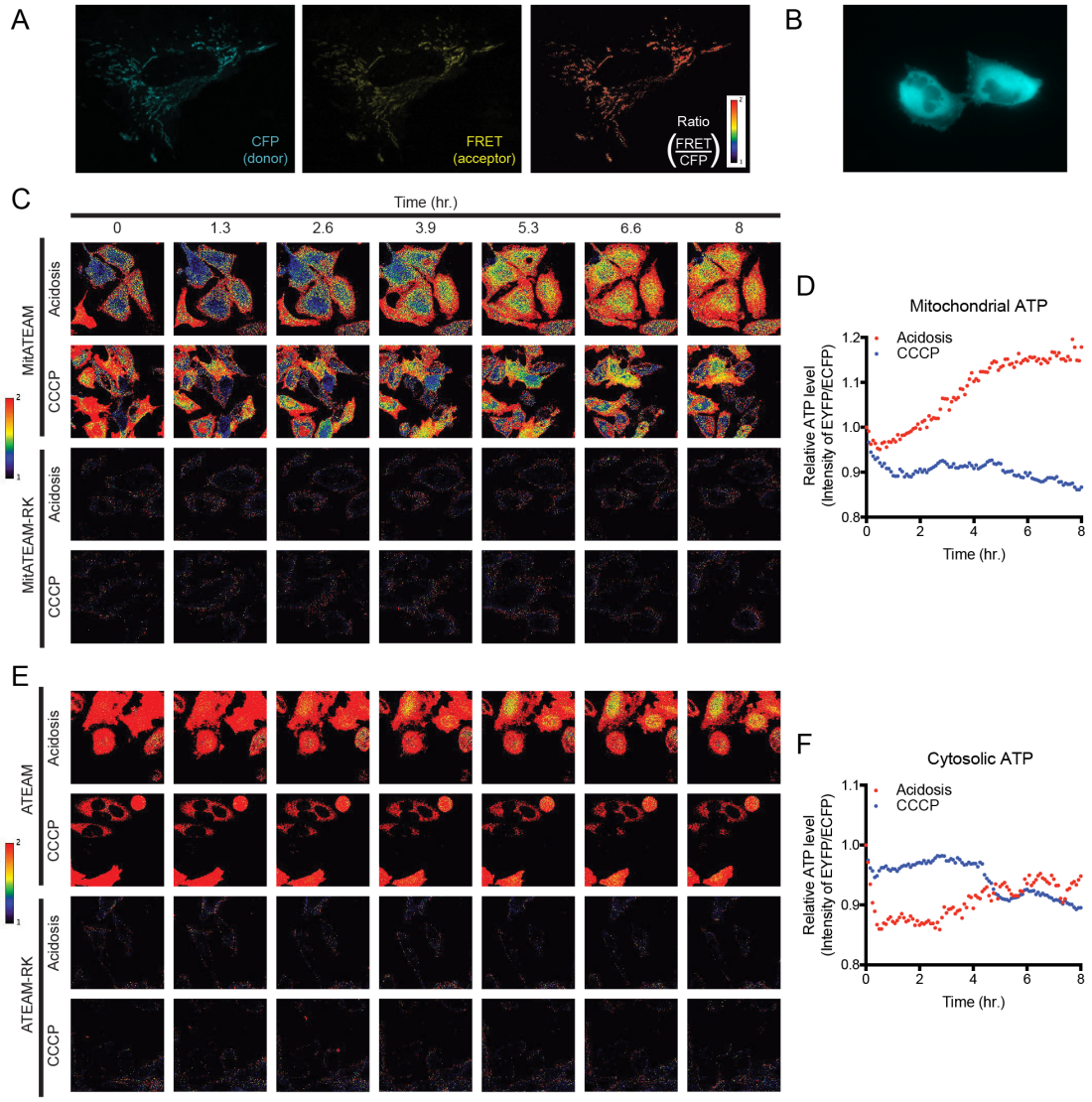

Figure 2.10. Supplement: Acidosis drives mitochondrial ATP synthesis
(**A**) Confocal images at 60X of Mit-ATEAM expressed in HeLa cells. Shown are the CFP and FRET channels as well as the ratio of FRET to CFP (indicating ATP). (**B**) Widefield image at 60X of ATEAM. CFP channel only is shown. (**C**) Confocal images of Mit-ATEAM and Mit-ATEAM(R122K/R126K) in HeLa cells. Cells were treated with acidosis or CCCP (1 μM) for eight hours. Images are pseudo-colored according to the FRET/CFP ratio and (**D**) quantification is given. (**E**) Confocal images of ATEAM and ATEAM(R122K/R126K) in HeLa cells. Cells were treated with acidosis or CCCP (1 μM) for eight hours. Images are pseudo-colored according to the FRET/CFP ratio and (**F**) quantification is given. Notably, the FRET/CFP ratios for Mit-ATEAM(R122K/R126K) and ATEAM(R122K/R126K) was negligible compared to nonmutated constructs.

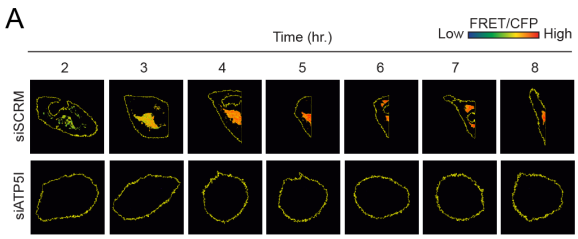

Figure 2.11. Supplement: Acidosis drives mitochondrial ATP synthesis
(**A**) Widefield microscopy of Mit-ATEAM was used to determine how acidosis affects mitochondrial ATP production in the context of siSCRM or siATP5I. Shown are pseudo-colored images of the FRET/CFP ratio.

Figure 2.12. MondoA senses G6P produced by mitochondrial-hexokinase
(**A**) Heatmap and $\log_2$ fold-changes of glycolytic and TCA metabolites measured from HeLa cells treated for four hours with acidic media using GC-MS. (**B**) Schematic illustrating how mtATP could contribute to MondoA transcriptional activity. As mtATP is exported from the mitochondria, mitochondrial-bound HK2 consumes it to produce G6P, resulting in MondoA activation. (**C**) Cellular fractionation of BJ-Tert cells indicating mitochondrial localization of Hk2, MondoA and Mlx. Succinate dehydrogenase A (SDHA) serves as a control for the mitochondria fraction. TXNIP mRNA levels of HeLa cells treated with acidosis and expressing a pool of four siRNAs against (**D**) ANT2 and (**E**) HK2, or (**F**) expressing HK2 and HK2(D657A). (**G**) TXNIP mRNA levels of BJ-Tert cells treated with acidosis and expressing mVDAC1-GFP and mVDAC1(E72Q)-GFP. HK2 localization was also analyzed by cellular fractionation and densitometry was used to quantify the relative amount of HK2 on the mitochondria. Of note, HK2 became increasingly enriched in the cytoplasmic fraction. (**H**) Schematic depicting the use of GFP(1-10) and GFP(11) to artificially tether mVDAC1 and HK2. HK2 localization was also analyzed by cellular fractionation, and densitometry was used to quantify the relative amount of HK2 on the mitochondria. (**I**) TXNIP mRNA levels of BJ-Tert cells treated with acidosis and expressing mVDAC1-GFP, mVDAC1(E72Q)-GFP and HK2-GFP(11). * $p<0.05$; ** $p<0.01$; *** $p<0.001$; **** $p<0.0001$; ns – not significant

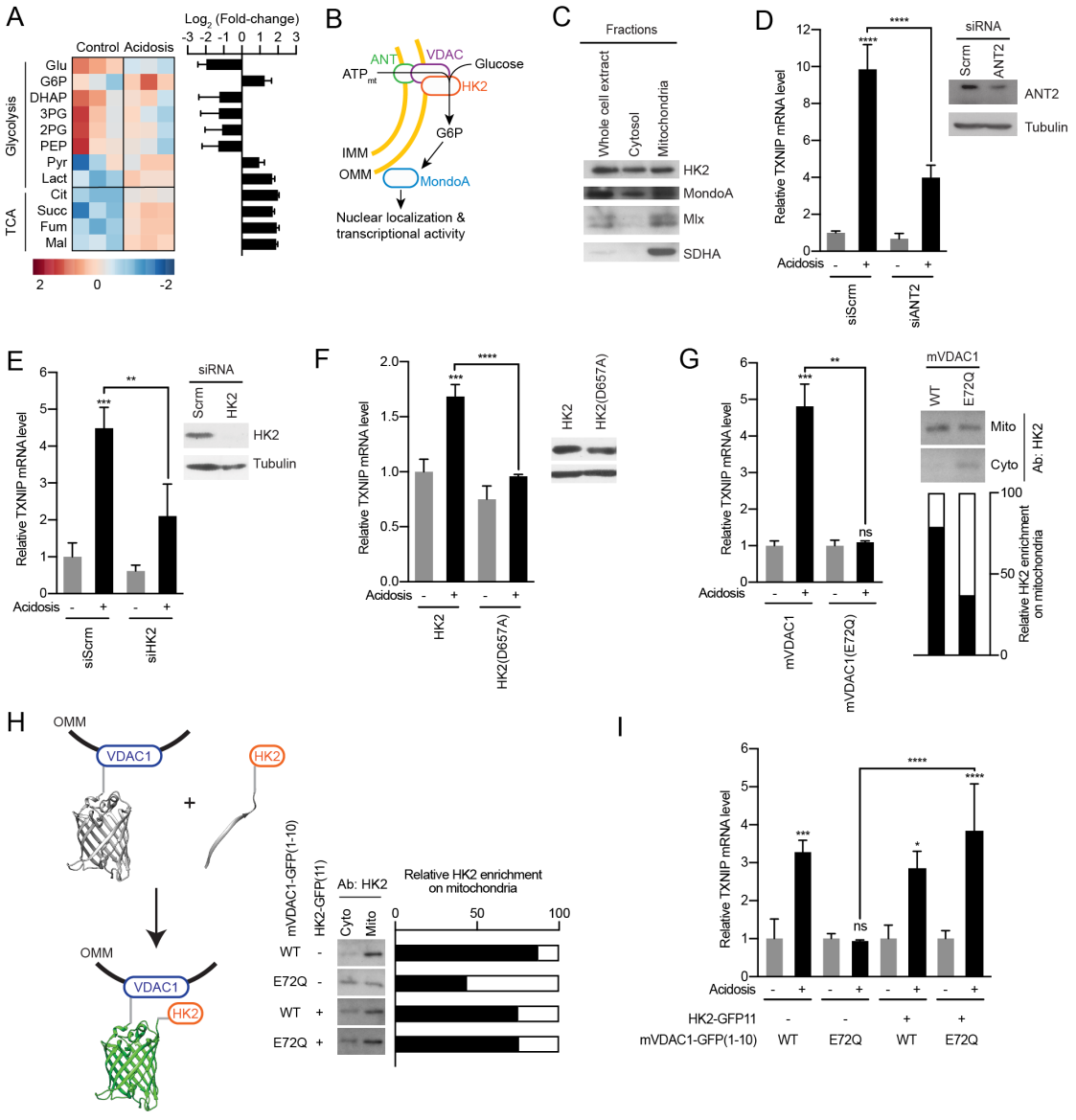
A
Log2 (Fold-change)
-3 -2 -1 0 1 2 3
Control Acidosis
Glycolysis
TCA
Glu
G6P
DHAP
3PG
2PG
PEP
Pyr
Lact
Cit
Succ
Fum
Mal
2 0 -2
B
ANT
VDAC
Glucose
ATPmit
HK2
G6P
IMM
OMM
MondoA
Nuclear localization & transcriptional activity
C
Fractions
Whole cell extract
Cytosol
Mitochondria
HK2
MondoA
Mlx
SDHA
D
siRNA
Scrm
ANT2
Relative TXNIP mRNA level
Acidosis
siScrm
siANT2
Tubulin
E
siRNA
Scrm
HK2
Relative TXNIP mRNA level
Acidosis
siScrm
siHK2
F
HK2
HK2(D657A)
Relative TXNIP mRNA level
Acidosis
G
mVDAC1
WT
E72Q
Mito
Cyto
Ab: HK2
Relative HK2 enrichment on mitochondria
Relative TXNIP mRNA level
Acidosis
mVDAC1
mVDAC1(E72Q)
ns
H
OMM
VDAC1
HK2
mVDAC1-GFP(1-10)
HK2-GFP(11)
Ab: HK2
Cyto
Mito
Relative HK2 enrichment on mitochondria
WT
E72Q
I
Relative TXNIP mRNA level
Acidosis
HK2-GFP11
mVDAC1-GFP(1-10)
WT
E72Q
ns

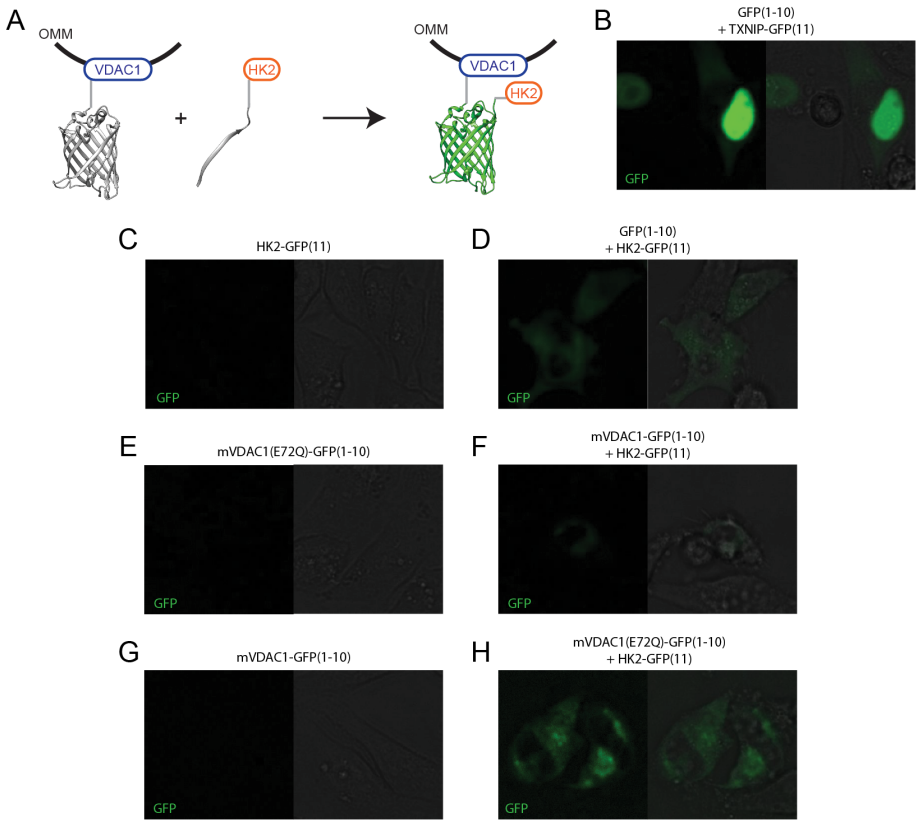

Figure 2.13. Supplement: MondoA senses G6P produced by mitochondrial-hexokinase

(**A**) Schematic depicting the use of GFP(1-10) and GFP(11) as a means of artificially tethering mVDAC1 and HK2 in the cell. Images of GFP signal in HeLa cells transfected with (**B**) TXNIP-GFP(11) and GFP(1-10) used as a positive control for alpha complementation, (**C**) HK2-GFP(11), (**D**) GFP(1-10) and HK2-GFP(11), (**E**) mVDAC1-GFP(1-10), (**F**) mVDAC1-GFP(1-10) and HK2-GFP(11), (**G**) mVDAC1(E72Q)-GFP(1-10), and (**H**) mVDAC1(E72Q)-GFP(1-10) and HK2-GFP(11).

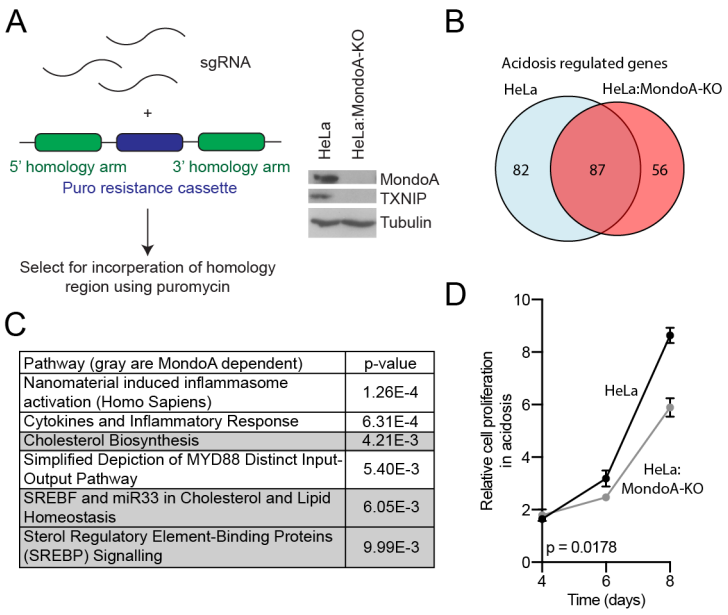

Pathway (gray are MondoA dependent)	p-value
Nanomaterial induced inflammasome activation (Homo Sapiens)	1.26E-4
Cytokines and Inflammatory Response	6.31E-4
Cholesterol Biosynthesis	4.21E-3
Simplified Depiction of MYD88 Distinct Input-Output Pathway	5.40E-3
SREBF and miR33 in Cholesterol and Lipid Homeostasis	6.05E-3
Sterol Regulatory Element-Binding Proteins (SREBP) Signalling	9.99E-3

Figure 2.14. The MondoA-dependent acidosis response
(**A**) Schematic depicting the strategy employed to knock out MondoA in HeLa cells. In brief, three sgRNAs, CRISPR/Cas9 and a homology construct were expressed. Homology-directed repair resulted in incorporation of a puromycin-resistance cassette. Puromycin was used to select for a pool of cells in which MondoA was lost. Immunoblot showing loss of MondoA. Of note, consistent with our previous findings, loss of MondoA prevented TXNIP expression. (**B**) RNA-sequencing was used to determine differentially regulated genes for HeLa and HeLa:MondoA-knockout cells treated with acidosis. (**C**) Over-representation analysis was used to determine the pathways that initiated by acidosis treatment. In gray are the pathways that lost in HeLa:MondoA-KO cells, indicating a dependence on MondoA. (**D**) Relative cell proliferation of cells treated with acidosis for eight days. Proliferation was determined by crystal violet staining.

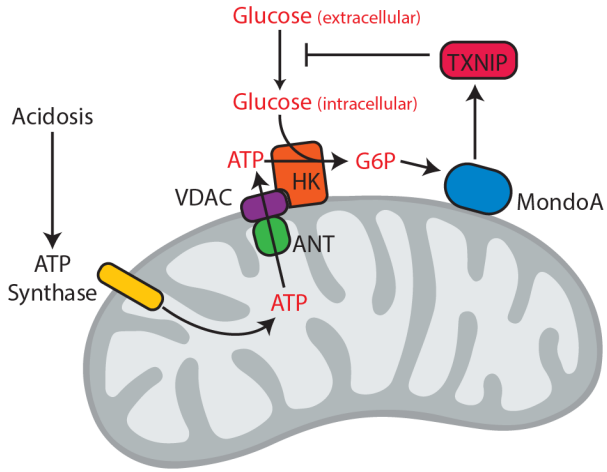

Figure 2.15. Model
A model depicting our findings. Acidosis drives mtATP synthesis. HK2 has preferential access to mtATP exported through ANT and VDAC. This leads to increased G6P synthesis, which activates MondoA. Finally, MondoA drives transcriptional circuits that control nutrient utilization in the cell, including TXNIP.

CHAPTER 3

DIRECT ACTIVATION OF THE MONDOA/TXNIP AXIS BY PROTEIN SYNTHESIS INHIBITORS

3.1. Abstract

Although protein synthesis is tightly linked to nutrient availability, crosstalk between the ribosome and metabolic pathways is poorly understood. Here we describe a mechanism by which protein synthesis exerts control over glucose uptake. Using protein synthesis inhibitors, we show that the MondoA/TXNIP axis, which restricts glycolytic flux, is activated by a blockage of protein synthesis. This is primarily due to significant metabolic rewiring that leads to mitochondrial ATP (mtATP)generation. mtATP is exported from the mitochondria and consumed by mitochondria-bound hexokinase produces glucose-6-phosphate, which is a potent activator of the MondoA/TXNIP axis. Further, we show that the anticancer protein synthesis inhibitor, Rocaglamide A, requires TXNIP for its antiproliferative efficacy. Finally, we observed that the MondoA/TXNIP axis is necessary for an adaptive response to protein synthesis inhibition. These findings provide a mechanistic link between the rate of protein synthesis, mitochondrial ATP synthesis, the MondoA/TXNIP axis and glucose availability.

3.2. Introduction

A unifying characteristic of oncogenes is their ability to drive anabolic metabolism to support the biosynthesis of macromolecules. Oncogenes also impose significant metabolic stress on cells (Hsieh and Dang, 2016). As a result of increased protein synthesis, cancer cells experience depletion of local nutrient supplies, accumulation of ROS, and many other metabolic challenges that if unchecked would result in cell death. In order to prevent apoptosis, the ribosome must convey information about translation flux to the pathways that control nutrient availability. Recently protein

synthesis inhibitors have received attention as potential anticancer therapies. Inhibitors of translation initiation are among the most promising candidate therapies (Martineau et al., 2014; Santagata et al., 2013). Yet the full mechanistic and biological consequences of targeting translation initiation have not been described.

The MondoA/TXNIP axis is a nexus of glucose homeostasis. Mechanistically, glucose-6-phosphate (G6P) drives translocation of the MondoA transcription factor from the outer mitochondrial membrane (OMM) to the nucleus where it binds DNA in the promoters of its target genes and recruits cofactors that initiate transcription. We recently showed that MondoA also requires mtATP for its transcriptional activity. An important target gene of MondoA is TXNIP, a negative regulator of glucose uptake. Previous reports have shown that protein synthesis inhibitors drive TXNIP expression, yet the mechanistic details remain unknown (Santagata et al., 2013).

Here we report that protein synthesis inhibitors activate the MondoA/TXNIP axis and restrict glucose uptake. Protein synthesis inhibitors cause widespread metabolic rewiring, including increased synthesis of mtATP, which is as a substrate for the production of G6P by mitochondria-bound hexokinase. The resultant increase in G6P drives MondoA transcriptional activity and TXNIP expression. We showed that the induction of the MondoA/TXNIP axis common among many protein synthesis inhibitors, including the elongation-initiation inhibitor Rocaglamide A (RocA). Importantly, the ability of RocA to restrict cell growth depends on its ability to initiate a transcriptional response by the MondoA/TXNIP axis. These findings expand our understanding of adaptive metabolism in response to protein synthesis inhibition. Further, it reinforces our previous findings that the MondoA/TXNIP axis is a metabolic switch that senses diverse

signals to control nutrient homeostasis.

3.3. Results

3.3.1. Translation inhibition drives TXNIP expression

Protein synthesis inhibitors drive expression of TXNIP (Santagata et al., 2013). To examine the generality of this finding, we performed an unbiased analysis of genes that correlate with TXNIP expression using the Gene-tissue Expression Database (GTEx). We identified a positive correlation between TXNIP and eukaryotic elongation factor 2 kinase (EEF2K), which negatively regulates mRNA translation elongation by phosphorylating and inactivating eukaryotic elongation factor 2 (Figures 3.1A and 3.2A; (White-Gilbertson et al., 2009). In contrast, we observed that EIF4A1 and EIF4E, both essential components of the elongation initiation machinery, were anticorrelated with TXNIP expression (Figure 3.2B). We extended these findings to cancerous tissues and observed that in breast cancers, TXNIP negatively correlates with elongation-initiation factor EIF4G1 and the ribosomal biogenesis genes RRP12 and RRP1 (Figure 3.1B). These data support the general model that a high rate of translation suppresses TXNIP expression.

We previously showed that mTOR is a negative regulator of the MondoA/TXNIP axis and that treating cells with mTOR inhibitors leads to induction of TXNIP expression (Kaadige et al., 2015). Given that enhanced protein synthesis is a predominant feature of mTORC1 activity, we investigated how protein synthesis inhibitors affect the MondoA/TXNIP axis. Treating HeLa cells with cycloheximide (CHX), which interferes with the translocation step of protein synthesis, led to a robust induction of TXNIP. In

comparison, the effects of the mTOR inhibitor, Torin, on TXNIP expression were more modest (Figure 3.1C), suggesting that CHX induces TXNIP via a pathway parallel to mTOR. We extended this finding to nontransformed cell lines including C2C12 and L6 myoblasts and HEK293 embryonic kidney cells, and found in all cases that CHX drove TXNIP expression (Figures 3.3A-C).

Given that oncogenes repress the MondoA/TXNIP axis, we sought to determine how CHX affects TXNIP expression in a variety of transformed cells. CHX drove TXNIP expression in HRAS(G12V)-transformed MEFS, $TSC2^{-/-}$ MEFs and MYC(T58A)-overexpressing MDA-MB-231 cells (Figures 3.1D-E and 3.3D). Finally, emetine and puromycin, which block translation elongation, also increased TXNIP expression (Figure 3.1F). Together, these findings demonstrate that TXNIP is induced broadly in response to protein synthesis inhibition, and suggest that TXNIP can be induced independent of oncogenic events. It is possible that the MondoA/TXNIP axis is 1) a sensor of protein synthesis and 2) a component of an adaptive response pathway initiated by a blockade in protein synthesis. We therefore investigated the mechanism by which protein synthesis inhibitors induce TXNIP expression.

3.3.2. Protein synthesis inhibitors drive MondoA transcriptional activity

We evaluated the contribution of MondoA to TXNIP induction by protein synthesis inhibitors. We treated wild type and $MondoA^{-/-}$ mouse embryonic fibroblasts (MEFs) with CHX. In the absence of MondoA, CHX treatment did not induce expression of TXNIP or another MondoA target gene, ARRDC4, a TXNIP paralogue (Figures 3.4A and 3.5A). Ectopic expression of MondoA rescued TXNIP induction in $MondoA^{-/-}$ MEFs

(Figure 3.4B). MondoA:Mlx heterodimerization is necessary for translocation to the nucleus and DNA binding (Peterson et al., 2010). Expressing MondoA(I766P), which is unable to bind Mlx, did not rescue CHX-driven TXNIP expression (Figure 3.4B), illustrating the requirement for functional MondoA:Mlx heterocomplexes. Consistent with this observation, we observed increased nuclear localization of MondoA in response to CHX when analyzed by immunofluorescence (Figure 3.4C). We evaluated the occupancy of MondoA on the promoter of TXNIP by chromatin immunoprecipitation (ChIP). CHX treatment led to increased occupancy of MondoA on the TXNIP promoter (Figure 3.4D).

MondoA-dependent TXNIP expression is mediated by a CACGAG carbohydrate-response element about 80 bp upstream of the transcription start site (Minn et al., 2005). MondoA:Mlx binds to the ChoRE and recruits cofactors to initiate transcription (Peterson et al., 2010). We used a TXNIP luciferase reporter assay to evaluate ChoRE-dependent transcription (Figure 3.4E). Cells were treated with CHX and one hour prior to determining luciferase expression, we washed out CHX by replacing the media with fresh glucose-free DMEM. This allowed for accumulated luciferase mRNA to be translated. Cells treated with CHX had increased luciferase activity, and this effect was entirely dependent on an intact ChoRE (Figure 3.4F). Thus, protein synthesis inhibition drives MondoA transcriptional activity.

3.3.3. Metabolic rewiring by protein synthesis inhibition

Because MondoA is a glucose dependent transcription factor, we determined the requirement for glucose in CHX-driven TXNIP expression. HeLa cells were treated with

CHX in DMEM or glucose-free DMEM. Surprisingly, TXNIP was induced in the presence and in the apparent absence of glucose (Figure 3.6A). FBS contains glucose (about 5 mM), which may provide a source of glucose to support MondoA-dependent TXNIP expression. This did not seem to be the case in our previous studies (Peterson et al., 2010; Stoltzman et al., 2008). We dialyzed FBS to remove small molecules including glucose then treated cells with CHX in glucose-free DMEM + 10% dialyzed FBS. This prevented the induction of TXNIP in response to CHX (Figure 3.6B). Adding glucose back rescued TXNIP induction (Figure 3.6C). In addition to greatly increasing the expression of TXNIP at all glucose levels, CHX decreased the glucose threshold ~ 5 fold at which TXNIP expression is induced. Thus, protein synthesis inhibitors sensitize the MondoA/TXNIP axis to low levels of glucose.

Given that MondoA transcriptional activity is tightly linked to nutrient abundance, in particular abundance of G6P and mtATP, we sought to determine how inhibiting protein synthesis affects the metabolic state of the cell. GC-MS was used to evaluate metabolite levels in cells treated with CHX. We observed significant changes in the levels of glycolytic intermediates and TCA cycle intermediates (Figures 3.6D and 3.6E and data not shown). G6P levels were significantly enriched following CHX treatment (Figure 3.6E), thus accumulated G6P likely explains why protein synthesis inhibitors trigger the MondoA/TXNIP axis. Considering that the increase in G6P was much greater than that observed for other glycolytic intermediates, we hypothesized that protein synthesis inhibition enhances the activity of hexokinase, which catalyzes the production G6P.

3.3.4. Protein synthesis inhibition drives mtATP production

We previously showed that MondoA is a sensor of mtATP in Chapter 2. We first investigated the requirement of the TCA cycle for CHX-driven TXNIP expression. We addressed this question by treating cells with dichloroacetic acid (DCA), an inhibitor of PDH kinase. DCA prevents phosphorylation and inactivation of PDH, thus increasing in the amount of pyruvate that is metabolized in the TCA cycle. DCA treatment further increased CHX-driven TXNIP (Figure 3.7A). Conversely, by using pyruvate-free media CHX-driven TXNIP expression was blunted (Figure 3.7B). Glutamine can also be a source of carbons for the TCA cycle, therefore we used glutamine-free and pyruvate/glutamine-free media. While glutamine-free media had no effect, pyruvate/glutamine-free media prevented CHX-driven TXNIP expression (Figure 3.7B).

Pyruvate and glutamine are anaplerotic substrates that are converted to oxaloacetate and α-ketoglutarate, respectively. Dimethyl-α-ketoglutarate (DMK) and oxaloacetate (OAA) supplementation rescued the depletion in CHX-driven TXNIP expression caused by withdrawing pyruvate and glutamine (Figure 3.7C). NAD^+, which is used as a substrate in the TCA cycle, was able to rescue the decrease in TXNIP induction caused by withdrawing pyruvate and glutamine (Figure 3.8A). Finally, we treated HeLa cells with CHX and the ETC inhibitors metformin (ETC complex I inhibitor) or oligomycin (ATP synthase inhibitor). Inhibiting oxidative phosphorylation disrupted CHX-driven TXNIP induction (Figure 3.7D). Together these data demonstrate the importance of the TCA cycle and oxidative phosphorylation in protein synthesis inhibition-driven TXNIP expression.

We next determined how protein synthesis inhibition affects mtATP. We

expressed a mitochondrial-targeted ATP FRET-biosensor (Mit-ATEAM) in HeLa cells and used live cell imaging to quantify fluorescence. CHX treatment caused massive cell death (data not shown) and could not be used for these experiments. Instead we used a different protein synthesis inhibitor, Rocaglamide A (RocA), which targets the elongation-initiation factor EIF4A. RocA induces TXNIP expression to the same degree as CHX (Figure 3.9A). Inhibiting protein synthesis by RocA lead to increased FRET signal indicating accumulation of ATP in the mitochondria (Figure 3.9B). We next used siRNA to deplete levels of ATP5I, an essential component of the ATP synthase. This prevented CHX-driven TXNIP expression (Figure 3.9C). Together these data suggest that protein synthesis inhibition triggers the MondoA/TXNIP axis by increasing mitochondria ATP synthesis.

3.3.5. Elongation initiation and the MondoA/TXNIP axis

Dysregulation of mRNA translation is a hallmark of cancer and is induced by numerous oncogenes (Ali et al. 2017). Eukaryotic translation initiation factors (eIFs) are commonly overexpressed in cancer and several oncogenes converge on the activation of eIFs (Ali et al., 2017). It is therefore thought that inhibiting elongation initiation may selectively target and eradicate cancer cells. We therefore asked whether inhibiting elongation initiation triggers the MondoA/TXNIP axis.

We knocked down EIF4E in HeLa cells using siRNA. EIF4E depletion led to an increase in TXNIP mRNA levels (Figure 3.10A). Surprisingly, TXNIP protein levels dramatically increased as well (Figure 3.10B). This suggests that TXNIP may undergo cap-independent translation. Consistent with this, it was recently shown that TXNIP

undergoes both cap-dependent and IRES-mediated translation (Lampe et al., 2018). Considering that TXNIP is induced by inhibiting elongation initiation, and that translation of TXNIP occurs in a cap-independent manner, we hypothesized that drugs targeting elongation initiation would induce both TXNIP mRNA and protein.

Rocaglates are a class of phytochemicals that selectively kill cancer cells, the most common being Rocaglamide A (RocA). RocA targets EIF4A and converts it to a sequence-selective translation inhibitor by increasing EIF4A/mRNA affinity and blocking scanning of the preinitiation complex (Iwasaki et al., 2016). Low nanomolar-doses of RocA induced TXNIP expression in HeLa cells (Figure 3.10C), which led to a decrease in glucose uptake (Figure 3.11B). RocA also drove an increase in TXNIP protein levels in the triple-negative breast cancer cells (TNBC) cell lines MDA-MB-157 and MDA-MB-231 (Figure 3.10D).

We next asked whether the MondoA/TXNIP axis is required for RocA to suppress growth. Using shRNAs, we blunted TXNIP expression in MDA-MB-157 cells. We then treated cells with 100 nM RocA for three days and determined relative cell viability using crystal violet staining. We observed that TXNIP knock down protected MDA-MB-157 cells from growth suppression by RocA (Figure 3.10E). In line with this finding, TXNIP$^{-/-}$ MEFs were also less susceptible to RocA than wild type MEFs (Figure 3.12A). These findings demonstrate that the MondoA/TXNIP axis is required for RocA-induced growth suppression.

3.3.6. MondoA/TXNIP in a RocA-induced stress response

We next determined the role of MondoA/TXNIP in the growth suppression initiated by RocA treatment. Using CRISPR/Cas9 genome editing we knocked out MondoA and TXNIP in HeLa cells (Figure 3.13A). We next conducted mRNA-sequencing on cells treated with RocA to determine the differentially regulated genes for each cell type. MondoA and TXNIP are responsible for 23% and 16% of the RocA-dependent gene expression signature, respectively (Figure 3.13B). As expected TXNIP was highly induced by RocA and its expression was highly dependent on MondoA (Figure 3.13C). ARRDC4 induction was less robust but was also MondoA-dependent (Figure 3.13C). By comparing the Log_2Fold-Change for each cell type we identified a novel MondoA/TXNIP regulated gene, Ras-related Associated with Diabetes (RRAD; Figures 3.13C-E), which was induced upon treatment with RocA in HeLa but not in HeLa:MondoA-KO and HeLa:TXNIP-KO cells (Figures 3.13C-E). RRAD is a negative regulator of glycolysis and may work collaboratively with TXNIP and ARRDC4 to suppress glycolysis following RocA treatment (Casey et al., 2008; Liu et al., 2015; Shang et al., 2016; Yan et al., 2016; Zhang et al., 2014).

3.4. Discussion

The ribosome is centrally situated to process and transmit information throughout the cell. Translational flux is tightly linked to nutrient availability, yet how the ribosome conveys the need for increased nutrients has remained unknown. Here we describe a mechanism by which the protein synthesis exerts control over the MondoA/TXNIP axis and glucose uptake.

We and others previously showed that the MondoA/TXNIP axis is tightly linked to metabolic reprogramming. MondoA simultaneously senses glucose and mtATP through the production of G6P by mitochondria-bound hexokinase (see Chapter 2). Here we show that a blockade in protein synthesis leads to metabolic rewiring, including an increase in mtATP synthesis and overall levels of G6P, leading to activation of the MondoA/TXNIP axis.

The anticancer translation inhibitor RocA drove an increase in TXNIP protein levels and a decrease in glucose uptake. We showed that the MondoA/TXNIP axis is a critical component of the growth suppressive properties of RocA. This is consistent with our finding that constitutive TXNIP expression in TNBC patient derived xenografts suppresses tumor growth *in vivo* (data not shown). These finding illustrate that activating the MondoA/TXNIP axis may have clinical benefit in suppressing tumor growth, and that RocA may be a way to achieve this. Importantly, protein synthesis inhibitors appear to drive TXNIP expression regardless of the oncogenic insult. The *in vivo* effects of RocA on the MondoA/TXNIP axis and its role in cytotoxicity remain to be determined.

We determined the RocA-induced, MondoA-dependent changes in gene expression. This analysis revealed that TXNIP and ARRDC4 are the most highly MondoA-dependent genes following RocA treatment. Our findings here indicate that MondoA/TXNIP axis controls a significant portion of the adaptive response to protein synthesis inhibition. By examining the lists for dysregulated transcripts that showed dependence on MondoA or TXNIP, we identified RRAD as a potential target.

In conclusion our studies showed that protein synthesis regulates the MondoA/TXNIP axis. Inhibiting protein synthesis rewires metabolism. Further

experiments will be needed to determine the mechanism by which MondoA senses G6P.

3.5. Experimental procedures

3.5.1. Cell culture

Cells were incubated at 37 °C in 5% CO2. DMEM with penicillin/streptomycin and 10% FBS (Gibco) was used for murine embryonic fibroblasts, HeLa, MDA-MB-231, L6, C2C12 and 293T (all from ATCC) and MDA-MB-157 cells (a gift from Andrea Bild, University of Utah). $TSC2^{-/-}$ and $TSC2^{-/-}$:hTSC2 MEFs are a gift of Brendan Manning, Harvard University. $MondoA^{-/-}$ MEFs were created from Day 15 embryos as described previously (Stoltzman et al., 2011).

3.5.2. Plasmids

pcDNA3.1-MondoA-V5, pcDNA3-Mlx-FLAG, LXSH-MondoA, and LXSH-MondoA(I766P) as well as TXNIP promoter luciferase reporter plasmids (wild type and ChoRE mutant) were described (Sans et al., 2006; Stoltzman et al., 2011). pcDNA3-Mit-ATEAM (pcDNA3-mitAT1.03) was a gift of Hiroyuki Noji, Rikkyo University (Imamura et al., 2009). pLKO.1-shScrm and pLKO.1-shTXNIP were obtained from Sigma Aldrich. Standard molecular cloning techniques were used to generate pLVX-TetOne-Puro-MYC(T58A). Transfections were performed using Lipofectamine 2000 (Thermo Fisher) or Lipofectamine 3000 (Thermo Fisher).

3.5.3. Protein synthesis inhibitor treatments

Media was replaced with glucose-free DMEM with penicillin/streptomycin and 10% FBS for six hours. Media was then replaced with glucose-free DMEM with penicillin/streptomycin, 10% FBS, and translation inhibitors for 16 hours. Unless otherwise indicated, compounds were added at the following concentration: Cycloheximide (Sigma Aldrich), 50 μg/ml; emetine (Sigma Aldrich), 50 μg/ml; puromycin (Sigma Aldrich), 100 μg/ml; and Rocaglamide A (Santa Cruz), 25-100 nM. Serum dialysis experiment?

3.5.4. Quantitative real-time PCR

Total RNA was extracted using the RNAeasy Kit (Qiagen). cDNA was synthesized from 0.1-1 μg RNA using GoScript reverse transcription kit (Promega). qPCR was performed using OneTaq Hot Start DNA Polymerase (Heidelberger et al., 1957), SYBR/ROX Combo PCR DNA Fluorescence Dye (Thermo Fisher) and dNTPs (Thermo Fisher).

3.5.5. Immunofluorescence

Cells were transfected with plasmids containing MondoA-V5 and FLAG-Mlx using Lipofectamine 2000 (Thermo Fisher). Following treatment, cells were fixed on glass coverslips using ice-cold 100% methanol for 15 minutes, following which we followed standard immunofluorescence procedures. Mouse anti-V5 (Thermo Fisher) antibody was used at 1:2000, rabbit anti-FLAG (Cell Signaling) antibody was used at 1:2000,

3.5.6. Metabolomics

GC-MS was used to determine metabolite levels as described previously (Chapter 2). Five biological replicates were used for each treatment type.

3.5.7. Chromatin immunoprecipitation

MondoA-V5 was transfected into cells. Chromatin was cross-linked and sheared as in Peterson et al. 2010. Chromatin was incubated overnight with anti-V5 antibody (Thermo Fisher) or mouse IgG (Sigma Aldrich). M-280 sheep anti-mouse Dynabeads (Thermo Fisher) were used to capture and purify immunocomplexes. DNA was purified using a QIAquick PCR Purification Kit (Qiagen) and analyzed using quantitative PCR as described above. Primers were previously described (Shen et al., 2015).

3.5.8. Promoter activity assay

TXNIP promoter luciferase assays were performed as described previously (Stoltzman et al., 2008).

3.5.9. FRET

Widefield microscopy was used to conduct live cell imaging on cells expressing Mit-ATEAM as described previously (Chapter 2).

3.5.10. Immunoblotting

Immunoblotting was performed as described previously (Kaadige et al., 2015). Primary antibodies were used at a dilution of 1:1000 anti-MLXIP (Proteintech, 13614-1-

AP), 1:2000 anti-VDUP1 (MBL, K0205-3), 1:15,000 anti-Tubulin (Molecular Probes, 236-10501) and 1:1,000 anti-EIF4E (BioLegend, 693002). Secondary were used at a dilution of 1:5000 anti-rabbit (GE Life Sciences, NA-934) and 1:15,000 anti-mouse (GE Life Sciences, NA-931).

3.5.11. Cell viability assay

Crystal violet was used to determine relative cell viability/proliferation as described previously (Chapter 2).

3.5.12. Statistical methods

Data represents the mean ± S.D. for five biological replicates for metabolomics experiments and three biological replicates for all other experiments. ANOVA was performed to determine significance.

3.6. References

Abdelsaid, M.A., Matragoon, S., and El-Remessy, A.B. (2013). Thioredoxin-interacting protein expression is required for VEGF-mediated angiogenic signal in endothelial cells. Antioxid Redox Signal *19*, 2199-2212.

Ali, M.U., Ur Rahman, M.S., Jia, Z., and Jiang, C. (2017). Eukaryotic translation initiation factors and cancer. Tumour Biol *39*, 1010428317709805.

Carleton, J.B., Berrett, K.C., and Gertz, J. (2017). Multiplex Enhancer Interference Reveals Collaborative Control of Gene Regulation by Estrogen Receptor alpha-Bound Enhancers. Cell Syst *5*, 333-344 e335.

Carroll, P.A., Diolaiti, D., McFerrin, L., Gu, H., Djukovic, D., Du, J., Cheng, P.F., Anderson, S., Ulrich, M., Hurley, J.B*., et al.* (2015). Deregulated Myc requires MondoA/Mlx for metabolic reprogramming and tumorigenesis. Cancer Cell *27*, 271-285.

Casey, W.M., Brodie, T., Yoon, L., Ni, H., Jordan, H.L., and Cariello, N.F. (2008). Correlation analysis of gene expression and clinical chemistry to identify biomarkers of

skeletal myopathy in mice treated with PPAR agonist GW610742X. Biomarkers *13*, 364-376.

Cermelli, S., Jang, I.S., Bernard, B., and Grandori, C. (2014). Synthetic lethal screens as a means to understand and treat MYC-driven cancers. Cold Spring Harb Perspect Med *4*, 1-18.

Chen, J., Jing, G., Xu, G., and Shalev, A. (2014). Thioredoxin-interacting protein stimulates its own expression via a positive feedback loop. Mol Endocrinol *28*, 674-680.

Dang, C.V. (2013). MYC, metabolism, cell growth, and tumorigenesis. Cold Spring Harb Perspect Med *3*, 1-13.

DeBalsi, K.L., Wong, K.E., Koves, T.R., Slentz, D.H., Seiler, S.E., Wittmann, A.H., Ilkayeva, O.R., Stevens, R.D., Perry, C.G., Lark, D.S.*, et al.* (2014). Targeted metabolomics connects thioredoxin-interacting protein (TXNIP) to mitochondrial fuel selection and regulation of specific oxidoreductase enzymes in skeletal muscle. J Biol Chem *289*, 8106-8120.

Elgort, M.G., O'Shea, J.M., Jiang, Y., and Ayer, D.E. (2010). Transcriptional and Translational Downregulation of Thioredoxin Interacting Protein Is Required for Metabolic Reprogramming during G(1). Genes Cancer *1*, 893-907.

Evan, G., and Littlewood, T. (1998). A matter of life and cell death. Science *281*, 1317-1322.

Evan, G.I., Wyllie, A.H., Gilbert, C.S., Littlewood, T.D., Land, H., Brooks, M., Waters, C.M., Penn, L.Z., and Hancock, D.C. (1992). Induction of apoptosis in fibroblasts by c-myc protein. Cell *69*, 119-128.

Heidelberger, C., Chaudhuri, N.K., Danneberg, P., Mooren, D., Griesbach, L., Duschinsky, R., Schnitzer, R.J., Pleven, E., and Scheiner, J. (1957). Fluorinated pyrimidines, a new class of tumour-inhibitory compounds. Nature *179*, 663-666.

Herwig, R., Hardt, C., Lienhard, M., and Kamburov, A. (2016). Analyzing and interpreting genome data at the network level with ConsensusPathDB. Nat Protoc *11*, 1889-1907.

Hsieh, A.L., and Dang, C.V. (2016). MYC, metabolic synthetic lethality, and cancer. Recent Results Cancer Res *207*, 73-91.

Hui, S.T., Andres, A.M., Miller, A.K., Spann, N.J., Potter, D.W., Post, N.M., Chen, A.Z., Sachithanantham, S., Jung, D.Y., Kim, J.K.*, et al.* (2008). Txnip balances metabolic and growth signaling via PTEN disulfide reduction. Proc Natl Acad Sci U S A *105*, 3921-3926.

Imamura, H., Nhat, K.P., Togawa, H., Saito, K., Iino, R., Kato-Yamada, Y., Nagai, T., and Noji, H. (2009). Visualization of ATP levels inside single living cells with fluorescence resonance energy transfer-based genetically encoded indicators. Proc Natl Acad Sci U S A *106*, 15651-15656.

Iwasaki, S., Floor, S.N., and Ingolia, N.T. (2016). Rocaglates convert DEAD-box protein eIF4A into a sequence-selective translational repressor. Nature *534*, 558-561.

Kaadige, M.R., Looper, R.E., Kamalanaadhan, S., and Ayer, D.E. (2009). Glutamine-dependent anapleurosis dictates glucose uptake and cell growth by regulating MondoA transcriptional activity. Proc Natl Acad Sci U S A *106*, 14878-14883.

Kaadige, M.R., Yang, J., Wilde, B.R., and Ayer, D.E. (2015). MondoA-Mlx transcriptional activity is limited by mTOR-MondoA interaction. Mol Cell Biol *35*, 101-110.

Kamburov, A., Stelzl, U., Lehrach, H., and Herwig, R. (2013). The ConsensusPathDB interaction database: 2013 update. Nucleic Acids Res *41*, D793-800.

Lampe, S., Kunze, M., Scholz, A., Brauss, T.F., Winslow, S., Simm, S., Keller, M., Heidler, J., Wittig, I., Brune, B.*, et al.* (2018). Identification of the TXNIP IRES and characterization of the impact of regulatory IRES trans-acting factors. Biochim Biophys Acta *1861*, 147-157.

Li, F., Wang, Y., Zeller, K.I., Potter, J.J., Wonsey, D.R., O'Donnell, K.A., Kim, J.W., Yustein, J.T., Lee, L.A., and Dang, C.V. (2005). Myc stimulates nuclearly encoded mitochondrial genes and mitochondrial biogenesis. Mol Cell Biol *25*, 6225-6234.

Link, J.M., Ota, S., Zhou, Z.Q., Daniel, C.J., Sears, R.C., and Hurlin, P.J. (2012). A critical role for Mnt in Myc-driven T-cell proliferation and oncogenesis. Proc Natl Acad Sci U S A *109*, 19685-19690.

Liu, J., Zhang, C., Wu, R., Lin, M., Liang, Y., Liu, J., Wang, X., Yang, B., and Feng, Z. (2015). RRAD inhibits the Warburg effect through negative regulation of the NF-kappaB signaling. Oncotarget *6*, 14982-14992.

Martineau, Y., Muller, D., and Pyronnet, S. (2014). Targeting protein synthesis in cancer cells. Oncoscience *1*, 484-485.

Minn, A.H., Hafele, C., and Shalev, A. (2005). Thioredoxin-interacting protein is stimulated by glucose through a carbohydrate response element and induces beta-cell apoptosis. Endocrinology *146*, 2397-2405.

Parmenter, T.J., Kleinschmidt, M., Kinross, K.M., Bond, S.T., Li, J., Kaadige, M.R., Rao, A., Sheppard, K.E., Hugo, W., Pupo, G.M.*, et al.* (2014). Response of BRAF-mutant melanoma to BRAF inhibition is mediated by a network of transcriptional regulators of glycolysis. Cancer Discov *4*, 423-433.

Peterson, C.W., Stoltzman, C.A., Sighinolfi, M.P., Han, K.S., and Ayer, D.E. (2010). Glucose controls nuclear accumulation, promoter binding, and transcriptional activity of the MondoA-Mlx heterodimer. Mol Cell Biol *30*, 2887-2895.

Ren, Y., Shi, Y., Wang, Y., Li, Y., Wu, S., Li, H., Zhang, Y., and Duan, H. (2010). p38 MAPK pathway is involved in high glucose-induced thioredoxin interacting protein induction in mouse mesangial cells. FEBS Lett *584*, 3480-3485.

Sans, C.L., Satterwhite, D.J., Stoltzman, C.A., Breen, K.T., and Ayer, D.E. (2006). MondoA-Mlx heterodimers are candidate sensors of cellular energy status: mitochondrial localization and direct regulation of glycolysis. Mol Cell Biol *26*, 4863-4871.

Santagata, S., Mendillo, M.L., Tang, Y.C., Subramanian, A., Perley, C.C., Roche, S.P., Wong, B., Narayan, R., Kwon, H., Koeva, M.*, et al.* (2013). Tight coordination of protein translation and HSF1 activation supports the anabolic malignant state. Science *341*, 1238303.

Shang, R., Wang, J., Sun, W., Dai, B., Ruan, B., Zhang, Z., Yang, X., Gao, Y., Qu, S., Lv, X.*, et al.* (2016). RRAD inhibits aerobic glycolysis, invasion, and migration and is associated with poor prognosis in hepatocellular carcinoma. Tumour Biol *37*, 5097-5105.

Shen, L., O'Shea, J.M., Kaadige, M.R., Cunha, S., Wilde, B.R., Cohen, A.L., Welm, A.L., and Ayer, D.E. (2015). Metabolic reprogramming in triple-negative breast cancer through Myc suppression of TXNIP. Proc Natl Acad Sci U S A *112*, 5425-5430.

Stoltzman, C.A., Kaadige, M.R., Peterson, C.W., and Ayer, D.E. (2011). MondoA senses non-glucose sugars: regulation of thioredoxin-interacting protein (TXNIP) and the hexose transport curb. J Biol Chem *286*, 38027-38034.

Stoltzman, C.A., Peterson, C.W., Breen, K.T., Muoio, D.M., Billin, A.N., and Ayer, D.E. (2008). Glucose sensing by MondoA:Mlx complexes: a role for hexokinases and direct regulation of thioredoxin-interacting protein expression. Proc Natl Acad Sci U S A *105*, 6912-6917.

White-Gilbertson, S., Kurtz, D.T., and Voelkel-Johnson, C. (2009). The role of protein synthesis in cell cycling and cancer. Mol Oncol *3*, 402-408.

Wu, N., Zheng, B., Shaywitz, A., Dagon, Y., Tower, C., Bellinger, G., Shen, C.H., Wen, J., Asara, J., McGraw, T.E.*, et al.* (2013). AMPK-dependent degradation of TXNIP upon energy stress leads to enhanced glucose uptake via GLUT1. Mol Cell *49*, 1167-1175.

Yan, Y., Xie, M., Zhang, L., Zhou, X., Xie, H., Zhou, L., Zheng, S., and Wang, W. (2016). Ras-related associated with diabetes gene acts as a suppressor and inhibits Warburg effect in hepatocellular carcinoma. Onco Targets Ther *9*, 3925-3937.

Zhang, C., Liu, J., Wu, R., Liang, Y., Lin, M., Liu, J., Chan, C.S., Hu, W., and Feng, Z. (2014). Tumor suppressor p53 negatively regulates glycolysis stimulated by hypoxia through its target RRAD. Oncotarget *5*, 5535-5546.

Figure 3.1. TXNIP induction by protein synthesis inhibitors
Heatmaps representing TXNIP mRNA levels relative to (**A**) EF2 kinase in skin tissues (GTEx), and (**B**) EIF4G1 (elongation initiation), RRP12 (ribosomal biogenesis) and RRP1 (ribosomal biogenesis) in breast cancer (TCGA). Pearson and Spearman correlation statistics are reported below. (**C**) TXNIP mRNA levels in HeLa cells following treatment with CHX (50 μg/mL) or Torin (250 nM). TXNIP mRNA levels after CHX treatment of (**D**) normal or HRAS(G12V)-transformed MEFs, (**E**) $TSC2^{-/-}$ MEFs expressing empty vector or human-TSC2. Cells were treated with 50 μg/mL CHX for 16 hours. (**F**) TXNIP mRNA levels in HeLa cells after treatment with the translation elongation inhibitors CHX (50 μg/mL), emetine (50 μg/mL) and puromycin (100 μg/mL).

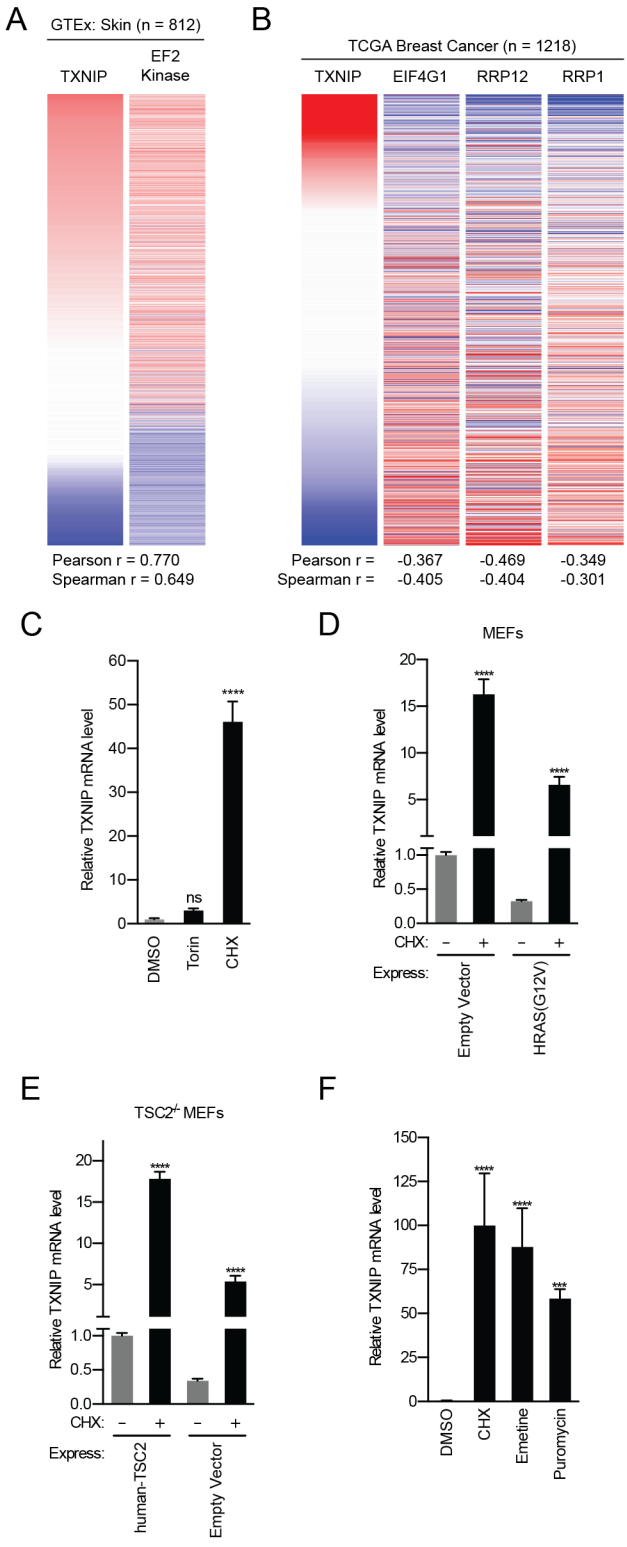
A
GTEx: Skin (n = 812)
TXNIP
EF2 Kinase
Pearson r = 0.770
Spearman r = 0.649
B
TCGA Breast Cancer (n = 1218)
TXNIP
EIF4G1
RRP12
RRP1
Pearson r = -0.367 -0.469 -0.349
Spearman r = -0.405 -0.404 -0.301
C
Relative TXNIP mRNA level
ns
****
DMSO
Torin
CHX
D
MEFs
Relative TXNIP mRNA level
CHX:
Express:
Empty Vector
HRAS(G12V)
E
TSC2-/- MEFs
Relative TXNIP mRNA level
CHX:
Express:
human-TSC2
Empty Vector
F
Relative TXNIP mRNA level
***
DMSO
CHX
Emetine
Puromycin

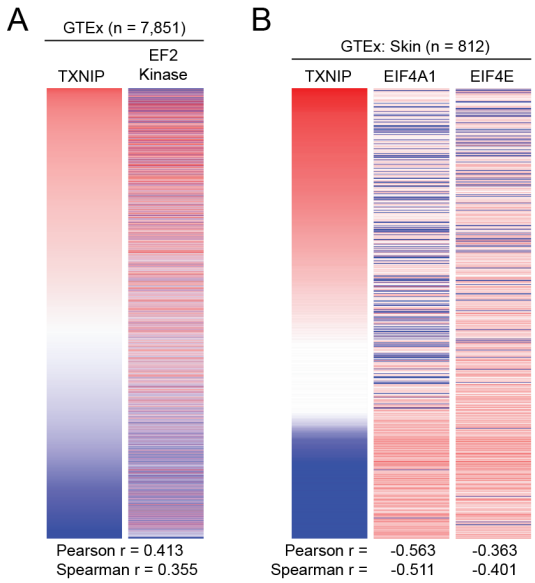

Figure 3.2. Supplement: TXNIP expression correlates with genes that control mRNA translation

Heatmaps representing mRNA levels of TXNIP relative to (**A**) EF2 kinase (GTEx: all tissues), and (**B**) EIF4A1 and EIF4E (GTEx: skin). Pearson and Spearman correlation statistics are reported below.

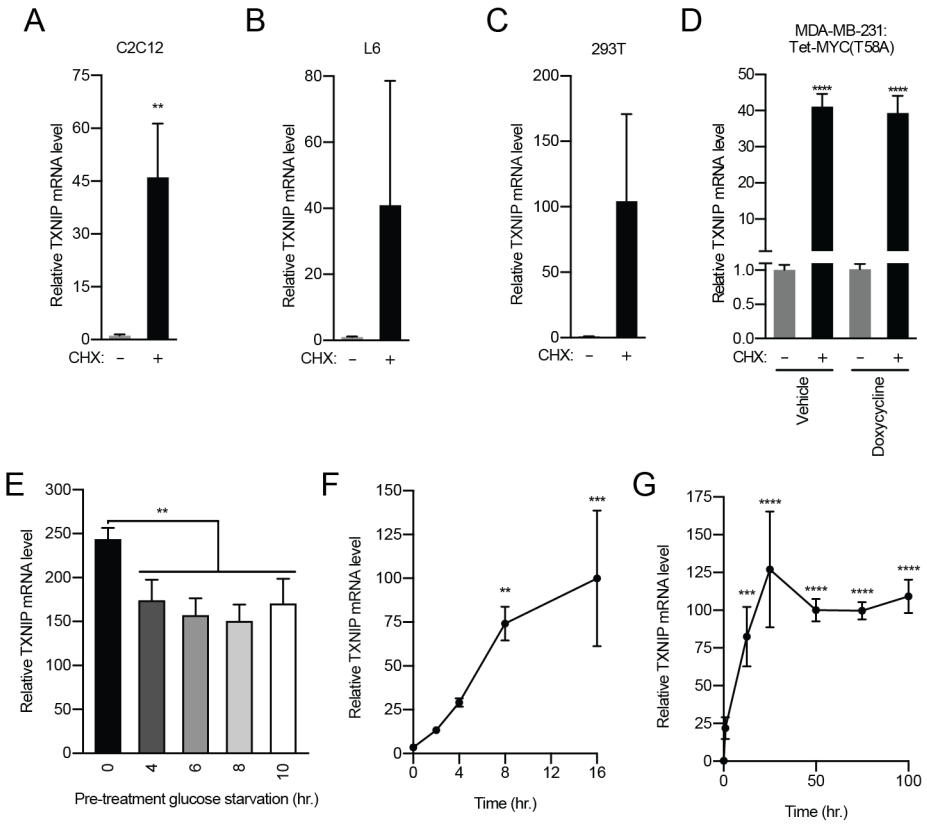

Figure 3.3. Supplement: Protein synthesis inhibitors induce TXNIP expression
TXNIP mRNA levels following CHX treatment of (**A**) C2C12 mouse myoblasts, (**B**) L6 rat myoblasts, (**C**) 293T embryonic kidney cells, and (**D**) MDA-MB-231 expressing tet-inducible MYC(T58A) with or without doxycycline. TXNIP mRNA levels following CHX treatment of HeLa cells with varying (**E**) pretreatment glucose-starvation time, (**F**) treatment time, (**G**) CHX concentration.

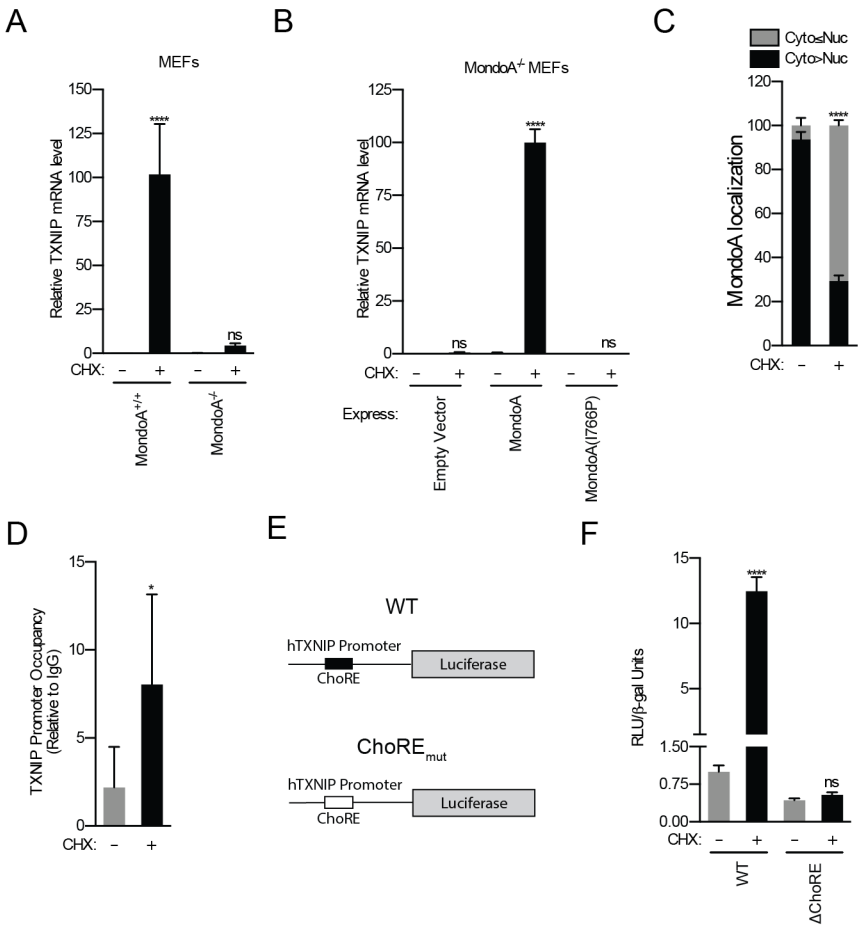

Figure 3.4. Protein synthesis inhibition drives MondoA transcriptional activity
TXNIP mRNA levels following CHX treatment of (**A**) MondoA$^{+/+}$ and MondoA$^{-/-}$ MEFs, and (**B**) MondoA$^{-/-}$ MEFs expressing empty vector, MondoA or MondoA(I766P). Notably, MondoA(I766P) cannot interact with its obligate partner Mlx. (**C**) Immunofluorescence was used to assess the localization of MondoA in response to CHX. (**D**) Depiction of TXNIP-promoter luciferase reporter constructs. Wild type or ChoRE$_{mut}$ TXNIP promoter was directly upstream of TXNIP. (**E**) HeLa cells expressing luciferase constructs were treated with CHX for 16 hours. One hour prior to assessing cells for luciferase activity, we washed out CHX by replacing media with glucose-free DMEM. This allowed for translation of accumulated luciferase message. (**F**) Chromatin-immunoprecipitation was used to determine the enrichment of MondoA on the TXNIP promoter in response to CHX.

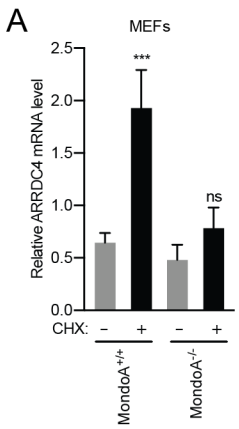

Figure 3.5. Supplement: Protein synthesis inhibition drives MondoA transcriptional activity
(A) ARRDC4 mRNA levels following CHX treatment of MondoA$^{+/+}$ and MondoA$^{-/-}$ MEFs.

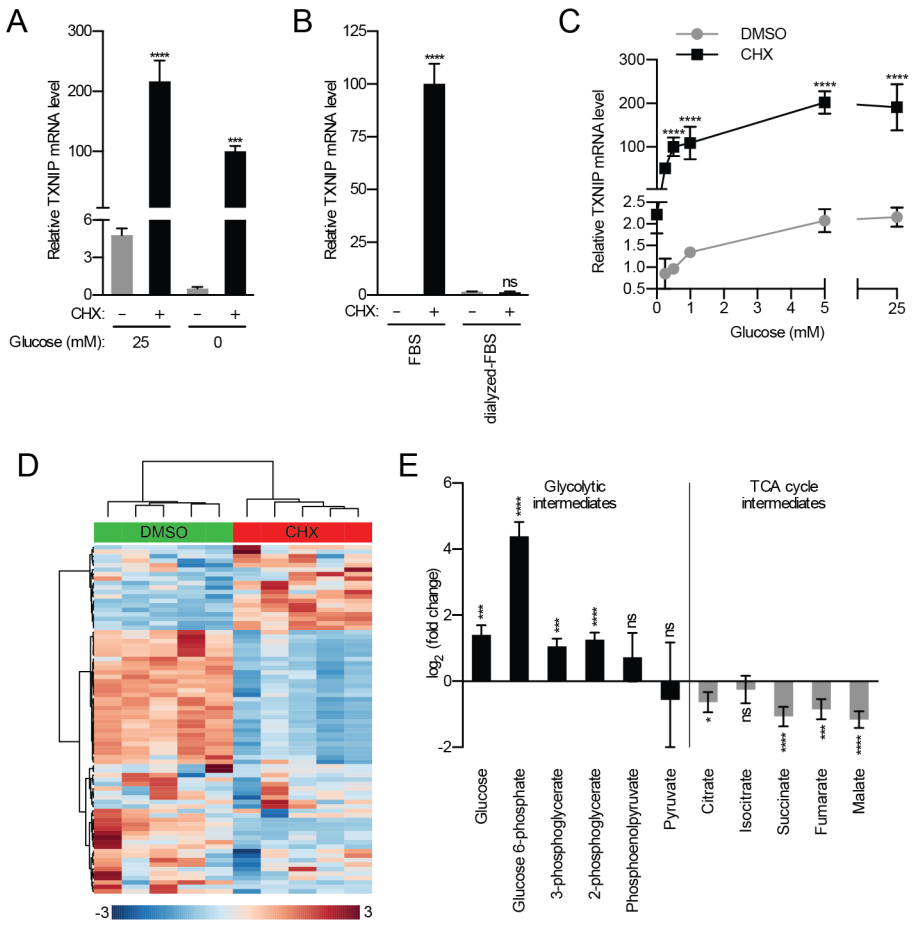

Figure 3.6. Metabolic rewiring after treatment with protein synthesis inhibitors
Prior to treatment with protein synthesis inhibitors, cells were starved of glucose for six hours. This ensure that TXNIP levels were at a minimum. We then measured TXNIP mRNA levels in HeLa cells treated with CHX in (**A**) DMEM or glucose-free DMEM + 10% FBS, (**B**) glucose-free DMEM + 10% FBS or dialyzed FBS, and (**C**) glucose-free DMEM + 10% dialyzed FBS + varying amounts of glucose. (**D**) GC-MS was used to assess metabolite levels in HeLa cells treated with CHX. Of note, CHX has a broad impact on all metabolic pathways we analyzed. (**E**) Log_2(fold change) of glycolytic and TCA cycle intermediates from HeLa cells treated with CHX (relative to DMSO treatment).

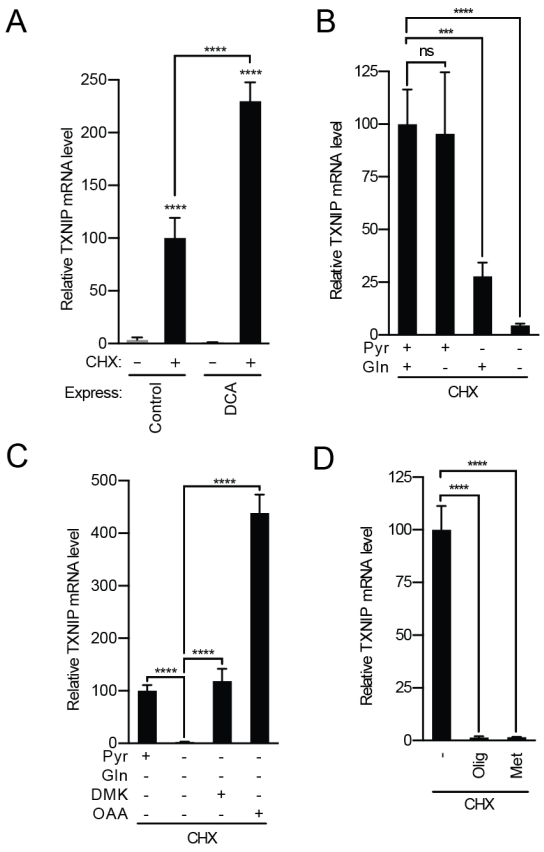

Figure 3.7. CHX-driven TXNIP expression requires the TCA cycle
(**A**) TXNIP mRNA levels in HeLa cells treated with CHX and dichloroacetic acid (DCA), which inhibits PDH kinase, thus enhancing pyruvate metabolism in the TCA cycle. TXNIP mRNA levels in HeLa cells treated with CHX in (**B**) glucose-free DMEM with or without pyruvate and glutamine, and (**C**) glucose-free DMEM without pyruvate or glutamine, and supplemented with dimethyl-α-ketoglutarate (DMK) and oxaloacetate (OAA). (**D**) TXNIP mRNA levels in HeLa cells treated with CHX and electron transport chain inhibitors metformin (Met) and oligomycin (Olig).

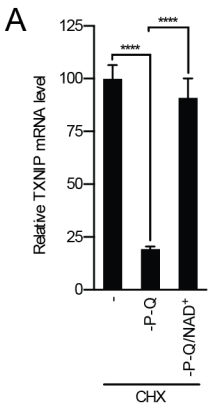

Figure 3.8. Supplement: CHX-driven TXNIP expression requires TCA cycle
(A) TXNIP mRNA levels following CHX treatment of HeLa cells in glucose-free DMEM, glucose-free DMEM without pyruvate (P) or glutamine (Q), glucose-free DMEM without pyruvate or glutamine supplemented with NAD^+ (4mM).

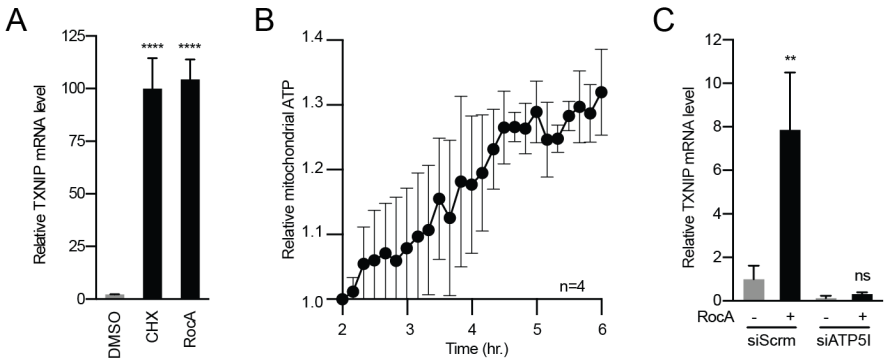

Figure 3.9. Protein synthesis inhibition drives mitochondrial ATP synthesis
(A) TXNIP mRNA levels following treatment of HeLa cells with CHX or Rocaglamide A (RocA, 100 nM). (**B**) A mitochondrial-targeted ATP FRET biosensor (Mit-ATEAM) was used to determine mtATP levels in HeLa cells treated with the protein synthesis inhibitor Rocaglamide A. TXNIP mRNA levels in HeLa cells treated with CHX and (**C**) TXNIP mRNA levels following CHX treatment of HeLa cells with siSCRM or siATP5I.

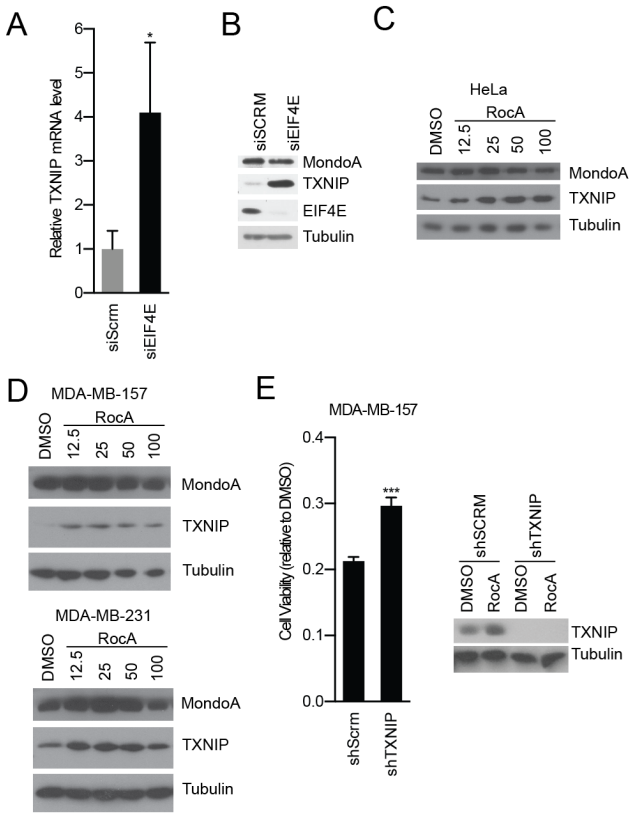

Figure 3.10. TXNIP is a key feature of cytotoxicity elicited by protein synthesis inhibition

HeLa cells treated with siEIF4E and the impact on (**A**) TXNIP mRNA and (**B**) protein levels. Immunoblot showing TXNIP protein levels following RocA treatment of (**C**) HeLa cells and (**D**) the triple-negative breast cancer cell lines MDA-MB-157 and MDA-MB-231. (**E**) MDA-MB-157 cells were generated to express control scrambled shRNA (shScrm) or shTXNIP. Cells were then treated with RocA for two days following which cell viability was analyzed by crystal violet.

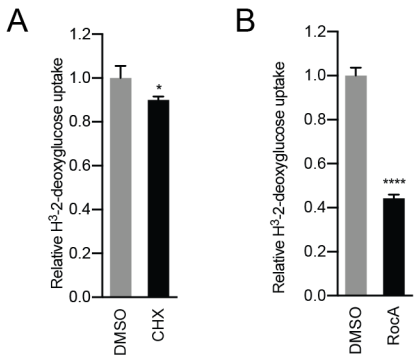

Figure 3.11. Supplement: Protein synthesis inhibition restricts glucose uptake. Glucose uptake in HeLa cells treated with (**A**) CHX and (**B**) RocA.

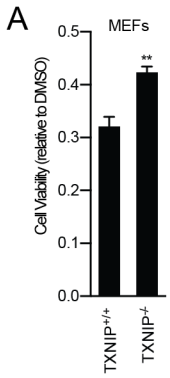

Figure 3.12. Supplement: TXNIP is a key feature of cytotoxicity elicited by protein synthesis inhibition.
$TXNIP^{+/+}$ or $TXNIP^{-/-}$ MEFS were treated with RocA for two days then cell viability was analyzed by crystal violet.

Figure 3.13. Protein synthesis inhibitors initiate a MondoA/TXNIP-dependent stress response.
(**A**) Immunoblot of HeLa cells in which MondoA and TXNIP have been knocked out using CRISPR/Cas9. (**B**) RNA-sequencing was conducted for HeLa, HeLa:MondoA-KO and HeLa:TXNIP-KO cells treated with RocA. Shown above is a venn-diagram indicating overlap in differentially regulated genes (log_2(fold change) of at least 2). Of note, MondoA and TXNIP are necessary for about 11% and 25% of gene expression induced by RocA respectively. Plots showing log_2FC for HeLa cells compared to (**C**) log_2FC for HeLa:MondoA-KO cells and (**D**) log_2FC for HeLa:TXNIP-KO cells. TXNIP, ARRDC4 and RRAD are indicated. (**E**) Data tracks showing the aligned reads for RRAD in HeLa, HeLa:MondoA-KO and HeLa:TXNIP-KO cells treated with DMSO or RocA. (**F**) Schematic depicting the effects of protein synthesis on mitochondria metabolism and MondoA activity. During protein synthesis inhibition, the mitochondrial ATP is increase and its export from the mitochondria drives the synthesis of G6P by mitochondria-linked hexokinase. G6P signals to MondoA to translocate to the nucleus and drive expression of TXNIP and other stress-responsive genes.

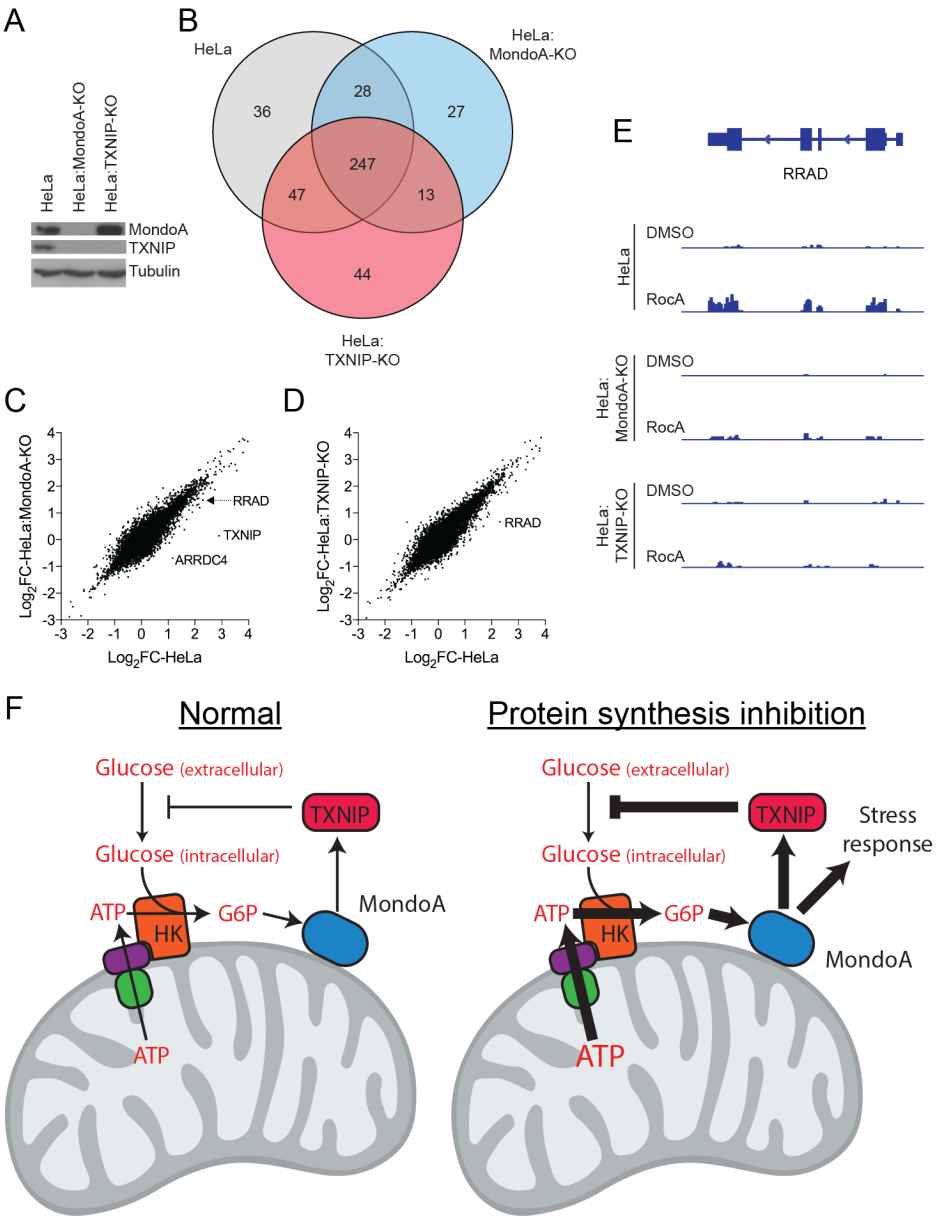
A
HeLa
HeLa:MondoA-KO
HeLa:TXNIP-KO
MondoA
TXNIP
Tubulin
B
HeLa
HeLa: MondoA-KO
HeLa: TXNIP-KO
36
28
27
247
47
13
44
C
Log2FC-HeLa:MondoA-KO
Log2FC-HeLa
RRAD
TXNIP
ARRDC4
D
Log2FC-HeLa:TXNIP-KO
Log2FC-HeLa
RRAD
E
RRAD
HeLa
DMSO
RocA
HeLa: MondoA-KO
DMSO
RocA
HeLa: TXNIP-KO
DMSO
RocA
F
Normal
Protein synthesis inhibition
Glucose (extracellular)
TXNIP
Glucose (intracellular)
ATP
HK
G6P
MondoA
ATP
Glucose (extracellular)
TXNIP
Stress response
Glucose (intracellular)
ATP
HK
G6P
MondoA
ATP

CHAPTER 4

THE MONDOA-DEPENDENT TRANSCRIPTOME

4.1. Abstract

MondoA is a basic helix-loop-helix leucine zipper (bHLH-Zip) transcription factor that drives expression of thioredoxin-interacting protein (TXNIP). We recently demonstrated that Myc is a transcriptional repressor of TXNIP expression, and that Myc and MondoA compete for a binding site in the TXNIP promoter. While Myc-dependent transcription has been well-studied, little is known about the full complement of genes regulated by MondoA. Further, it is known that TXNIP can play a role in transcription, yet specific genes that TXNIP regulates are unknown. Here we use CRISPR/Cas9 editing and next-generation sequencing to address these questions. We observed significant overlap in the genes that are differentially regulated by MondoA and TXNIP, therefore, we suggest that MondoA requires TXNIP for its transcriptional activity. We show that Myc/MondoA competition extends to thousands of sites across the genome, and specifically characterize the reciprocal regulation of electron transport chain biogenesis. During Myc overexpression, loss of MondoA sensitized cells to apoptosis. Thus, by antagonizing Myc transcriptional activity, MondoA acts as a safeguard against Myc-driven cell death.

4.2. Introduction

MondoA is a bHLH-Zip transcription factor that senses and controls metabolic states of the cell. Mechanistically, MondoA senses high levels of glucose-6-phosphate (G6P) and responds by translocating to the nucleus where it controls transcription of genes involved in nutrient homeostasis. The most well-characterized MondoA target gene is thioredoxin-interacting protein (TXNIP), a negative regulator of glucose uptake. Thus,

MondoA and TXNIP form an axis that senses and regulates glucose uptake.

We previously showed that in triple-negative breast cancer (TNBC) Myc-drives aerobic glycolysis at least in part by suppressing TXNIP expression. MondoA and Myc compete for a binding site in the TXNIP promoter and thus, differentially regulate its expression (Shen et al., 2015). Consistent with our findings in TNBC, Myc/MondoA antagonism also occurs in $BRAF^{V600E}$ melanomas (Parmenter et al., 2014). However, in neuroblastoma and Myc-overexpressing B-cell leukemia, Myc and MondoA cooperate to drive expression of target genes (Carroll et al., 2015). Further studies are needed to determine the mechanisms by which MondoA and Myc compete and cooperate.

Little is known about the other genes that MondoA regulates. TXNIP expression is highly, if not entirely dependent on MondoA in nearly all extra-hepatic tissues, yet other MondoA target genes are not as straightforward. Other MondoA-regulated genes are appear to be context specific. For example, while in kidney epithelial (HA1ER) cells, MondoA downregulates MYC (Stoltzman et al., 2008), in triple-negative breast cancer, MondoA doesn't have any apparent control over MYC expression (Figure 4.1A). Identifying a common set of MondoA-regulated genes will provide new insight into how Myc and MondoA coordinate the use and availability of nutrients.

We used CRISPR/Cas9 to generate clonal TNBC cell lines that had loss of MondoA or TXNIP expression. Using mRNA-sequencing, we determined that MondoA and TXNIP loss results in similar transcriptional profiles. We propose that MondoA requires TXNIP for its transcriptional activity. Additionally, we observed that MondoA loss led to increased Myc-dependent transcription and increased sensitivity to cells to Myc-driven cell death. We conducted a complete evaluation of the sites in the genome

that MondoA binds in quiescence and in the G1 phase of the cell cycle. We observed reciprocal binding of Myc and MondoA at the same sites during G0 and G1. Our findings demonstrate a wide-spread antagonism between MondoA and Myc in controlling gene expression.

4.3. Results

We generated cell lines that did lack expression of MondoA and TXNIP using CRISPR/Cas9 editing. In short, for each gene we coexpressed CRISPR/Cas9 and three sgRNAs (from the GeCKO v2 library). The CRISPR/Cas9 plasmid also contained GFP as a marker for transfection efficiency. We used fluorescence-assisted sorting to collect cells with the highest GFP expression. Cell clones were derived from single cells and screened for expression of MondoA and TXNIP using RT-qPCR and immunoblotting. We identified multiple clonal colonies that did not express MondoA or TXNIP (Figure 4.1A). As expected, loss of MondoA abolished TXNIP expression illustrating the necessity of MondoA for TXNIP expression (Stoltzman et al., 2008).

4.3.1. MondoA transcriptional activity requires TXNIP

In order to determine the consequence of MondoA and TXNIP loss on transcription, we conducted mRNA-sequencing on three clones for each knock-out type (231:MondoA-KO and 231:TXNIP-KO). We used principal component analysis to predict transcriptional variation for each clone. Both 231:MondoA-KO and 231:TXNIP-KO clones clustered away from parental MDA-MB-231 cells (Figure 4.1B). 231:TXNIP-KO clones 1 and 3 clustered with all three 231:MondoA-KO clones, suggesting that the

transcriptional profiles may be similar. We observed very little variance among two biological replicates of MDA-MB-231, demonstrating the fitness of the mRNA-sequencing data.

We next used DESeq2 to quantify expression as fragments per kilobase of transcript per million mapped reads (FPKM) and fold changes relative to MDA-MB-231. Using a threshold of $\log_2(\text{fold change}) \geq 1$, we identified 1256 and 1139 genes that were differentially regulated in 231:MondoA-KO and 231:TXNIP-KO clones, respectively, of which 844 were differentially regulated in both cell types (Figures 4.1C-E). Notably, we only considered genes that had an adjusted p-value of at least 20. We used RT-qPCR to validate the differential expression of several genes (data not shown).

We next performed Gene Set Enrichment Analysis (GSEA) using gene sets derived from differentially regulated genes from either 231:MondoA-KO or 231:TXNIP-KO cells. 231:MondoA-KO cells showed enrichment for both TXNIP upregulated and downregulated genes (Figure 4.1F). Similarly, 231:TXNIP-KO cells showed enrichment for both MondoA upregulated and downregulated genes (Figure 4.1G). Further, the degree to which genes are regulated in 231:MondoA-KO and 231:TXNIP-KO cells is similar (Figure 4.1H). Finally, we also observed significant overlap in differentially regulated genes from HeLa cells with loss of MondoA or TXNIP (Figure 4.1I). Together these findings indicate that loss of MondoA or TXNIP leads to highly similar gene expression profiles.

The high degree of similarity in gene expression between the 231:MondoA-KO and 231:TXNIP-KO led us to hypothesize that TXNIP positively regulates MondoA transcriptional activity. To address this model, we expressed exogenous TXNIP in

231:MondoA-KO1 and 231:TXNIP-KO1 cells (Figure 4.2A). In 231:MondoA-KO cells, exogenous expression of TXNIP had no effect on the expression of FOXA2, PGF and INHBB, indicating that TXNIP alone is not sufficient to regulate these genes (Figures 4.2B-4.2D). However, when TXNIP was expressed in 231:TXNIP-KO, we observed a restoration of FOXA2, PGF and INHBB expression. These results demonstrate that both MondoA and TXNIP are necessary for the regulation of a set of genes, and that TXNIP alone is not sufficient to control these genes. This suggests that MondoA and TXNIP cooperate in transcriptional regulation. This is consistent with the findings of Chen et al. showing that TXNIP regulates its own expression (Chen et al., 2014). Preliminary data from our lab suggests that TXNIP is necessary for nucleocytoplasmic shuttling of MondoA (data not shown). Because glucose controls the nucleocytoplasmic shuttling of MondoA, we propose that TXNIP plays a role in the nutrient-sensing by MondoA. A model that might explain this finding is that as TXNIP is downregulated, cells undergo a shift from oxidative metabolism to aerobic glycolysis. This results in decreased mtATP production, thus restricting MondoA transcriptional activity (Figure 4.2E).

4.3.2. MondoA and Myc antagonism

We recently showed that Myc is a transcriptional repressor of TXNIP, likely by competing with MondoA for a shared binding site in the TXNIP promoter (Shen et al., 2015). We sought to identify other genes that Myc and MondoA regulate antagonistically. We therefore analyzed our mRNA-sequencing data to determine how MondoA loss affects Myc-dependent transcription. We used GSEA to compare our mRNA-sequencing data to Myc target genes. Using the 231:MondoA-KO dataset, we

observed enrichment for Myc upregulated and downregulated genes (Figure 4.3A), suggesting that Myc transcription activity was enhanced at both upregulated and downregulated genes. Consistent with our findings showing that MondoA requires TXNIP (Chapter 4.3.1), 231:TXNIP-KO cells are also enriched for Myc regulated gene expression (Figure 4.3B). Using the differentially regulated genes identified in the analyses described above, we generated MondoA and TXNIP gene sets. These gene sets included the top 100 upregulated and downregulated genes for each genotype. We then compared the gene sets to multiple Myc-overexpression datasets obtained from GEO (GSE5823; Cappellen et al., 2007). Myc overexpression in MDA-MB-231, MCF7 and HeLa cells led to enrichment of MondoA and TXNIP regulated genes (Figures 4.3C and 4.3D and data not shown). Collectively these results demonstrate the opposing regulation of gene expression by MondoA and Myc (Figures 4.3E).

We next determined genome occupancy for Myc and MondoA during quiescence (G0) and the G1 phase of the cell cycle. Previously, we showed that MondoA transcriptional activity is high during G0 and low during G1, and conversely Myc expression and transcriptional activity is low during G0 and high during G1 (Elgort et al., 2010; Shen et al., 2015). We starved MDA-MB-231 cells of serum for 72 hours to ensure all cells entered G0. Serum was added back to some of the samples, and six hours later cells were harvested and chromatin-immunoprecipitation sequencing (ChIP-sequencing) was used to determine the genome occupancy of MondoA, Myc and PolII. Antibodies against endogenous MondoA, Myc and Polymerase II (PolII) were used to pulldown transcription factor/DNA complexes. DNA was purified, processed for sequencing, amplified and processed on an Illumina HiSeq 50. Sequencing reads were aligned to

genomic build hg19. Reads were normalized to input DNA and peaks were identified using MACS2. Peaks were identified using from the G0 MondoA ChIP and the G0 Myc ChIP, which we called "MondoA-bound" and "Myc-bound" regions, respectively. We identified significantly more Myc-bound regions than MondoA-bound regions (Figures 4.4 and 4.5); however, we recognized that MondoA is enriched at Myc-bound regions, but to a lesser extent. For both Myc-bound and MondoA-bound regions, Myc binding was increased during G1 and decreased during G0. Conversely, MondoA binding was increased during G0 and decreased during G1. We identified several regions where MondoA and Myc were both enriched, which we called "cobound regions." Meme analysis by John O'Shea showed enrichment for ChoRE-like sequences at the cobound regions (data not shown). This reciprocal binding by MondoA and Myc is further evidence that MondoA and Myc competitively regulate the same genes.

We next sought to characterize Myc/MondoA antagonism in a biological pathway. Myc is a master regulator of mitochondrial and ETC biogenesis (Dang, 2013; Li et al., 2005). Given that MondoA and Myc control many of the same genes, we hypothesized that MondoA also regulates ETC biogenesis. We conducted GSEA using mRNA-sequencing data from above, and observed increased expression of ETC genes in 231:MondoA-KO cells (Figure 4.6A). We used RT-qPCR to verify the results of the mRNA-sequencing (Figure 4.6B). Using the ChIP-sequencing data described above, we determined whether MondoA binds to ETC gene promoters. We observed enrichment for both MondoA and Myc on ETC gene promoters, suggesting that MondoA is a direct negative-regulator of ETC biogenesis (Figure 4.6C). Finally, we extended these findings to another cell type. We used gene expression data obtained from HeLa:MondoA-KO

cells (described in Chapters 2 and 3) and found that loss of MondoA in HeLa cells also lead to an enrichment of ETC genes (Figure 4.6D). These data suggest that Myc and MondoA competitively regulate ETC biogenesis.

Finally, we sought to determine the biological impact of Myc/MondoA antagonism. While the oncogenic effects of Myc are to drive cell growth and proliferation, in certain circumstances Myc overexpression drives cell death (Cermelli et al., 2014; Evan and Littlewood, 1998; Evan et al., 1992). Because it stimulates biosynthetic pathways, Myc innately drives metabolic stress by depleting nutrients. Myc requires other adaptions to counter the metabolic stress and support cell survival. When one or more of those adaptations are lost, the cell undergoes Myc-driven apoptosis (Myc synthetic lethality; Figure 4.7A). Yet loss of some adaptations only sensitizes cells to Myc synthetic lethality. One adaptation to high Myc activity is to activate transcription factors that target the same genes as Myc. For example, Mnt regulates Myc target genes in the opposite direction of Myc, and loss of Mnt leads to Myc synthetic lethality (Link et al., 2012). We therefore hypothesized that MondoA loss sensitizes cells to Myc-driven cell death. Further, we reasoned that synthetic lethality would be more evident as Myc levels and transcriptional activity increased (Figure 4.7B).

In order to test this hypothesis, we expressed Myc fused to estrogen-receptor (ER-Myc) in MDA-MB-231, 231:MondoA-KO and 231:TXNIP-KO cells. ER-Myc is constitutively cytoplasmic, yet when cells are treated with 4-hydroxytamoxifin (4OHT), ER-Myc translocates to the nucleus and is transcriptionally active (Figure 4.7C). Using a cell proliferation assay, we determined the response to 4OHT treatment relative to nontreated cells. We observed a decrease in 231:MondoA-KO cell viability compared to

MDA-MB-231 cells (Figure 4.7D). This suggests that MondoA is critical for cells to adapt to high Myc levels. The specific target genes MondoA that regulates to counter Myc synthetic lethality remains to be investigated. Further, it will be important to determine whether this result extend to other cell types. ER-Myc does not restrict cell viability in 231:TXNIP-KO cells as it does in 231:MondoA-KO cells (Figure 4.7D). While the gene expression profiles of 231:MondoA-KO and 231:TXNIP-KO cells are highly similar, this result illustrates the importance of nonoverlapping functions of the two cell types.

4.3.3. MondoA and TXNIP in tumorigenesis

Our gene expression and genome occupancy data suggest that MondoA and TXNIP act as tumor suppressors in TNBC. We sought to verify this idea using *in vivo* tumor growth assays. We injected MDA-MB-231, 231:MondoA-KO and 231:TXNIP-KO cells into the cleared mammary fat pad in NOD/SCID mice (Figure 4.8A). We tracked tumor growth over the next several weeks, then harvested tumors and analyzed for size and morphology. Surprisingly, loss of MondoA or TXNIP led to significant decreases in tumor size (Figure 4.8B).

We next determined how gene expression contributes to this decrease in tumor size. We therefore conducted mRNA-sequencing on MDA-MB-231, 231:MondoA-KO and 231:TXNIP-KO tumors. After aligning reads to the genome, we used DESeq2 to determine the differentially regulated genes. In this analysis, we also included MDA-MB-231, 231:MondoA-KO and 231:TXNIP-KO samples from tissue culture (Chapter 4.3.1). Hierarchical clustering and principle component analysis showed that MDA-MB-231

deviated from 231:MondoA-KO and 231:TXNIP-KO to a much greater extent in the tumors than in cell culture (Figures 4.9A and 4.9B). Consistent with this finding using a cutoff of $\log_2$(fold-change) ≥ 0.585, we observed about a three-fold increase in the number of differentially regulated genes in the 231:MondoA-KO and 231:TXNIP-KO relative to MDA-MB-231 tumor samples (data not shown). Consistent with what we observed in tissue culture, tumors derived from 231:MondoA-KO and 231:TXNIP-KO cells had similar transcriptional profiles (Figures 4.9A and 4.9B and data not shown). We conducted pathway analysis on the genes that are differentially regulated in tumors after MondoA loss. There was a significant enrichment for pathways involving interferon signaling, HDAC1/HDAC2 function and KRAS activity (Figure 4.9C). Functional studies will be needed to determine whether dysregulation of interferon, HDACs and/or KRAS are responsible for the decrease in tumorigenesis.

We compared differentially regulated genes from 231:MondoA-KO tumors, 231:MondoA-KO cells in culture and human mammary epithelial cells expressing an shRNA against MondoA. Using a log (fold change) ≥ 0.585, we observed 72 genes that overlapped in all three groups (Figure 4.9D). We conducted pathway analysis on these 72 genes and observed enrichment for interferon signaling, p63 activity, glutathione metabolism, selenium regulation, cell cycling and arachidonic acid metabolism. How these differentially regulated genes or pathways contribute to loss of tumorigenesis upon MondoA loss remains to be explored.

4.4 Discussion

Outlined in this Chapter is the impact that loss of MondoA or TXNIP has on TNBC transcription and tumorigenesis. We demonstrated that MondoA and TXNIP have similar transcriptional profiles. Given the finding that TXNIP is essential for its own transcription (Chen et al., 2014), we have proposed a model in which TXNIP supports MondoA transcriptional activity. TXNIP loss is sufficient to drive glucose uptake and aerobic glycolysis (Hui et al., 2008; Kaadige et al., 2009; Wu et al., 2013). We propose that TXNIP deletion in MDA-MB-231 of Hela cells drives a shift from oxidative metabolism to aerobic glycolysis. This shift reduces levels of mtATP, which is necessary to activate MondoA transcriptional activity (see Chapter 2).

Loss of MondoA or TXNIP led to increased expression of electron transport chain (ETC) and mRNA translation genes and decreased expression of genes involved in MAPK and VEGF signaling (Figure 4.1E). These findings were consistent with published reports showing that VEGF signaling requires TXNIP (Abdelsaid et al., 2013); MAPK signaling requires TXNIP (Ren et al., 2010); and TXNIP is necessary for proper control of mitochondrial metabolism and oxidative phosphorylation (DeBalsi et al., 2014). The MondoA/TXNIP axis is controlled by ETC (Chapter 2), mRNA translation (Chapter 3), and MAPK signaling (Elgort et al., 2010), leading us to propose that the MondoA/TXNIP axis is involved in feedback regulation of these diverse processes. ETC gene upregulation is also paradoxical with the increase in glucose uptake and aerobic glycolysis observed when MondoA and TXNIP are lost (Hui et al., 2008; Kaadige et al., 2009; Wu et al., 2013). We propose that the upregulation of ETC genes is required to accommodate the increased glucose uptake and metabolism.

We also expanded our understanding of Myc/MondoA antagonism by showing that it occurs at hundreds of genes. We demonstrated that Myc and MondoA compete in the regulation of ETC biogenesis. Conceptually, because the MondoA/TXNIP axis senses mitochondrial ATP (see Chapters 2 and 3) the negative regulation of ETC biogenesis by MondoA, establishes a negative feedback loop. As carbons enter the TCA cycle and fuel ETC-mediated ATP synthesis, MondoA becomes transcriptionally active and 1) restricts glucose uptake and flux of carbons into mitochondrial metabolism driving expression of TXNIP, and 2) directly downregulate nuclear-encoded ETC genes. Finally, we showed that in conditions where Myc is overexpressed, MondoA is necessary to counter Myc-driven apoptosis, indicating an essential role for MondoA in Myc-driven tumorigenesis. This is consistent with our reports demonstrating that in some cancers Myc and MondoA antagonistically regulate the same genes, and that in tumors with high Myc expression, loss of MondoA leads to synthetic lethality (Carroll et al., 2015) Parmenter et al., 2014; Shen et al., 2015; Wilde and Ayer, 2015).

The ChIP-sequencing data showed Myc and MondoA bind the same regions in the genome in a mutually exclusive manner. Of note, for the MondoA peaks, PolII binding was offset from the MondoA/Myc binding site about 150 bp, approximately the size of one nucleosome (Figure 4.5). This result has led us to hypothesize that MondoA might act as a pioneer factor, binding to chromatin-rich regions and recruiting factors that open/close chromatin. Yet how MondoA binds and its molecular functions at these regions has yet to be addressed.

4.5. Experimental procedures

4.5.1. Cell culture

MDA-MB-231 cells and its derivative lines were incubated at 37 ºC in 5% CO_2. Cells were passaged in DMEM (Gibco) with penicillin/streptomycin (Gibco), 10% FBS (Gibco) and 1% non-essential amino acids (Gibco) using standard cell culture practices.

4.5.2. mRNA-sequencing

Total RNA was extracted from cells using a Quick RNA Miniprep Kit (Zymo Research) according to manufacturer's recommendations. mRNA was isolated and library production performed using a Stranded mRNA-Seq Kit with mRNA Capture Beads (Kapa). Library quality was analyzed using an Agilent High Sensitivity D1000 ScreenTape. Single-end sequencing for 50 cycles was performed using an Illumina HiSeq.

4.5.3. Chromatin-immunoprecipitation sequencing

Chromatin-immunoprecipitation was performed as described previously (Shen et al., 2015). Library preparation was described as described previously (Carleton et al., 2017).

4.5.4. Bioinformatic analysis

Reads were aligned to hg19 using Novoalign. DESeq2 was used to determine the number of fragments for each gene, compute a value for fragments per kilobase of the gene per million fragments read (FPKM), determine R-log transformations, calculate

log_2(fold change) for each gene, and determine an adjusted p-value. Hierarchical clustering was performed using sample-distance matrices computed by DESeq2. Principle component analysis was performed for the R-log values using the R package. Gene Set Enrichment Analysis (GSEA) was conducted using the Broad Institute's publically available GSEA application. FPKM values were compared to published and unpublished gene sets. ConsensusPathDB (Max Planck Institute for Molecular Genetics) was used to conduct overrepresentation analysis on differentially regulated genes (Herwig et al., 2016; Kamburov et al., 2013). For ChIP-sequencing, MACS2 was used to identify bound regions, and DeepTools was used to visualize the data.

4.5.5. Orthotopic xenografts

All animal procedures were reviewed and approved by the University of Utah Institutional Animal Care and Use Committee. 100,000 cells (in 100 µl matrigel) were implanted into the cleared right inguinal mammary fat pad of NOD/SCID mice between 3 and 6 weeks old. Mice were calipered for tumor growth until the largest tumor (MDA-MB-231) reached 2 cm^3, at which time all mice in the study were euthanized and analyzed for tumors. Tumor weight was analyzed relative to brain weight.

4.5.6. Reverse transcriptase quantitative PCR

Total RNA was extracted from cells using the RNAeasy Kit (Qiagen). cDNA was synthesized from 200 ng RNA using GoScript reverse transcription kit (Promega). cDNA was diluted 10-fold and qPCR was performed using OneTaq Hot Start DNA Polymerase (Heidelberger et al., 1957), SYBR/ROX Combo PCR DNA Fluorescence Dye (Thermo

Fisher) and dNTPs (Thermo Fisher).

4.5.7. Immunoblotting

Immunoblotting was performed as described previously (Kaadige et al., 2015). Primary antibodies were used at a dilution of 1:1000 anti-MLXIP (Proteintech, 13614-1-AP), 1:1000 anti-TXNIP (Abcam, ab188865), and 1:15,000 anti-Tubulin (Molecular Probes, 236-10501).

4.5.8. Cell viability/proliferation

Cells were stained using crystal violet staining solution (0.05% crystal violet, 1% formaldehyde and 1% methanol in PBS). Plates were rocked gently at room temperature for one hour. Staining solution was then aspirated and water was used to wash wells several times. 1% SDS in water was used to solubilize crystal violet and relative amount of solubilized crystal violet was determined by measuring absorbance at 590 nm.

4.5.9. Statistical methods

Significance was determined using a two-tailed student's t-test. Where applicable, one-way or two-way ANOVA was performed prior to determining significance.

4.6. References

Abdelsaid, M.A., Matragoon, S., and El-Remessy, A.B. (2013). Thioredoxin-interacting protein expression is required for VEGF-mediated angiogenic signal in endothelial cells. Antioxid Redox Signal *19*, 2199-2212.

Carleton, J.B., Berrett, K.C., and Gertz, J. (2017). Multiplex Enhancer Interference Reveals Collaborative Control of Gene Regulation by Estrogen Receptor alpha-Bound Enhancers. Cell Syst *5*, 333-344 e335.

Carroll, P.A., Diolaiti, D., McFerrin, L., Gu, H., Djukovic, D., Du, J., Cheng, P.F., Anderson, S., Ulrich, M., Hurley, J.B., *et al.* (2015). Deregulated Myc requires MondoA/Mlx for metabolic reprogramming and tumorigenesis. Cancer Cell *27*, 271-285.

Cermelli, S., Jang, I.S., Bernard, B., and Grandori, C. (2014). Synthetic lethal screens as a means to understand and treat MYC-driven cancers. Cold Spring Harb Perspect Med *4*.

Chen, J., Jing, G., Xu, G., and Shalev, A. (2014). Thioredoxin-interacting protein stimulates its own expression via a positive feedback loop. Mol Endocrinol *28*, 674-680.

Dang, C.V. (2013). MYC, metabolism, cell growth, and tumorigenesis. Cold Spring Harb Perspect Med *3*.

DeBalsi, K.L., Wong, K.E., Koves, T.R., Slentz, D.H., Seiler, S.E., Wittmann, A.H., Ilkayeva, O.R., Stevens, R.D., Perry, C.G., Lark, D.S., *et al.* (2014). Targeted metabolomics connects thioredoxin-interacting protein (TXNIP) to mitochondrial fuel selection and regulation of specific oxidoreductase enzymes in skeletal muscle. J Biol Chem *289*, 8106-8120.

Elgort, M.G., O'Shea, J.M., Jiang, Y., and Ayer, D.E. (2010). Transcriptional and Translational Downregulation of Thioredoxin Interacting Protein Is Required for Metabolic Reprogramming during G(1). Genes Cancer *1*, 893-907.

Evan, G., and Littlewood, T. (1998). A matter of life and cell death. Science *281*, 1317-1322.

Evan, G.I., Wyllie, A.H., Gilbert, C.S., Littlewood, T.D., Land, H., Brooks, M., Waters, C.M., Penn, L.Z., and Hancock, D.C. (1992). Induction of apoptosis in fibroblasts by c-myc protein. Cell *69*, 119-128.

Heidelberger, C., Chaudhuri, N.K., Danneberg, P., Mooren, D., Griesbach, L., Duschinsky, R., Schnitzer, R.J., Pleven, E., and Scheiner, J. (1957). Fluorinated pyrimidines, a new class of tumour-inhibitory compounds. Nature *179*, 663-666.

Herwig, R., Hardt, C., Lienhard, M., and Kamburov, A. (2016). Analyzing and interpreting genome data at the network level with ConsensusPathDB. Nat Protoc *11*, 1889-1907.

Hui, S.T., Andres, A.M., Miller, A.K., Spann, N.J., Potter, D.W., Post, N.M., Chen, A.Z., Sachithanantham, S., Jung, D.Y., Kim, J.K., *et al.* (2008). Txnip balances metabolic and growth signaling via PTEN disulfide reduction. Proc Natl Acad Sci U S A *105*, 3921-3926.

Kaadige, M.R., Looper, R.E., Kamalanaadhan, S., and Ayer, D.E. (2009). Glutamine-dependent anapleurosis dictates glucose uptake and cell growth by regulating MondoA transcriptional activity. Proc Natl Acad Sci U S A *106*, 14878-14883.

Kaadige, M.R., Yang, J., Wilde, B.R., and Ayer, D.E. (2015). MondoA-Mlx transcriptional activity is limited by mTOR-MondoA interaction. Mol Cell Biol *35*, 101-110.

Kamburov, A., Stelzl, U., Lehrach, H., and Herwig, R. (2013). The ConsensusPathDB interaction database: 2013 update. Nucleic Acids Res *41*, D793-800.

Li, F., Wang, Y., Zeller, K.I., Potter, J.J., Wonsey, D.R., O'Donnell, K.A., Kim, J.W., Yustein, J.T., Lee, L.A., and Dang, C.V. (2005). Myc stimulates nuclearly encoded mitochondrial genes and mitochondrial biogenesis. Mol Cell Biol *25*, 6225-6234.

Link, J.M., Ota, S., Zhou, Z.Q., Daniel, C.J., Sears, R.C., and Hurlin, P.J. (2012). A critical role for Mnt in Myc-driven T-cell proliferation and oncogenesis. Proc Natl Acad Sci U S A *109*, 19685-19690.

Parmenter, T.J., Kleinschmidt, M., Kinross, K.M., Bond, S.T., Li, J., Kaadige, M.R., Rao, A., Sheppard, K.E., Hugo, W., Pupo, G.M.*, et al.* (2014). Response of BRAF-mutant melanoma to BRAF inhibition is mediated by a network of transcriptional regulators of glycolysis. Cancer Discov *4*, 423-433.

Ren, Y., Shi, Y., Wang, Y., Li, Y., Wu, S., Li, H., Zhang, Y., and Duan, H. (2010). p38 MAPK pathway is involved in high glucose-induced thioredoxin interacting protein induction in mouse mesangial cells. FEBS Lett *584*, 3480-3485.

Shen, L., O'Shea, J.M., Kaadige, M.R., Cunha, S., Wilde, B.R., Cohen, A.L., Welm, A.L., and Ayer, D.E. (2015). Metabolic reprogramming in triple-negative breast cancer through Myc suppression of TXNIP. Proc Natl Acad Sci U S A *112*, 5425-5430.

Stoltzman, C.A., Peterson, C.W., Breen, K.T., Muoio, D.M., Billin, A.N., and Ayer, D.E. (2008). Glucose sensing by MondoA:Mlx complexes: a role for hexokinases and direct regulation of thioredoxin-interacting protein expression. Proc Natl Acad Sci U S A *105*, 6912-6917.

Wilde, B.R., and Ayer, D.E. (2015). Interactions between Myc and MondoA transcription factors in metabolism and tumourigenesis. Br J Cancer *113*, 1529-1533.

Wu, N., Zheng, B., Shaywitz, A., Dagon, Y., Tower, C., Bellinger, G., Shen, C.H., Wen, J., Asara, J., McGraw, T.E.*, et al.* (2013). AMPK-dependent degradation of TXNIP upon energy stress leads to enhanced glucose uptake via GLUT1. Mol Cell *49*, 1167-1175.

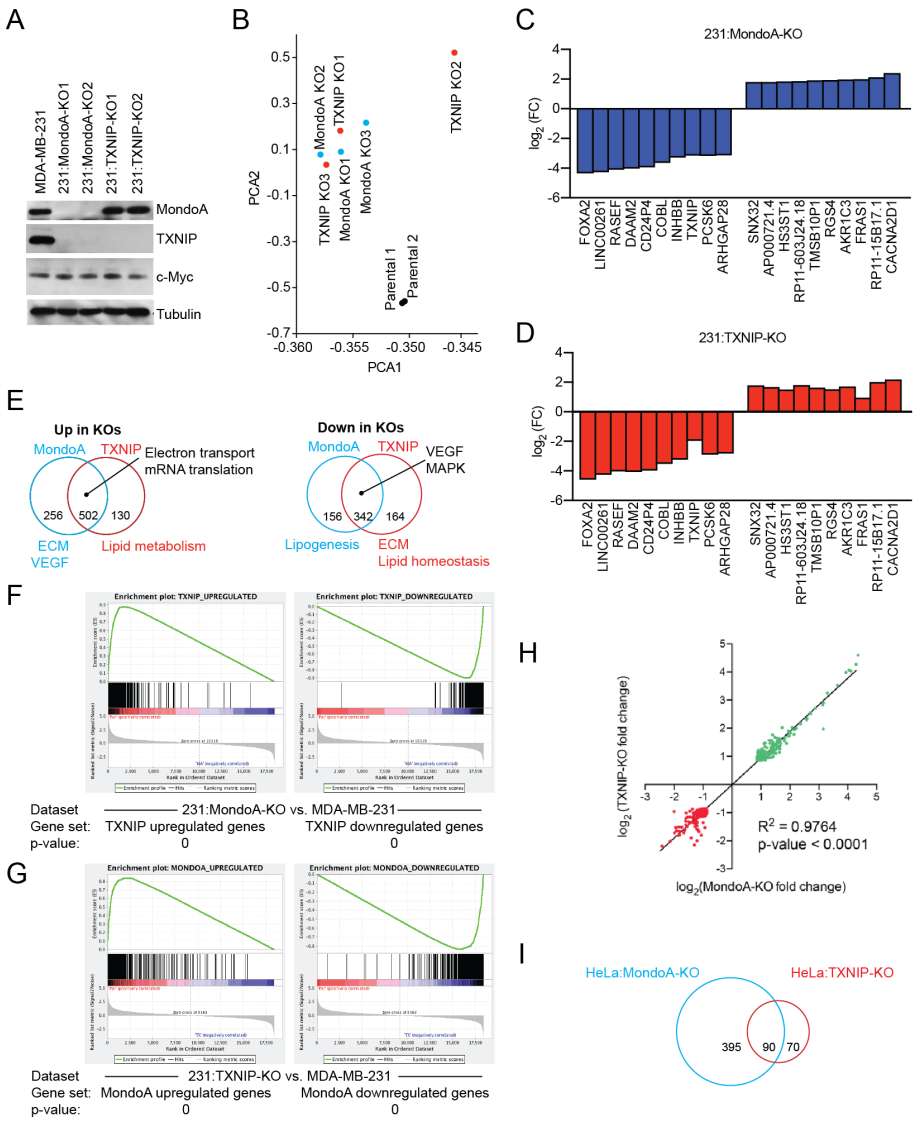

Figure 4.1. MondoA and TXNIP regulated genes
(**A**) CRISPR/Cas9 was used to generate clonal cell lines with MondoA or TXNIP loss. Immunoblot showing MondoA and TXNIP loss in MDA-MB-231, 231:MondoA-KO and 231:TXNIP-KO cells. (**B**) mRNA-sequencing was performed on parental cells and MondoA and TXNIP knockout clones. Principle component analysis showing variance among clonal colonies and parental cells. Log_2(fold changes) for several genes in (**C**) 231:MondoA-KO and (**D**) 231:TXNIP-KO cells. (**E**) Venn diagram indicating significant overlap in differentially regulated genes in 231:MondoA-KO and 231:TXNIP-KO cells. Two venn diagrams are depicted for genes upregulated in the knockout clones and genes downregulated in the knockout clones. GSEA was performed using (**F**) 231:MondoA-KO and (**G**) 231:TXNIP-KO datasets and comparing TXNIP- and MondoA-regulated genes sets, respectively. (**H**) Log_2(fold-change) in gene expression for 231:MondoA-KO cells compared to 231:TXNIP-KO cells. (**I**) Venn diagram indicating significant overlap in differentially regulated genes in HeLa:MondoA-KO and HeLa:TXNIP-KO cells.

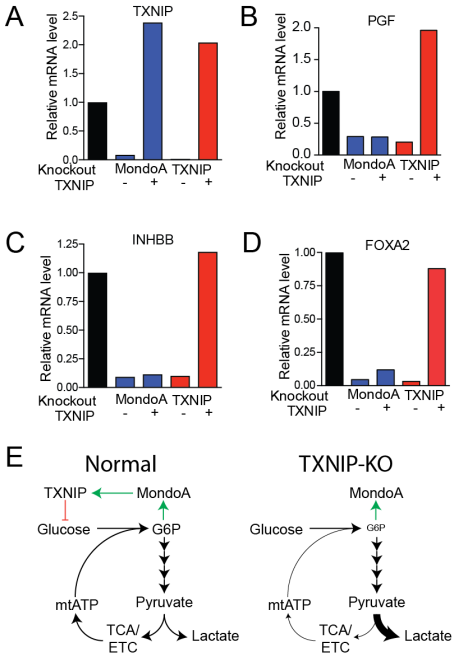

Figure 4.2. MondoA requires TXNIP
Exogenous TXNIP was expressed in 231:MondoA-KO and 231:TXNIP-KO cells. mRNA levels were determined for the MondoA/TXNIP target genes, (**A**) TXNIP, (**B**) PGF, (**C**) INHBB and (**D**) FOXA2. (**E**) Depiction of our model that supports MondoA transcriptional activity. Loss of TXNIP causes a shift from oxidative metabolism to aerobic glycolysis, leading to a decrease in mtATP production and MondoA transcriptional activity.

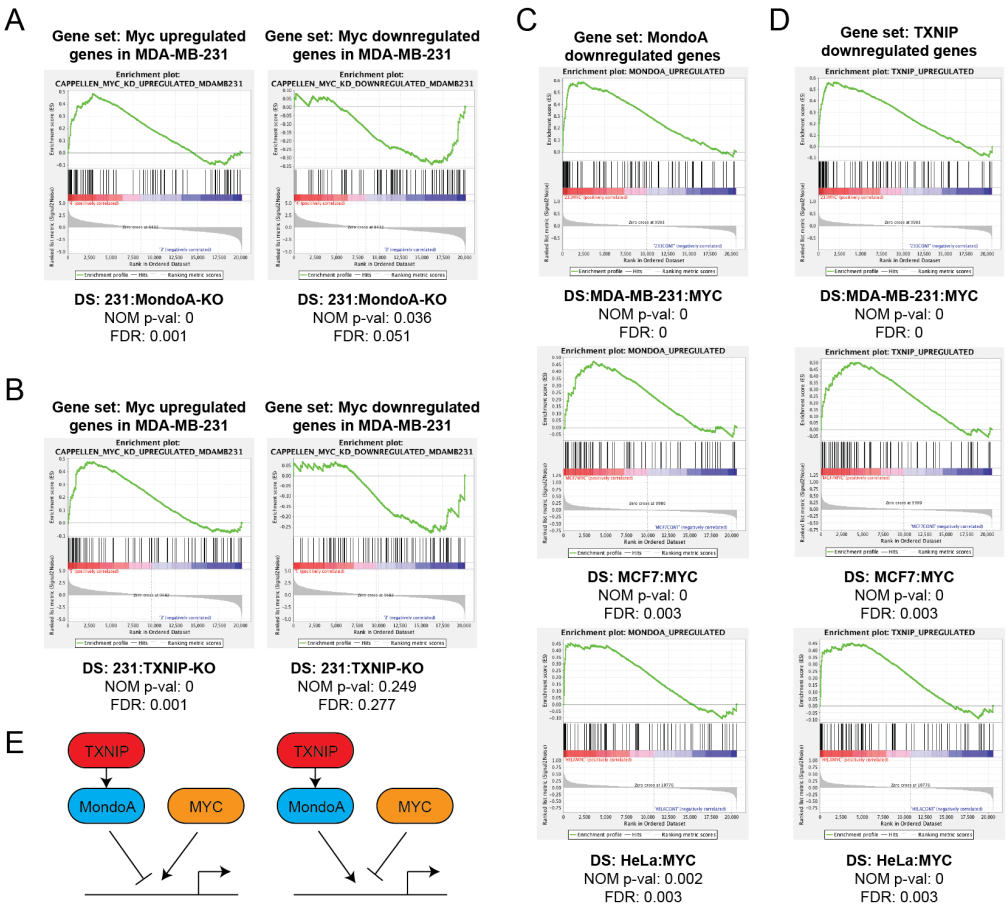

Figure 4.3. MondoA loss leads to Myc transcriptional activity
GSEA was performed using (**A**) 231:MondoA-KO and (**B**) 231:TXNIP-KO datasets and comparing Myc transcriptional regulation gene sets. GSEA was performed using (**C**) MondoA-regulated and (**D**) TXNIP-regulated gene sets compared to datasets from Myc overexpressing HeLa, MCF7 and MDA-MB-231 cells. (**E**) Schematic depicting Myc/MondoA antagonism.

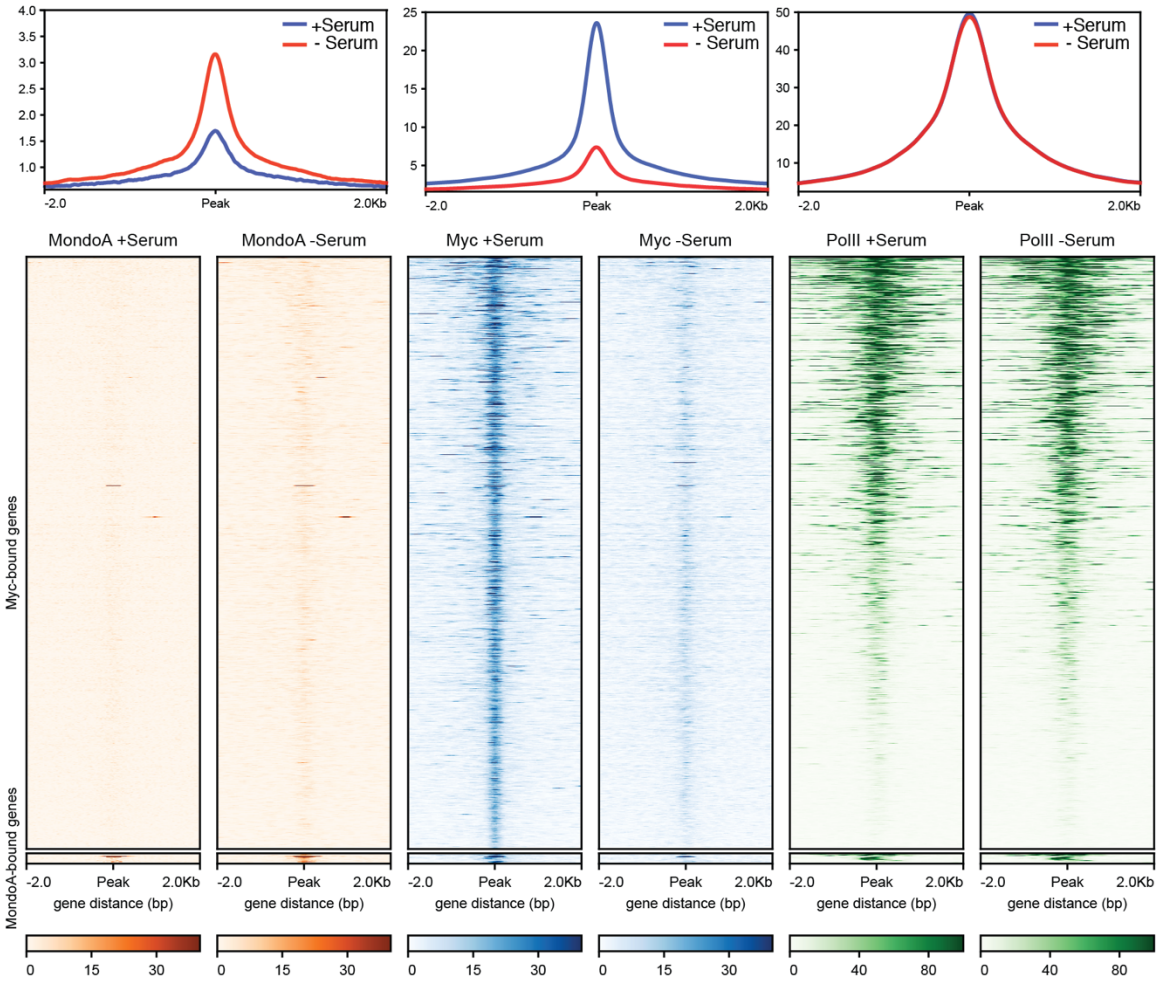

Figure 4.4. Myc and MondoA bind the same regions in the genome
ChIP-sequencing was performed on MDA-MB-231 cells in quiescence (-serum) or in the G1 phase of the cell cycle (+serum). The heatmaps shown are a depiction of abundance of MondoA (orange), Myc (blue) and PolII (green) at binding sites across the genome. The sites selected are based on enrichment over an input sample. Myc-bound genes (top) are the sites that were identified from the Myc-IP, +serum sample. MondoA-bound genes (bottom) are the sites that were identified from the MondoA-IP, -serum sample.

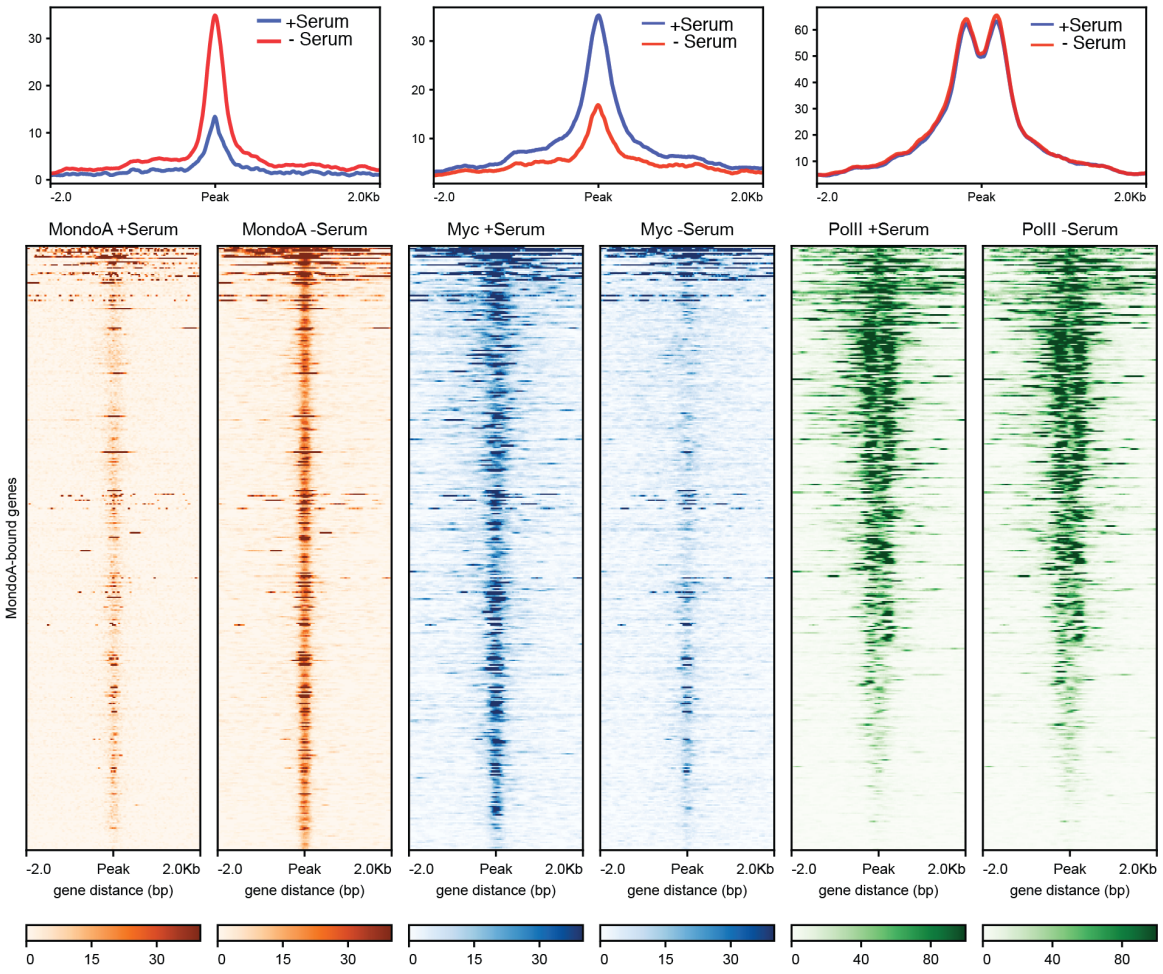

Figure 4.5. Myc and MondoA bind the same regions in the genome
ChIP-sequencing was performed on MDA-MB-231 cells in quiescence (-serum) or in the G1 phase of the cell cycle (+serum). The heatmaps shown are a depiction of abundance of MondoA (orange), Myc (blue) and PolII (green) at binding sites across the genome. The sites selected are based on enrichment over input of the MondoA-IP, -serum sample.

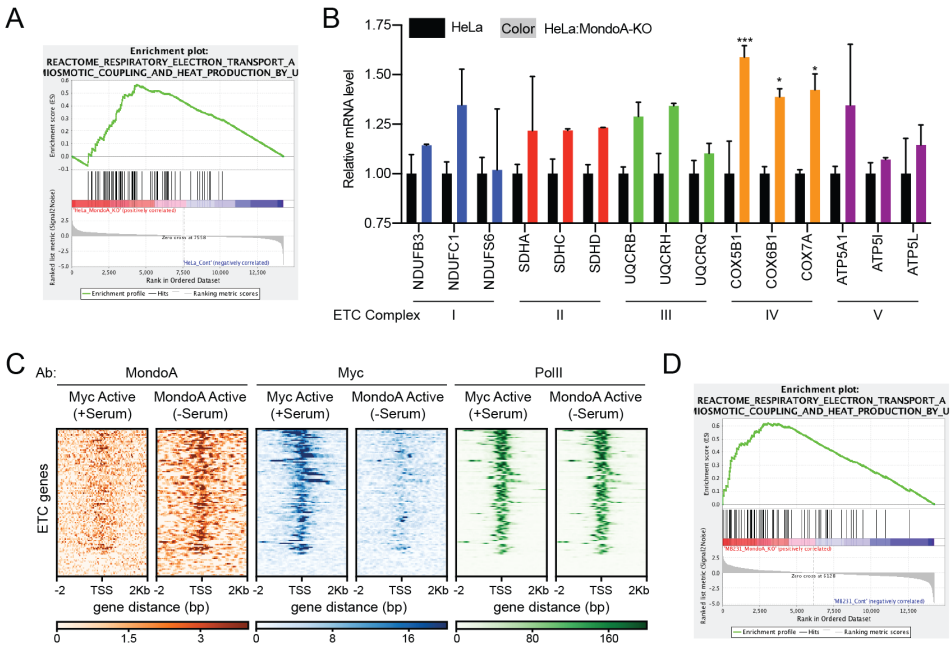

Figure 4.6. MondoA and Myc competitively regulate ETC biogenesis
(**A**) GSEA conducted for 231:MondoA-KO cell mRNA-sequencing data compared to the gene set, REACTOME_RESPIRATORY_TRANSPORT_CHEMOSMOTIC_COUPLING_AND_HEAT_PRODUCTION. (**B**) RT-qPCR for nuclear-encoded ETC genes in HeLa (black bars) and HeLa:MondoA-KO (colored bars) cells. Significantly regulated genes are indicated with asterisks. (**C**) Heatmaps shown are a depiction of abundance of MondoA (orange), Myc (blue) and PolII (green) at the promoters of nuclear-encoded ETC genes. (**D**) GSEA conducted for HeLa:MondoA-KO cell mRNA-sequencing data (Chapters 2 and 3) compared to the gene set, REACTOME_RESPIRATORY_TRANSPORT_CHEMOSMOTIC_COUPLING_AND_HEAT_PRODUCTION. * $p<0.05$; *** $p<0.001$

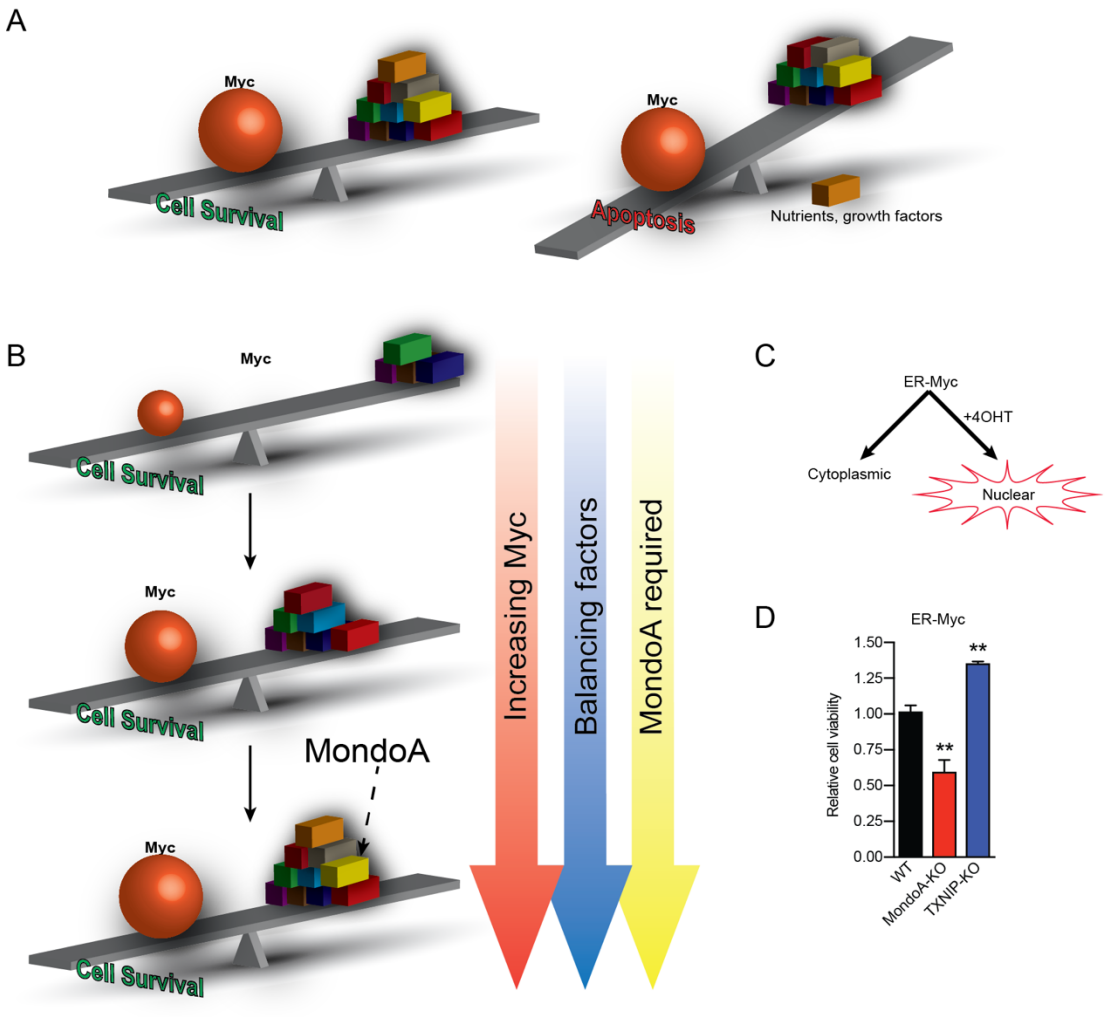

Figure 4.7. Myc synthetic lethality in MondoA-KO cells
(**A**) Depiction of the general concept of Myc synthetic lethality. Myc has several factors such as nutrients and growth factors that prevent Myc-driven apoptosis. When one or more of these factors are lost, the cells experience Myc-driven cell death. (**B**) Our model of MondoA in Myc synthetic lethality. We propose that as Myc levels increase, MondoA is required more to counter Myc transcriptional activity and Myc-driven cell death. (**C**) Depiction of how ER-Myc occurs. Briefly, ER-Myc is cytoplasmic, yet when cells are treated with 4-hydroxytamoxifin (4OHT), ER-Myc translocates to the nucleus and drives transcription. (**D**) Cell viability assay conducted after ER-Myc activation by 4OHT treatment in MDA-MB-231, 231:MondoA-KO and 231:TXNIP-KO cells.

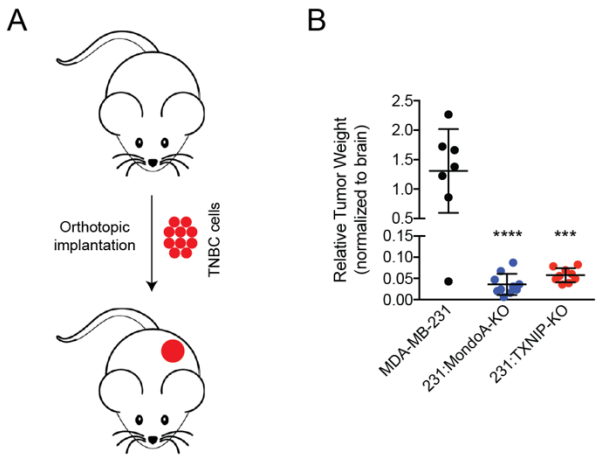

Figure 4.8. Orthotopic xenograft
(**A**) Depiction of experiment. Cells were implanted into cleared mammary fat pads. (**B**) Tumor to brain weight ratio was determined at the end of the experiment.

Figure 4.9. MondoA and TXNIP regulated gene expression *in vivo*
mRNA-sequencing was performed on tumor tissues derived from MDA-MB-231, 231:MondoA-KO and 231:TXNIP-KO cells. (A) Hierarchical clustering depicts how similar/dissimilar samples are from other samples. (B) Principle component analysis was performed to determine the level of variation in the samples. (C) Overrepresentation analysis was conducted using ConsensusPathDB. Shown here are the top most regulated pathways in response to MondoA loss. (D) Differentially regulated genes were compared to the differentially regulated genes for two other datasets: 231:MondoA-KO in cell culture (see above) and HMEC(siMondoA).

A

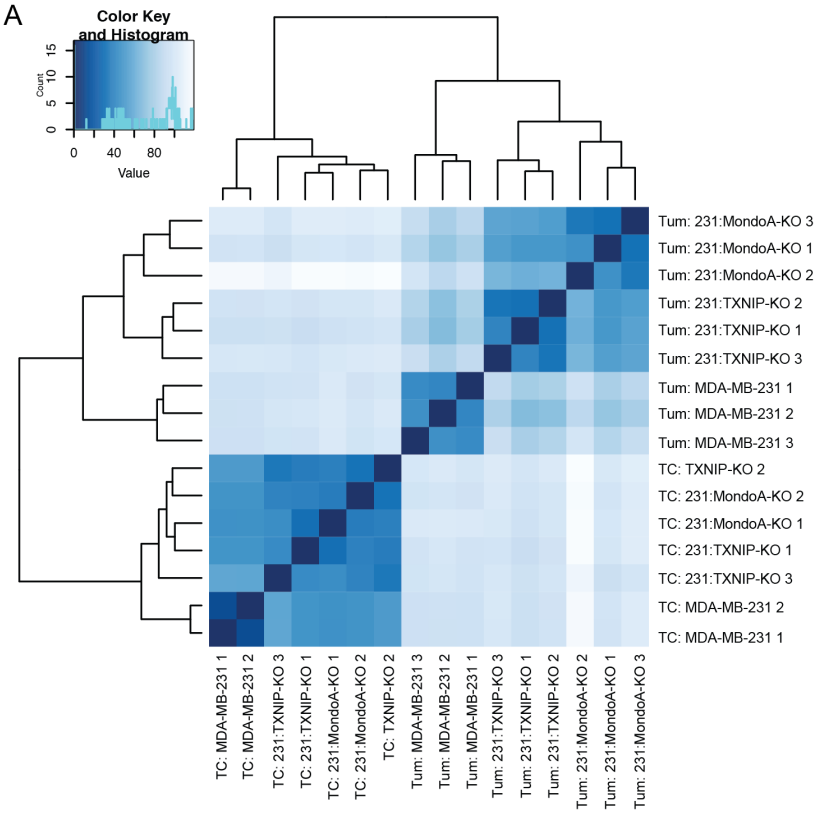

B

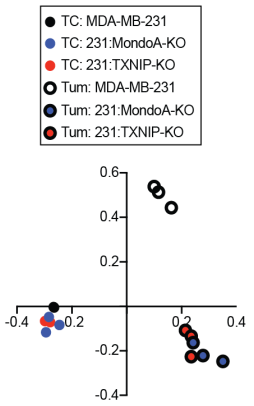

C

Gene Set	FDR (Nom. p-val = 0)
SANA_RESPONSE_TO_IFNG_UP	0
GSE42021_CD24HI_VS_CD24INT_TREG_THYMUS_DN	0
BROWNE_INTERFERON_RESPONSIVE_GENES	0
REACTOME_INTERFERON_ALPHA_BETA_SIGNALING	1.71E-04
REACTOME_INTERFERON_GAMMA_SIGNALING	1.47E-04
GSE42021_TREG_VS_TCONV_PLN_UP	1.28E-04
ZHANG_TLX_TARGETS_36HR_DN	4.90E-04
WUNDER_INFLAMMATORY_RESPONSE_AND_CHOLESTEROL_UP	1.14E-04
GSE37533_PPARG1_FOXP3_VS_FOXP3_TRANSDUCED_CD4_TCELL_DN	1.03E-04
NIKOLSKY_BREAST_CANCER_1Q21_AMPLICON	1.87E-04
SENESE_HDAC1_AND_HDAC2_TARGETS_DN	2.21E-04
KRAS.50_UP.V1_DN	4.15E-04
ICHIBA_GRAFT_VERSUS_HOST_DISEASE_D7_UP	3.89E-04
KOBAYASHI_EGFR_SIGNALING_24HR_DN	6.54E-04
AMIT_EGF_RESPONSE_480_MCF10A	4.91E-04
GSE42724_NAIVE_BCELL_VS_PLASMABLAST_UP	5.50E-04
RICKMAN_METASTASIS_DN	5.19E-04
ICHIBA_GRAFT_VERSUS_HOST_DISEASE_35D_UP	4.92E-04
ZHANG_TLX_TARGETS_DN	3.93E-04
NIKOLSKY_BREAST_CANCER_8Q12_Q22_AMPLICON	4.20E-04
BIDUS_METASTASIS_UP	7.35E-04
KRAS.LUNG.BREAST_UP.V1_UP	7.63E-04
RICKMAN_METASTASIS_UP	7.84E-04
KRAS.600_UP.V1_UP	0.00107079
SENESE_HDAC1_AND_HDAC2_TARGETS_UP	0.001145503
SENESE_HDAC2_TARGETS_UP	0.00143341
PEDERSEN_METASTASIS_BY_ERBB2_ISOFORM_1	0.001540864
HALLMARK_E2F_TARGETS	0.001633958
SENESE_HDAC1_TARGETS_UP	0.001654804
KRAS.600.LUNG.BREAST_UP.V1_UP	0.001615599
FERREIRA_EWINGS_SARCOMA_UNSTABLE_VS_STABLE_UP	0.001634404

D

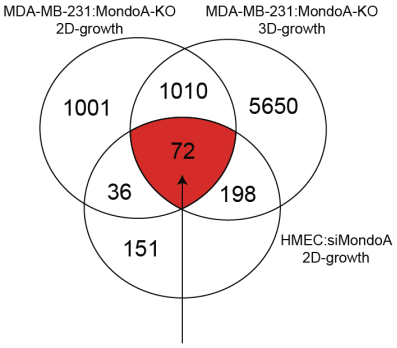

Response to interferon-gamma (p-val. = 0.001)
Glutathione metabolism (p-val.=0.002)
TAp63 targets (p-val. = 0.002)
Selenium regulation (p-val. = 0.003)
Regulation of cell division (p-val. = 0.004)
Arachidonic acid metabolism (p-val. = 0.006)

CHAPTER 5

CONCLUSION

The ability to sense nutrients and respond to maintain metabolic homeostasis is a central tenet of biology. Glucose is a fundamental nutrient for constructing and fueling cells. Controlling glucose availability is necessary for establishing proper metabolic states. The MondoA/TXNIP axis is a nexus of cellular glucose homeostasis. The MondoA transcription factor senses glucose availability and drives expression of its target gene thioredoxin-interacting protein (TXNIP), a negative regulator of glucose uptake. Thus, the MondoA/TXNIP axis controls glucose homeostasis. Dysregulation of the MondoA/TXNIP axis underlies a number of metabolic diseases including diabetes and cancer. In this dissertation, we explored the molecular mechanisms that trigger the MondoA/TXNIP axis as well MondoA-dependent transcriptional outputs.

MondoA resides on the outer mitochondrial membrane (OMM) (Sans et al., 2006). Our previous work demonstrated that MondoA senses glucose-6-phosphate (G6P) and responds by translocating to the nucleus and driving transcription (Stoltzman et al., 2008). MondoA also requires a signal from the electron transport chain (ETC) to become transcriptionally active, yet the identity of the ETC signal has remained unclear (Yu et al., 2010). By monitoring both glycolytic flux and oxidative phosphorylation, MondoA is centrally situated to be a master regulator of central carbon metabolism. The primary goal of this project was to identify the metabolic determinants of MondoA transcriptional activity.

In Chapter 2, we demonstrate that acidosis drives MondoA-dependent TXNIP expression. Treatment with low pH medium leads to intracellular acidification. Intracellular pH is a strong determinant of glycolytic flux and acidification leads to decreased glucose uptake (Gunnink et al., 2014; Webb et al., 2011). This finding led us to

investigate the molecular mechanisms by which acidosis triggers the MondoA/TXNIP axis. Acidosis treatment leads to hyperpolarization of the inner-mitochondrial membrane, which is sufficient to drive mitochondrial-ATP (mtATP) synthesis. Our results demonstrate that mtATP is a necessary signal for MondoA transcriptional activity. As mtATP is exported from the mitochondrial matrix, it is consumed by hexokinase to produce G6P, a potent activator of MondoA transcriptional activity. Future work will focus on how G6P stimulates MondoA transcriptional activity.

MondoA is necessary for cell proliferation under acidosis. Chapter 2 also outlined the MondoA-dependent transcriptional response to acidosis. MondoA is responsible for about 50% of acidosis-driven transcription. Among the pathways that MondoA regulates in response to acidosis is cholesterol biosynthesis. Given that cholesterol protects against acidosis-mediated membrane damage, we propose that MondoA drives a cell protective response to acidosis, of which cholesterol biosynthesis is a key feature (Zhou et al., 2009).

Results presented in Chapter 2 show that MondoA integrates signals from both glycolysis, and oxidative phosphorylation, to exert control over nutrient homeostasis. Given that MondoA, Mlx and hexokinase all localize to the OMM, we propose that they are part of a signaling center that senses and controls central carbon metabolism. Tethering signaling complexes to membranes is a common theme in biology. For example, the mTORC1/Ragulator complex is tethered to the lysosome where it senses nutrients from the lysosomal lumen and the cytosol (Saxton and Sabatini, 2017).

In Chapter 3 we demonstrate that protein synthesis inhibitors trigger the MondoA/TXNIP axis. Protein synthesis inhibition leads to significant metabolic rewiring

and increased production of mtATP. As was shown in Chapter 2, MondoA senses this increase in mtATP through the generation of G6P by mitochondria-bound hexokinase. Protein synthesis inhibitors likely enhance TCA cycle flux to drive ETC-mediated production of mtATP production. Thus, in the context of protein synthesis inhibition, the MondoA/TXNIP axis is also linked to mtATP production.

Protein synthesis inhibitors have been proposed as potential therapeutics for various cancers. Rocaglamide A (RocA) is an translation initiation inhibitor that drives apoptosis in a number of cancer types. RocA drives a robust increase in TXNIP expression and a reduction in glucose uptake. The induction of TXNIP is essential for full RocA-mediated growth suppression, suggesting a role for TXNIP in protecting against protein synthesis inhibition.

Chapter 3 concludes with analysis of the RocA-stimulated MondoA-dependent transcriptome. TXNIP and ARRDC4 are highly induced by RocA treatment and are almost entirely dependent on MondoA. We identified Ras-related Associated with Diabetes (RRAD) as a novel target of the MondoA/TXNIP axis. RRAD is a negative regulator of glycolysis, thus expanding our knowledge of the potential mechanisms by which the MondoA/TXNIP axis restricts glycolysis.

In Chapter 4, we determine the transcriptional consequences of MondoA and TXNIP loss in triple-negative breast cancer (TNBC). We made three key observations: 1) MondoA requires TXNIP for its transcriptional activity, 2) loss of MondoA or TXNIP results in increased Myc transcriptional activity, 3) loss of MondoA sensitizes cells to Myc-driven cell death, and 4) MondoA and TXNIP loss has a much greater impact on transcription in tumors compared to cells in culture.

We first demonstrate that TNBC cell lacking MondoA and TXNIP have a similar transcriptional profile. Importantly, TXNIP expression is highly, if not entirely, dependent on MondoA transcriptional activity. Yet, TXNIP is not sufficient to rescue gene expression in the context of MondoA-loss. We therefore propose that the transcriptional activity of MondoA is dependent on TXNIP. This is consistent with the results of other labs showing that TXNIP drives its own transcription in a positive-feedback loop (Chen et al., 2014). A potential model is that TXNIP loss causes a shift from oxidative metabolism to aerobic glycolysis. This causes a decrease in mtATP production, thus limiting MondoA transcriptional activity.

Second, MondoA and TXNIP loss led to increased Myc transcriptional activity. Loss of MondoA or TXNIP in TNBC cells results in enrichment of genes that are directly regulated by Myc. In addition to driving differential gene expression, Myc and MondoA antagonistically bind the same sites in the genome. Further, loss of MondoA sensitizes cells to Myc-driven cell death. This is consistent with observations in neuroblastoma and Myc-amplified B-cell leukemia in which MondoA loss led to Myc-driven cell death (Carroll et al., 2015).

Finally, in orthotopic TNBC xenografts, MondoA and TXNIP loss led to far more differentially regulated genes than cells growth in culture. This suggests that MondoA and TXNIP more broadly regulate transcription *in vivo*. Future studies will investigate why MondoA and TXNIP might be more transcriptionally active in tumors. A possible explanation is that stresses caused by the tumor microenvironment, such as acidosis, trigger the MondoA/TXNIP axis, resulting in increased transcription.

The work presented here shows in multiple contexts that MondoA senses multiple

metabolic states. By simultaneously sensing glucose and mtATP through the production of G6P at the mitochondria, we recognize the following: 1) Not all pools of ATP are equal. mtATP pools specifically trigger MondoA/TXNIP-dependent regulation of glucose uptake, 2) MondoA and hexokinase make up a signaling center on the surface of the mitochondria to control glucose homeostasis, and 3) MondoA is a coincidence detector that integrates glycolytic and mitochondrial metabolites in order to control nutrient homeostasis.

How MondoA senses G6P remains to be determined. Further studies on the molecular mechanisms that control the MondoA/TXNIP axis and its impact on metabolism and cancer will provide important insights into an adaptive response to central carbon metabolism and ultimately aid in therapeutic approaches for cancer. Further, in-depth analyses of the genes regulated by MondoA will uncover biological consequences of MondoA-transcriptional activity.

5.1. References

Carroll, P.A., Diolaiti, D., McFerrin, L., Gu, H., Djukovic, D., Du, J., Cheng, P.F., Anderson, S., Ulrich, M., Hurley, J.B., *et al.* (2015). Deregulated Myc requires MondoA/Mlx for metabolic reprogramming and tumorigenesis. Cancer Cell *27*, 271-285.

Chen, J., Jing, G., Xu, G., and Shalev, A. (2014). Thioredoxin-interacting protein stimulates its own expression via a positive feedback loop. Mol Endocrinol *28*, 674-680.

Folli, F., Corradi, D., Fanti, P., Davalli, A., Paez, A., Giaccari, A., Perego, C., and Muscogiuri, G. (2011). The role of oxidative stress in the pathogenesis of type 2 diabetes mellitus micro- and macrovascular complications: avenues for a mechanistic-based therapeutic approach. Curr Diabetes Rev *7*, 313-324.

Gunnink, S.M., Kerk, S.A., Kuiper, B.D., Alabi, O.D., Kuipers, D.P., Praamsma, R.C., Wrobel, K.E., and Louters, L.L. (2014). Alkaline pH activates the transport activity of GLUT1 in L929 fibroblast cells. Biochimie *99*, 189-194.

Sans, C.L., Satterwhite, D.J., Stoltzman, C.A., Breen, K.T., and Ayer, D.E. (2006). MondoA-Mlx heterodimers are candidate sensors of cellular energy status: mitochondrial localization and direct regulation of glycolysis. Mol Cell Biol *26*, 4863-4871.

Saxton, R.A., and Sabatini, D.M. (2017). mTOR signaling in growth, metabolism, and disease. Cell *169*, 361-371.

Stoltzman, C.A., Peterson, C.W., Breen, K.T., Muoio, D.M., Billin, A.N., and Ayer, D.E. (2008). Glucose sensing by MondoA:Mlx complexes: a role for hexokinases and direct regulation of thioredoxin-interacting protein expression. Proc Natl Acad Sci U S A *105*, 6912-6917.

Webb, B.A., Chimenti, M., Jacobson, M.P., and Barber, D.L. (2011). Dysregulated pH: a perfect storm for cancer progression. Nat Rev Cancer *11*, 671-677.

Yu, F.X., Chai, T.F., He, H., Hagen, T., and Luo, Y. (2010). Thioredoxin-interacting protein (Txnip) gene expression: sensing oxidative phosphorylation status and glycolytic rate. J Biol Chem *285*, 25822-25830.

Zhou, Y., Doyen, R., and Lichtenberger, L.M. (2009). The role of membrane cholesterol in determining bile acid cytotoxicity and cytoprotection of ursodeoxycholic acid. Biochim Biophys Acta *1788*, 507-513.

APPENDIX

INTERACTIONS BETWEEN MYC AND MONDOA TRANSCRIPTION FACTORS IN METABOLISM AND TUMOURIGENESIS

Blake R. Wilde* and Donald E. Ayer

*I, Blake R. Wilde, along with Donald E. Ayer wrote this article.

Reprinted with permission from British Journal of Cancer, Vol. 113, p. 1529-1533

MINIREVIEW

BJC

British Journal of Cancer (2015) 113, 1529–1533 | doi: 10.1038/bjc.2015.360

Keywords: Myc; MondoA; cancer metabolism; transcription; TXNIP; tumourigenesis

Interactions between Myc and MondoA transcription factors in metabolism and tumourigenesis

Blake R Wilde[1] and Donald E Ayer*[,1]

[1]*Department of Oncological Sciences, Huntsman Cancer Institute, University of Utah, 2000 Circle of Hope, Salt Lake City, UT 84112-5550, USA*

Metabolic reprogramming towards aerobic glycolysis is a common feature of transformed cells and can be driven by a network of transcription factors. It is well established that c-Myc and hypoxia-inducible factor-1α (HIF-1α) contribute to metabolic reprogramming by driving the expression of glycolytic target genes. More recently, the c-Myc-related transcription factor MondoA has been shown to restrict glucose uptake and aerobic glycolysis via its induction of thioredoxin-interacting protein (TXNIP). Three recent studies demonstrate that complex and cancer type-specific interactions between c-Myc, MondoA and HIF-1α underlie metabolism, tumourigenesis and drug response. In triple-negative breast cancer, c-Myc blocks MondoA-dependent activation of TXNIP to stimulate aerobic glycolysis. In contrast, in neuroblastoma, N-Myc requires MondoA for metabolic reprogramming and tumourigenesis. Finally, the therapeutic response of $BRAF^{V600E}$ melanoma cells to vemurafenib requires downregulation of c-Myc and HIF-1α and upregulation of MondoA-TXNIP, and the subsequent reprogramming away from aerobic glycolysis. In this minireview we highlight the findings in these three studies and present a working model to explain why c-Myc and MondoA function cooperatively in some cancers and antagonistically in others.

THE PLAYERS AND THEIR ROLES

The MYC family of proto-oncogenes (c-Myc, L-Myc, N-Myc or collectively Myc) encode basic helix-loop-helix leucine zipper (bHLHZip) transcription factors that have roles in normal and oncogenic physiology (Eilers and Eisenman, 2008; Meyer and Penn, 2008). Aberrant Myc activity leads to increased cell proliferation and growth and Myc family members are commonly dysregulated in cancer. Cancers of many different tissue types have dysregulated Myc and, when paired with other mutations, Myc can drive tumourigenesis. Myc's normal and pathological functions have been the subject of many excellent reviews and will not be discussed here. Rather, we focus on the interplay between Myc and related bHLHZip factors that comprise an extended Myc network. This extended Myc network functions to match nutrient availability with nutrient utilisation, supporting cell growth and tumourigenesis.

Myc requires dimerisation with another bHLHZip transcription factor, Max, for DNA binding and the recruitment of transcriptional machinery. All Myc paralogues dimerise with Max and the different heterocomplexes have many common target genes, although each heterocomplex has a unique subset of target genes and expression patterns. Generally, Myc/Max complexes influence cell growth by driving the expression genes involved in key biosynthetic pathways and by supporting glycolysis and glutaminolysis (Dang, 2012b). Myc can also act as a transcriptional repressor at certain promoters that is critical to its function in driving cell growth and proliferation (Walz *et al*, 2014).

A complete functional characterisation of Myc proteins is difficult because they do not function in isolation (O'Shea and Ayer, 2013). Rather, their activity is potentially regulated by a dizzying array of additional protein partnerships mediated by families of related bHLHZip transcription factors. The first level of regulation is mediated by the Mad family of transcriptional repressors (Mxd1, Mxi1, Mxd3, Mxd4) that also interact with Max.

*Correspondence: Dr DE Ayer; E-mail: don.ayer@hci.utah.edu

Received 31 July 2015; revised 10 September 2015; accepted 15 September 2015; published online 15 October 2015

Furthermore, Max can also interact with Mnt, which is related to the Mad family, and Mga, which has a T-Box DNA-binding domain in addition to its bHLHZip domain (Hurlin and Huang, 2006). The Mxd/Max complexes repress many of the same targets that are activated by Myc/Max complexes (Iritani *et al*, 2002); however, no comprehensive genome-wide occupancy studies have been conducted. The second level of regulation is mediated by a Max-like bHLHZip protein called Mlx. Mlx can interact with Mxd1 and Mxd4 and potentially Mnt. Mxd/Mlx, Mxd/Max and Myc/Max all bind similar DNA sites *in vitro*, suggesting overlapping transcriptional targets *in vivo*, but again no comprehensive genome-wide study is available (O'Shea and Ayer, 2013). The third level of regulation is that Mlx interacts with the Mondo family of bHLHZip transcriptional activators. There are two Mondo paralogues, MondoA (or MlxIP) and carbohydrate response element-binding protein (ChREBP, MondoB or MlxIPL) (Figure 1). Mondo/Mlx complexes are important nutrient sensors and share a similar DNA-binding sequence with the rest of the network heterocomplexes (O'Shea and Ayer, 2013). The existence of multiple Myc-related bHLHZip factors, their assembly into different heterocomplexes and the participation of these heterocomplexes in potentially overlapping networks suggests that functional output of Myc/Max complexes is likely dictated by many mechanisms: (1) competitive or collaborative interactions with other network complexes at shared targets, (2) competition for limiting Max or Mlx or (3) different complexes may regulate distinct effector pathways that compete or collaborate to control cell growth and tumourigenesis. In this review we focus on the last possibility as three recent papers demonstrate that Myc/Max and MondoA/Mlx complexes play critical roles in matching the cellular demand for nutrients with nutrient availability (Parmenter *et al*, 2014; Carroll *et al*, 2015; Shen *et al*, 2015).

THE MONDO FAMILY

In normal physiology, MondoA and ChREBP are ubiquitously expressed with the highest expression in skeletal muscle and liver, respectively, and are important regulators of glucose-dependent transcription (Peterson and Ayer, 2011). MondoA/Mlx localise primarily to the cytoplasm and translocate to the nucleus in response to increased extracellular glucose concentrations. The mechanistic details of how the heterocomplex senses extracellular glucose are still being worked out, but current data suggest that MondoA/Mlx complexes sense intermediates in the upper portion of the glycolytic pathway (O'Shea and Ayer, 2013). For MondoA, an allosteric mechanism where a glucose-derived metabolite binds directly to the conserved N-terminus to trigger nuclear accumulation, promoter binding and transcriptional activation of target genes seems to be key (Peterson *et al*, 2010). The transcriptional activity of MondoA/Mlx complexes also requires mitochondrial electron transport (Yu *et al*, 2010) that enables their nuclear import and promoter binding. Thus, MondoA/Mlx complexes sense the status of two key bioenergetic pathways, allowing cells to adapt to changes in glycolytic flux or mitochondrial activity.

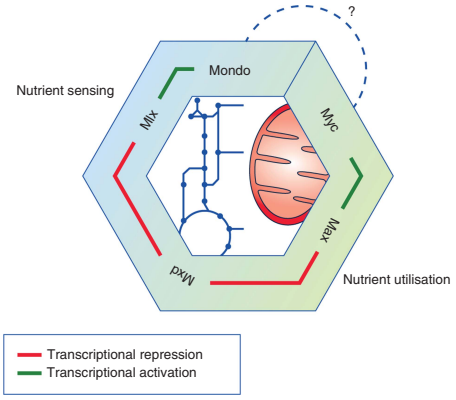

Figure 1. The extended Myc network. Transcriptional activation and repression mediated by Myc/Max and Max/Mxd respectively drive a transcriptional profile that coordinates nutrient utilisation. Transcriptional activation and repression by Mondo/Mlx make up a nutrient sensing branch of the network.

The most well-characterised direct and glucose-dependent target gene of MondoA/Mlx is thioredoxin-interacting protein (TXNIP), a member of the α-arrestin family (O'Shea and Ayer, 2013). TXNIP has pleiotropic functions in different cellular stress response pathways, with one of its most striking features being a potent negative regulator of glucose uptake. It can suppress both insulin-dependent and insulin-independent glucose uptake by limiting the localisation of glucose transporters to the plasma membrane (Wu *et al*, 2013). Furthermore, in some cell types TXNIP can drive degradation of hypoxia-inducible factor-1α (HIF-1α) (Shin *et al*, 2008), a central regulator of glycolytic gene expression under hypoxic growth conditions. Thus, the glucose-stimulated and MondoA-dependent induction of TXNIP triggers a negative feedback loop that restricts glucose uptake until glucose homeostasis can be restored. Furthermore, the dependence of the MondoA/TXNIP axis on electron transport ensures that cells with defective oxidative phosphorylation maintain a high glycolytic rate to support cellular bioenergetics.

Given that TXNIP is a potent negative regulator of glucose uptake and aerobic glycolysis, it is not surprising that its expression is reduced in many cancer types and low TXNIP expression correlates with poor clinical outcome in several cancers including breast and gastric cancer (Shin *et al*, 2008; Chen *et al*, 2010; Shen *et al*, 2015). MondoA is absolutely required for TXNIP expression, yet MondoA is not a frequent target for mutational inactivation in cancer. Rather, the activity of MondoA at the TXNIP promoter is suppressed by activation of common oncogenic or pro-growth pathways, for example Ras, PI3K and mTOR (Elgort *et al*, 2010; Kaadige *et al*, 2015). The prevalence of Ras, PI3K and mTOR activation across cancer types suggests broad suppression of the MondoA/TXNIP axis in tumourigenesis.

THE EXPANDED NETWORK IN TRIPLE-NEGATIVE BREAST CANCER

The triple-negative breast cancer (TNBC) accounts for 15–20% of breast cancer cases. Typically, TNBCs occur earlier in life, reoccur more frequently and have decreased overall survival. The TNBCs lack expression of the oestrogen receptor (ER), progesterone receptor (PR) and HER2, and hence the 'triple-negative' nomenclature (Foulkes *et al*, 2010). The TNBCs are more metabolic than other breast cancer subclasses, and thus understanding how nutrients support their growth and survival may provide pathways for therapeutic development. Consistent with Myc's role in regulating aerobic glycolysis, c-Myc expression correlates with the glycolytic phenotype of TNBCs (Palaskas *et al*, 2011). In contrast, there is no general correlation between c-Myc levels or Myc activity and glutamine utilisation or glutamine-dependence in TNBC (Timmerman *et al*, 2013; Shen *et al*, 2015). These findings prompted us to study how c-Myc controls glucose metabolism in TNBC (Shen *et al*, 2015). As expected, c-Myc knockdown reduced

glucose uptake in multiple TNBC cell lines. Surprisingly, TXNIP was induced in c-Myc knockdown TNBC cells and its induction was required for the reduction in glucose uptake resulting from c-Myc knockdown. This finding suggests that in addition to its canonical function of driving the expression of glycolytic target genes, c-Myc can also drive glucose metabolism by repressing TXNIP. Mechanistically, c-Myc can bind to proximal double E-box carbohydrate response element (ChoRE) in the TXNIP promoter, also the known MondoA/Mlx binding site. Furthermore, TXNIP induction following c-Myc knockdown is entirely dependent on MondoA. Thus, either c-Myc recruits dominant transcriptional repression machinery to the TXNIP promoter or displaces strongly activating MondoA/Mlx complexes from the TXNIP promoter by direct competition. MondoA levels increase at the TXNIP promoter following c-Myc knockdown, supporting the second model.

In the TNBC line MDA-MB-157, Myc-driven expression of glycolytic target genes and its repression of TXNIP contribute to Myc-driven glucose metabolism to approximately the same extent (Shen *et al*, 2015). Further studies are needed to determine whether these mechanisms are similarly balanced in other cancer types or whether cancer type-specific mechanisms dictate their relative contributions. Elevated c-Myc drives expression of genes that encode many biosynthetic pathways placing a demand on biosynthetic precursors such as glucose and glutamine (Dang, 2012a). In TNBC, c-Myc-dependent repression of TXNIP increases glucose uptake that helps to match nutrient demand with nutrient availability. A c-Myc_{high}/$TXNIP_{low}$ gene signature correlates with reduced overall survival and reduced metastasis-free survival in breast cancer, particularly in TNBC, highlighting the clinical significance of c-Myc-dependent repression of TXNIP (Shen *et al*, 2015).

It is striking that the c-Myc_{high}/$TXNIP_{low}$ signature only correlates with poor clinical outcome in TNBC and not in other subtypes of breast cancer. Furthermore, the gene signature only correlates with poor clinical outcome in tumours that also harbour mutations in the tumour suppressor gene TP53 (Shen *et al*, 2015). TP53 is mutated in between 60% and 90% of TNBCs (Turner *et al*, 2013), and this may explain why c-Myc_{high}/$TXNIP_{low}$ only correlates with poor clinical outcome in this breast cancer subtype. Thus, there may be functional cooperation between c-Myc_{high}/$TXNIP_{low}$ and mutation of TP53. Importantly, this cooperation does not appear to depend on established connections between dysregulated c-Myc expression and TP53 mutation (Shen *et al*, 2015). Thus, in TNBC, c-Myc and MondoA, via their opposing regulation of TXNIP expression, function antagonistically.

THE EXPANDED NETWORK IN $BRAF^{V600}$ MELANOMA

c-Myc and MondoA antagonism also appears to be at play in melanomas that harbour the activated alleles of the BRAF kinase (Parmenter *et al*, 2014). The BRAF-mutant melanomas are highly glycolytic and their sensitivity to the BRAF inhibitor vemurafenib correlates with a dramatic suppression of glucose uptake and aerobic glycolysis. Vemurafenib treatment reduces the membrane expression of the GLUT1 and GLUT3 glucose transporters and decreases expression of hexokinase II, the first rate-limiting enzyme in glycolysis. Importantly, $BRAF^{V600}$ melanomas rendered resistant to vemurafenib by expression of $NRAS^{Q61K}$ do not reprogramme their metabolism in response to drug treatment.

Vemurafenib treatment of $BRAF^{V600}$ melanomas drives upregulation of TXNIP and its paralogue ARRDC4 that contributes to its suppression of glucose uptake and aerobic glycolysis (Parmenter *et al*, 2014). MondoA occupancy at the TXNIP and ARRDC4 promoters increases in response to vemurafenib treatment and this increase is blocked by expression of $NRAS^{Q61K}$. As expected, MondoA is required for upregulation of TXNIP in response to vemurafenib. MondoA is also required for the decrease in glucose uptake and cell proliferation driven by vemurafenib. These results strongly implicate the MondoA/TXNIP axis as a key effector of the vemurafenib therapeutic response.

Vemurafenib treatment also results in dramatic downregulation of c-Myc and HIF-1α. Furthermore, functional experiments show that downregulation of c-Myc and HIF-1α is required for vemurafenib to suppress glucose metabolism in $BRAF^{V600}$ melanomas. Unlike TNBCs, where c-Myc knockdown is sufficient to upregulate TXNIP, c-Myc knockdown in one $BRAF^{V600}$ melanoma cell line only increases TXNIP slightly (Parmenter *et al*, 2014). Thus, other mechanisms, in addition to c-Myc downregulation, must also contribute to vemurafenib-dependent induction of TXNIP. Together, these experiments establish that activation of the MondoA/TXNIP axis along with reduction of c-Myc and HIF-1α are required in combination for vemurafenib to reprogramme metabolism away from glucose metabolism and suppress growth in $BRAF^{V600}$ melanomas. Given these findings, it is not surprising that vemurafenib-treated melanomas become dependent on glutamine (Hernandez-Davies *et al*, 2015). Together, these studies suggest that c-Myc and MondoA work in opposition in these cancers.

THE EXPANDED NETWORK IN NEUROBLASTOMA

In contrast to TNBC and $BRAF^{V600}$ melanomas, c-Myc and MondoA cooperate in reprogramming metabolism and supporting tumourigenesis in neuroblastoma (Carroll *et al*, 2015). Neuroblastoma is the most common extracranial solid tumour in children. Approximately 20% of neuroblastomas have N-Myc amplification that coorelates with advanced-stage disease and poor clincal outcome (Louis and Shohet, 2015). In N-Myc-overexpressing neuroblastomas, loss of MondoA or Mlx results in cell death, demonstrating that the MondoA/Mlx heterodimer is required for N-Myc-dependent cell growth and tumourigenesis. This finding extends to other Myc-amplified cells including human B-cell leukaemia and transformed neural stem cells. In contast, neuroblastoma cells that lack N-Myc amplification do not require MondoA for viability; however, overexpression of N-Myc in these cells drives MondoA dependence. Together, these data suggest that neuroblastoma cells with high N-Myc expression depend on MondoA/Mlx for their growth and survival.

There are over 1000 Myc/Max and MondoA/Mlx co-regulated genes in neuroblastoma cells including many metabolic genes (Carroll *et al*, 2015). Multiple MondoA-dependent pathways are required for N-Myc-driven survival/growth, providing the mechanistic basis of the dependence of N-Myc-overexpressing cells on MondoA. For example, MondoA depletion reduces N-Myc-driven expression of genes involved in glutamine uptake and utilisation, resulting in reduced global cellular biosynthesis, reduced mitochondrial metabolic capacity and a subsequent reduction in oxygen consumption. MondoA loss results in reduced activity of many nutrient utilisation and biosynthetic pathways. These findings suggest that MondoA supports the metabolic changes driven by and required by N-Myc overexpression. Furthermore, cells driven by N-Myc overepression have an increased demand for biosynthetic and bioeneregetic substrates that cannot be met by low MondoA levels. This mismatch eventually leads to apoptosis and a blockade of tumourigenesis. The patholgical significance of the cooperation between N-Myc and MondoA is highlighted by the finding that the highest expression of a seven-gene signature comprising MondoA and six metabolic genes correlates with poor clinical outcome in neuroblastoma and hepatocellular carcinoma. Reflecting the

apparent functional differences in the extended Myc network in TNBC and neuroblastoma, this same gene signature does not correlate with clinical outcome in invasive breast carcinoma.

CONCLUSIONS

These three studies highlight the complex interactions between the members of the extended Myc network in metabolism and tumourigenesis (Parmenter *et al*, 2014; Carroll *et al*, 2015; Shen *et al*, 2015). The studies in TNBC and $BRAF^{V600}$ melanoma suggest that MondoA and Myc function antagonistically in controlling glucose uptake/glycolysis. In contrast, in neuroblastoma, N-Myc amplification drives a dependence on MondoA and Mlx (Figure 2). These findings seem contradictory, but we suggest that the activities of Myc and MondoA function principally to match the demand for biosynthetic precursors with their availability. We speculate that in TNBC, TXNIP suppression by Myc increases the availability of glucose to support Myc-driven biosynthetic reactions. In contrast, in neuroblastoma, N-Myc increases MondoA levels that in turn activate glutaminolysis and lipogenesis to support N-Myc-driven biosynthetic reactions. Together, these data suggest that in cells or tumours that depend primarily on glucose catabolism to fuel biosynthesis, Myc and MondoA will function antagonistically. In contrast, in cells or tumours that depend primarily on catabolism of glutamine and lipids to fuel biosynthesis, Myc and MondoA will function collaboratively.

How broadly the complex interplay between Myc and MondoA extends across tumourigenesis remains to be explored. Current data suggest that the primary function of the MondoA/TXNIP axis is in growth and tumour suppression. For example, TXNIP is downregulated in many tumour types and is only infrequently upregulated in tumours (O'Shea and Ayer, 2013). Furthermore, MondoA is not strongly downregulated in tumours, but several common oncogenic drivers suppress its transcriptional activity at the TXNIP promoter. It will be interesting to determine whether tumours that show suppression of the MondoA/TXNIP axis are particularly dependent on glucose. MondoA has been proposed to function as an oncogene in B-cell acute lymphoblastic leukaemia (Wernicke *et al*, 2012). The function of c-Myc in B-ALL is not well studied, but elevated c-Myc levels do associate with increased risk of persistent disease (Allen *et al*, 2014). Whether MondoA is required for B-ALL growth and tumourigenesis or is required to support other c-Myc-driven B-cell lymphomas such as Burkitt's and diffuse large B-cell should be investigated (Slack and Gascoyne, 2011). As argued above, these Myc-driven tumours may be particularly dependent on glutamine or lipid catabolic pathways.

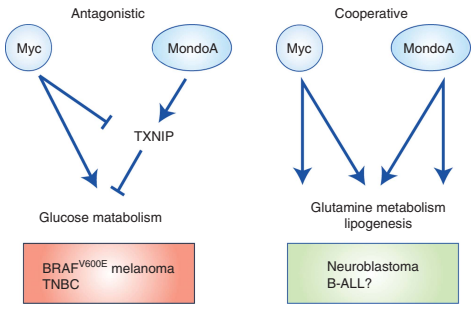

Figure 2. Myc and MondoA coordinate nutrient utilisation. In triple-negative breast cancer and melanoma, Myc and MondoA competitively influence glucose metabolism, whereas in neuroblastoma and possibly B-ALL, MondoA and Myc cooperatively drive glutamine metabolism and lipogenesis.

The highlighted studies indicate that Myc/Max complexes have cell-type differences in their transcriptional targets. For example, in neuroblastoma, N-Myc/Max increases the expression of MondoA and TXNIP (Carroll *et al*, 2015), whereas in TNBC/ c-Myc represses TXNIP without influencing MondoA levels (Shen *et al*, 2015). These cell-type differences may reflect differences in the pallet of co-activators/co-repressors available in a given cell type, or they may reflect more indirect mechanisms such as c-Myc- or MondoA-driven changes in cell metabolism. Furthermore, the relationship between MondoA and Myc may be influenced by the relative level of Myc amplification and/or the specific Myc homologue that is deregulated (Murphy *et al*, 2008). With the discovery of Max almost 25 years ago and the demonstration that Myc/Max complexes functioned as transcriptional activators, there was hope that determining 'how' c-Myc functioned in normal and pathological settings would follow directly from determining the cohort of Myc/Max transcriptional targets. However, as many studies now highlight, studying Myc in isolation provides only partial answer to what is a complex multidimensional puzzle.

ACKNOWLEDGEMENTS

We thank members of the Ayer lab for helpful discussions. DEA is supported by R01GM055668 and W81XWH1410445 from the Department of Defense.

CONFLICT OF INTEREST

The authors declare no conflict of interest.

REFERENCES

Allen A, Gill K, Hoehn D, Sulis M, Bhagat G, Alobeid B (2014) C-myc protein expression in B-cell acute lymphoblastic leukemia, prognostic significance? *Leuk Res* **38**: 1061–1066.

Carroll PA, Diolaiti D, Mcferrin L, Gu H, Djukovic D, Du J, Cheng PF, Anderson S, Ulrich M, Hurley JB, Raftery D, Ayer DE, Eisenman RN (2015) Deregulated Myc requires MondoA/Mlx for metabolic reprogramming and tumorigenesis. *Cancer Cell* **27**: 271–285.

Chen JL, Merl D, Peterson CW, Wu J, Liu PY, Yin H, Muoio DM, Ayer DE, West M, Chi JT (2010) Lactic acidosis triggers starvation response with paradoxical induction of TXNIP through MondoA. *PLoS Genet* **6**: e1001093.

Dang CV (2012a) Links between metabolism and cancer. *Genes Dev* **26**: 877–890.

Dang CV (2012b) MYC on the path to cancer. *Cell* **149**: 22–35.

Eilers M, Eisenman RN (2008) Myc's broad reach. *Genes Dev* **22**: 2755–2766.

Elgort MG, O'Shea JM, Jiang Y, Ayer DE (2010) Transcriptional and translational downregulation of thioredoxin interacting protein is required for metabolic reprogramming during G1. *Genes Cancer* **1**: 893–907.

Foulkes WD, Smith IE, Reis-Filho JS (2010) Triple-negative breast cancer. *N Engl J Med* **363**: 1938–1948.

Hernandez-Davies JE, Tran TQ, Reid MA, Rosales KR, Lowman XH, Pan M, Moriceau G, Yang Y, Wu J, Lo RS, Kong M (2015) Vemurafenib resistance reprograms melanoma cells towards glutamine dependence. *J Transl Med* **13**: 210.

Hurlin PJ, Huang J (2006) The MAX-interacting transcription factor network. *Semin Cancer Biol* **16**: 265–274.

Iritani BM, Delrow J, Grandori C, Gomez I, Klacking M, Carlos LS, Eisenman RN (2002) Modulation of T-lymphocyte development, growth and cell size by the Myc antagonist and transcriptional repressor Mad1. *EMBO J* **21**: 4820–4830.

Kaadige MR, Yang J, Wilde BR, Ayer DE (2015) MondoA-Mlx transcriptional activity is limited by mTOR-MondoA interaction. *Mol Cell Biol* **35**: 101–110.

Louis CU, Shohet JM (2015) Neuroblastoma: molecular pathogenesis and therapy. *Annu Rev Med* **66**: 49–63.

Meyer N, Penn LZ (2008) Reflecting on 25 years with MYC. *Nat Rev Cancer* **8**: 976–990.

Murphy DJ, Junttila MR, Pouyet L, Karnezis A, Shchors K, Bui DA, Brown-Swigart L, Johnson L, Evan GI (2008) Distinct thresholds govern Myc's biological output in vivo. *Cancer Cell* **14**: 447–457.

O'Shea JM, Ayer DE (2013) Coordination of nutrient availability and utilization by MAX- and MLX-centered transcription networks. *Cold Spring Harb Perspect Med* **3**: a014258.

Palaskas N, Larson SM, Schultz N, Komisopoulou E, Wong J, Rohle D, Campos C, Yannuzzi N, Osborne JR, Linkov I, Kastenhuber ER, Taschereau R, Plaisier SB, Tran C, Heguy A, Wu H, Sander C, Phelps ME, Brennan C, Port E, Huse JT, Graeber TG, Mellinghoff IK (2011) 18F-Fluorodeoxy-glucose positron emission tomography marks MYC-overexpressing human basal-like breast cancers. *Cancer Res* **71**: 5164–5174.

Parmenter TJ, Kleinschmidt M, Kinross KM, Bond ST, Li J, Kaadige MR, Rao A, Sheppard KE, Hugo W, Pupo GM, Pearson RB, Mcgee SL, Long GV, Scolyer RA, Rizos H, Lo RS, Cullinane C, Ayer DE, Ribas A, Johnstone RW, Hicks RJ, Mcarthur GA (2014) Response of BRAF-mutant melanoma to BRAF inhibition is mediated by a network of transcriptional regulators of glycolysis. *Cancer Discov* **4**: 423–433.

Peterson CW, Ayer DE (2011) An extended Myc network contributes to glucose homeostasis in cancer and diabetes. *Front Biosci (Landmark Ed)* **16**: 2206–2223.

Peterson CW, Stoltzman CA, Sighinolfi MP, Han KS, Ayer DE (2010) Glucose controls nuclear accumulation, promoter binding, and transcriptional activity of the MondoA-Mlx heterodimer. *Mol Cell Biol* **30**: 2887–2895.

Shen L, O'Shea JM, Kaadige MR, Cunha S, Wilde BR, Cohen AL, Welm AL, Ayer DE (2015) Metabolic reprogramming in triple-negative breast cancer through Myc suppression of TXNIP. *Proc Natl Acad Sci USA* **112**: 5425–5430.

Shin D, Jeon JH, Jeong M, Suh HW, Kim S, Kim HC, Moon OS, Kim YS, Chung JW, Yoon SR, Kim WH, Choi I (2008) VDUP1 mediates nuclear export of HIF1alpha via CRM1-dependent pathway. *Biochim Biophys Acta* **1783**: 838–848.

Slack GW, Gascoyne RD (2011) MYC and aggressive B-cell lymphomas. *Adv Anat Pathol* **18**: 219–228.

Timmerman LA, Holton T, Yuneva M, Louie RJ, Padro M, Daemen A, Hu M, Chan DA, Ethier SP, Van'T Veer LJ, Polyak K, Mccormick F, Gray JW (2013) Glutamine sensitivity analysis identifies the xCT antiporter as a common triple-negative breast tumor therapeutic target. *Cancer Cell* **24**: 450–465.

Turner N, Moretti E, Siclari O, Migliaccio I, Santarpia L, D'incalci M, Piccolo S, Veronesi A, Zambelli A, Del Sal G, Di Leo A (2013) Targeting triple negative breast cancer: is p53 the answer? *Cancer Treat Rev* **39**: 541–550.

Walz S, Lorenzin F, Morton J, Wiese KE, Von Eyss B, Herold S, Rycak L, Dumay-Odelot H, Karim S, Bartkuhn M, Roels F, Wustefeld T, Fischer M, Teichmann M, Zender L, Wei CL, Sansom O, Wolf E, Eilers M (2014) Activation and repression by oncogenic MYC shape tumour-specific gene expression profiles. *Nature* **511**: 483–487.

Wernicke CM, Richter GH, Beinvogl BC, Plehm S, Schlitter AM, Bandapalli OR, Prazeres Da Costa O, Hattenhorst UE, Volkmer I, Staege MS, Esposito I, Burdach S, Grunewald TG (2012) MondoA is highly overexpressed in acute lymphoblastic leukemia cells and modulates their metabolism, differentiation and survival. *Leuk Res* **36**: 1185–1192.

Wu N, Zheng B, Shaywitz A, Dagon Y, Tower C, Bellinger G, Shen CH, Wen J, Asara J, Mcgraw TE, Kahn BB, Cantley LC (2013) AMPK-dependent degradation of TXNIP upon energy stress leads to enhanced glucose uptake via GLUT1. *Mol Cell* **49**: 1167–1175.

Yu FX, Chai TF, He H, Hagen T, Luo Y (2010) Thioredoxin-interacting protein (Txnip) gene expression: sensing oxidative phosphorylation status and glycolytic rate. *J Biol Chem* **285**: 25822–25830.